Ministry of Higher Education and Scientific Research
HASSIBA BENBOUALI UNIVERSITY OF CHLEF
Faculté des Sciences Exactes et Informatique
DEPARTMENT OF PHYSICS

THESIS

Presented for obtaining the degree of Doctor in Physics

Option: Theoretical physics

Submitted By:
TAIBI ZEYNEB

Titled:

Mathematical and Numerical Analysis of the Non Linear Schrödinger Equation

Defended on 11/02/2026 before the jury composed of:

Benarous Mohamed	Professor	University of Chlef	Chair
Hocine Ahmed	Professor	University of Chlef	Examiner
Boukabcha Hocine	Professor	University of Khemis Miliana	Examiner
Chaachoua Sameut Houria	Professor	University of Chlef	Supervisor
P.S vinayagam	Professor	PSG College of Arts & Science India	Co-Supervisor

University year: 2025-2026.

Acknowledgments

In the name of Allah, the Most Gracious, the Most Merciful. All praise is due to Allah, the Lord of the Worlds, for the strength and patience He granted me to complete this work.

I express my sincere gratitude to my supervisor, Pr. Chaachoua Sameut, for her invaluable guidance, support, and constant advice throughout this journey. I also warmly thank Pr. Benarous Mohamed for his mentorship and support; I am truly grateful for his valuable suggestions, from which I have greatly benefited.

I would like to extend my deepest thanks to Pr. Ahmed Hocine For being so helpful, which provided me with significant motivation. I am also sincerely grateful to Pr. Boukabcha Hocine for accepting to be an examiner and a member of the jury. Finally, a precious thought for my family, for their unconditional love and support during all these years, and for giving me the strength and perseverance to carry on with this thesis to its completion.

Abstract

This thesis presents a comprehensive analytical and numerical investigation of localized nonlinear wave structures governed by integrable Higher-Order Nonlinear Schrödinger (HNLS)-type equations. Motivated by recent advances in nonlinear wave physics and the increasing relevance of higher-order dispersive and nonlinear effects, this work demonstrates that the interplay between dispersion, nonlinearity, and higher-order terms constitutes a powerful framework for energy localization and control rather than a limitation.

The study begins with a detailed overview of fundamental nonlinear wave phenomena, including solitons, breathers, and rogue waves, together with a rigorous analysis of modulation instability as the underlying mechanism for localized structure formation. Numerical tools, particularly the Split-Step Fourier Method (SSFM), are introduced and validated through the relative L^2 error norm and trajectory tracking based on the center-of-mass formalism.

From an analytical perspective, the thesis employs the 3×3 Lax pair representation and the Darboux Transformation to construct exact solutions for integrable systems. These methods are applied to benchmark models such as the Hirota and Sasa–Satsuma equations, illustrating the iterative generation of higher-order solitonic and breather solutions and confirming the robustness of the analytical framework.

The dynamics of the HNLS equation with constant coefficients are investigated in detail, revealing the role of spectral parameters in shaping wave morphology, including Akhmediev breathers, Kuznetsov–Ma solitons, and the Peregrine soliton as a limiting rational solution. The individual influence of higher-order physical parameters is isolated, highlighting the dominant role of third-order dispersion in inducing center-of-mass shifts and trajectory drift.

Finally, the thesis extends the analysis to generalized HNLS equations with time-dependent coefficients, demonstrating that active modulation of dispersion and nonlinearity enables precise waveform engineering. Numerical simulations confirm the stability and physical relevance of the Darboux-derived solutions, with relative L^2 errors on the order of 10^{-4}, validating that the observed dynamics arise from intentional parametric control rather than numerical artifacts.

Overall, this work provides a unified analytical–numerical framework for understanding and managing localized nonlinear wave phenomena, offering insights relevant to next-generation nonlinear physical systems in optics, hydrodynamics, and related fields.

Résumé

Cette thèse présente une étude analytique et numérique approfondie des structures d'ondes non linéaires localisées régies par des équations intégrables de type équation de Schrödinger non linéaire d'ordre supérieur (HNLS). Motivée par les avancées récentes en physique des ondes non linéaires et par l'importance croissante des effets dispersifs et non linéaires d'ordre supérieur, cette étude montre que l'interaction entre dispersion, non-linéarité et termes d'ordre supérieur constitue un cadre puissant pour la localisation et le contrôle de l'énergie, plutôt qu'une contrainte.

Le travail débute par une présentation détaillée des phénomènes fondamentaux des ondes non linéaires, notamment les solitons, les breathers et les ondes scélérates, ainsi qu'une analyse rigoureuse de l'instabilité de modulation en tant que mécanisme précurseur de la formation des structures localisées. Les outils numériques, en particulier la méthode de Fourier à pas fractionnés (Split-Step Fourier Method, SSFM), sont introduits et validés à l'aide de la norme d'erreur relative L^2 et du suivi de la trajectoire basé sur le centre de masse.

Sur le plan analytique, la thèse exploite la représentation par paire de Lax 3×3 et la transformation de Darboux pour construire des solutions exactes de systèmes intégrables. Ces méthodes sont appliquées à des modèles de référence tels que les équations de Hirota et de Sasa–Satsuma, illustrant la génération itérative de solutions solitoniques et de breathers d'ordre supérieur, et confirmant la robustesse du cadre analytique.

La dynamique de l'équation HNLS à coefficients constants est ensuite étudiée en détail, mettant en évidence le rôle des paramètres spectraux dans la morphologie des ondes, notamment les breathers d'Akhmediev, les solitons de Kuznetsov–Ma et le soliton de Peregrine comme cas rationnel limite. L'influence individuelle des paramètres physiques d'ordre supérieur est analysée, soulignant le rôle dominant de la dispersion du troisième ordre dans le déplacement du centre de masse et la dérive des trajectoires.

Enfin, la thèse étend l'analyse aux équations HNLS généralisées à coefficients dépendant du temps, démontrant que la modulation temporelle de la dispersion et de la non-linéarité permet une ingénierie contrôlée des formes d'onde. Les simulations numériques confirment la stabilité et la pertinence physique des solutions issues de la transformation de Darboux, avec des erreurs relatives L^2 de l'ordre de 10^{-4}, attestant que les dynamiques observées résultent d'une gestion paramétrique intentionnelle plutôt que d'instabilités numériques.

Dans l'ensemble, ce travail propose un cadre analytique et numérique unifié pour la com-

préhension et la maîtrise des phénomènes d'ondes non linéaires localisées, ouvrant des perspectives pour les systèmes physiques non linéaires de nouvelle génération en optique, en hydrodynamique et dans des domaines connexes.

Contents

List of Figures

General introduction

Nonlinear wave dynamics represent a cornerstone of modern mathematical physics and applied nonlinear science, with profound implications across optics, hydrodynamics, plasma physics, and condensed matter systems [1, 2]. In contrast to linear wave theory, which relies on the principle of superposition and assumes that waves pass through one another without interaction, nonlinear dispersive systems support localized coherent structures that arise from the intrinsic, self-sustaining balance between dispersion and nonlinearity [3]. These structures, most notably solitons, breathers, and rogue waves, constitute the fundamental carriers of energy localization and extreme event formation in nonlinear media [4]. The discovery of these waves traces back to the observation of the "Great Wave of Translation" by John Scott Russell in 1834, but it was the mathematical formalisation of these concepts in the late $20^{(th)}$ century that transformed them into a unified field of study [5]. The nonlinear Schrödinger (NLS) equation has since emerged as a universal model describing the slow modulation of weakly nonlinear wave packets in dispersive environments [6]. Its integrable structure has enabled the discovery of exact analytical solutions that reveal the rich morphological diversity of nonlinear waves, proving that nonlinearity is not merely a perturbation of linear theory but a generator of entirely new physical states [7, 8]. Classical solitons propagate without distortion or loss of identity. In contrast, breather solutions exhibit a complex periodic exchange of energy between localisation and delocalisation, effectively 'breathing' as they move through space or time. One of the most intriguing phenomena is the rogue wave, which is characterised by its sudden emergence and extreme amplitude, often reaching three to four times the height of the surrounding waves. Mathematically, these "monsters of the deep" arise as rational limiting cases of breather solutions, specifically the Peregrine soliton, and are closely linked to modulation instability mechanisms. Recent advances have significantly deepened our understanding of these dynamics, showing that extreme waves can emerge deterministically from coherent backgrounds rather than from stochastic processes alone [9]. This deterministic view has revolutionised oceanic safety and optical telecommunications, where predicting 'giant pulses' is crucial. In optical systems, transitions from breathers to rogue waves have been observed in fibre experiments, confirming the predictive power of NLS-type integrable models and establishing the breather as the parent structure of extreme energy peaks [10].

The formal history of this dispersive wave environment gained momentum in 1967 with the work of Benney and Newell, followed by Zakharov's derivation of the NLS equation in 1968 [11]. The field reached a mathematical zenith in 1972 when Zakharov and Sha-

bat identified the Lax pair for the NLS equation, enabling the use of the Inverse Scattering Transform (IST) to solve the equation exactly [6]. However, as emphasised by Ankiewicz and Akhmediev [12], to accurately describe ultrashort pulse propagation and extreme events in realistic media such as sub-picosecond pulses in modern waveguides it is necessary to move beyond the standard NLS equation. This has led to the formulation of higher-order nonlinear Schrödinger (HNLS) equations, such as the Hirota and Sasa-Satsuma models, which incorporate third-order dispersion, self-steepening, and stimulated Raman scattering . According to Ankiewicz [13], these higher-order solitary wave solutions are not merely mathematical extensions but are essential for capturing the spatial-temporal symmetry breaking induced by the physical properties of the medium.

A fundamental feature of these integrable nonlinear systems is the existence of a Lax pair, which facilitates the application of the Darboux transformation as a systematic and recursive algebraic method for constructing exact solutions [14]. Originally proposed by Gaston Darboux in 1882 and later adapted for soliton theory by Matveev in 1979 [15], this transformation allows for the generation of complex multi-soliton and mixed-state solutions from simple seed solutions. By using this method, one can "engineer" interactions between different species of waves, such as the coexistence of dark solitons and Akhmediev breathers [16]. While early studies focused primarily on homogeneous media with constant coefficients, modern technological applications increasingly require non-autonomous models with time-dependent parameters. This shift towards dispersion and nonlinearity management allows for the active engineering of waveforms, providing a "control switch" to modulate amplitude, width, and trajectory drift [17].

This thesis is motivated by recent developments in the field and presents a comprehensive analytical and numerical investigation of localised nonlinear wave structures governed by integrable HNLS-type equations. The central aim of the work is to demonstrate that the interplay between dispersion, nonlinearity and higher-order effects is not an obstacle to be overcome, but rather a set of tools to be mastered. The work unifies the mathematical elegance of the Darboux method with the practical demands of numerical stability, as verified through the Split-Step Fourier Method (SSFM) and the tracking of the Relative L^2 Error Norm. The work seeks to provide a definitive framework for understanding how energy can be precisely localized and managed in the next generation of nonlinear physical systems [18]. The work is organised as follows:

- ❖ In Chapter 1, the fundamental physics of nonlinear wave phenomena is established, along with the numerical tools required for their study.

- **Concepts:** The article provides a historical overview of solitons, breathers , rogue waves and advanced wave structures and mixed states.
- **Modulation Instability (MI):** A thorough investigation of the MI mechanism is presented as a prerequisite to localised wave formation. This encompasses the analysis of G_{max} dynamics (maximum spectral growth rate) to ascertain stability thresholds and wave amplification.
- **Numerical Methodology:** The split-step Fourier method (SSFM) is introduced in conjunction with the relative L_2 error norm for the purpose of ensuring stability.
- **Trajectory Tracking:** The concept of the Center of Mass (x_{cm}) is established as a mathematical metric with which to monitor pulse shifts and trajectory drift.

❖ In Chapter 2, the reader will encounter an exposition on the analytical apparatus employed to derive exact solutions for integrable systems.

- **Techniques:** The following detailed formulation is presented: the Lax Pair (3×3) and the Darboux Transformation (DT).
- **Applications:** The aforementioned methodologies are employed in the context of the Hirota and Sasa-Satsuma equations, with the objective of constructing benchmark solitonic and breather solutions.
- **Analytical Validation:**The following demonstration is intended to illustrate the iterative capabilities of the DT in the generation of higher-order nonlinear structures from elementary seed solutions.

❖ In Chapter 3, the Higher-Order Nonlinear Schrödinger (HNLS) equation is investigated in the context of homogeneous media, i.e. time-independent coefficients.

- **Spectral Parameters:** This study explores the manner in which the spectral parameter, denoted by the symbol λ, governs wave morphology. It identifies the Akhmediev (spatial periodicity) and Kuznetsov-Ma (temporal periodicity) regimes.
- **Higher-Order Complexity:**The present study analyses Multi-Akhmediev breathers and Peregrine solitons as the limiting rational case for rogue waves.
- **Coefficient Influence:**The physical contribution of each parameter is isolated by the following methodology:
  - It is evident that the parametera_1 (Group Velocity Dispersion) exerts a significant influence on the process of spatial stretching.

- The function a_2 (Self-Focusing Nonlinearity) is responsible for the redistribution of energy.
- It has been determined that a_3 (third-order dispersion) is the primary driver for the centre of mass (x_{cm}) shift.

❖ Chapter 4 is concerned with the generalized HNLS equation, with time-dependent coefficients $a_i(t)$.

- **Active Management:**The demonstration is made that temporal modulation of dispersion and nonlinearity allows for "Waveform Engineering," regulating amplitude growth and localization width.
- **Numerical Substantiation:** The robustness of the Darboux-derived solutions is verified through simulations using the SSFM.
- **Results:** A high-fidelity relative L_2 error of approximately 6×10^{-4} has been demonstrated to confirm that the observed dynamics, such as targeted trajectory drift in x_{cm}, are physical results of intentional parametric management as opposed to numerical instability.

Chapter 1

Historical Background of Waves: Solitons, Breathers, and Rogue Waves

1.1 Introduction

The field of nonlinear science has undergone a profound paradigm shift over the last century, evolving from isolated observations of solitary waves into a unified mathematical framework that describes extreme energy localization in nature [19]. Theoretically predicted by nonlinear evolution equations (NLEEs) and experimentally observed in diverse physical media, including nonlinear optics, hydrodynamics, and plasma physics, the soliton, breather, and rogue wave represent distinct manifestations of the fundamental balance between dispersion and nonlinearity [20, 21, 22, 23, 24, 25].

A salient characteristic of such nonlinear structures is their capacity for morphological transitionality. Specifically, in the event of a branch of a breather solution possessing an unlimited temporal frame, the genesis of a rogue wave can be facilitated. This occurrence can be attributed to the capacity of a propagating breather to undergo spontaneous or induced splitting into distinct entities, thus providing a theoretical basis for the transition mechanisms observed in both laboratory water tanks and optical fibres. Utilising the theory of Modulation Instability (MI), the classification of breathers within complex systems, such as the nonlinear Schrödinger-Maxwell-Bloch system, has been rigorously addressed [26]. Furthermore, experimental investigations in water wave tanks have demonstrated that the

initial amplitude and wave steepness are the decisive parameters governing the evolution of these nonlinear waveforms [27].

In order to address the complex dynamics under consideration, the employment of nonlinear models that possess a Lax pair and are solvable via the Darboux transformation is necessary. These integrable systems represent a significant component of nonlinear wave theory, encompassing the Nonlinear Schrödinger (NLS) equation and its higher-order extensions. Notable models include the Hirota equation [28], which accounts for third-order dispersion, the Sasa-Satsuma equation, and the derivative NLS (DNLS) equation [29, 30].

The formal study of nonlinear dispersive environments was initiated in 1967 with the contributions of Benney and Newell [31]. This was followed by Zakharov's seminal 1968 study, which derived the NLS equation while investigating the stability of periodic waves in deep water [32]. The field reached a mathematical zenith in 1972 when Zakharov and Shabat discovered the Lax pair for the NLS equation, enabling the use of the Inverse Scattering Transform (IST) to solve the equation exactly [33]. The Darboux transformation, named after the French mathematician Jean-Gaston Darboux who proposed the technique in 1882 [34], was elegantly adapted for soliton theory by Matveev in 1979 [35]. This transformation provides a universal algorithmic method for constructing high-order solutions, such as multi-Akhmediev breathers and complex mixed states. These mixed interactions, particularly the coexistence of dark solitons and Akhmediev breathers, represent the cutting edge of vector nonlinear dynamics as established by Baronio et al [36]. Finally, in order to establish a connection between analytical theory and physical reality, this thesis employs a numerical stability framework of a rigorous nature. The maximum gain (G_{max}) of the modulation instability is analysed in order to determine the growth rate of perturbations (ϵ). Temporal evolution is computed via the split-step Fourier method (SSFM), with the results being validated through the relative L^2 error norm and the centre of mass (x_{cm}) trajectory. This ensures the conservation of power and the integrity of wave dynamics [18, 37]

1.2 Integrable systems

However, given the lack of consensus among scientists regarding the precise interpretation of the term 'integrable', the definition of integrable systems remains a challenging endeavour. This ambiguity in definition contributes to the elusiveness of the concept of integrability. Contemporary working definitions frequently cite the presence of a Lax pair,

the existence of an infinite number of symmetries or conservation rules, the solvability of the system using the inverse scattering transform (IST), or the occurrence of a sufficient number of initial integrals in involution (Liouville integrability). The complexity of this subject is evidenced by the existence of a publication exclusively dedicated to the definition of integrability [38].

Integrable systems are defined as nonlinear differential equations that can be solved analytically. Given that the majority of nonlinear differential equations are known to behave chaotically, making explicit solutions impossible, such systems are extremely rare. Despite their rarity, integrable systems have created fascinating areas of mathematics, including fluid dynamics, quantum field theory, differential geometry, and complex analysis [39].

An ensemble of linear partial differential equations (PDEs) in an auxiliary function can be linked to a fully integrable nonlinear PDE. The original PDE must be satisfied for these linear PDEs to be compatible. This associated set is termed a Lax pair, representing a reformulation of the original nonlinear system into the compatibility condition for a linear system. Lax's discovery of such a linear system for the extensively studied KdV equation, which represents a variety of nonlinear wave phenomena such as shallow water waves and ion acoustic waves in plasmas, marks the beginning of the history of Lax pairs [40]. Lax's discovery enabled the application of the then newly discovered inverse scattering transform method for solving the KdV problem to a variety of integrable equations. In 1979, it was recognized that the Lax pair formulation, originally introduced by Peter Lax, admits a geometric interpretation in terms of a zero–curvature representation. This reformulation significantly deepened the structural understanding of integrable nonlinear evolution equations.

A Lax pair consists of two linear operators L and P satisfying

$$\frac{dL}{dt} = [P, L], \tag{1.1}$$

which ensures the isospectral evolution of L and provides the analytical foundation of the inverse scattering transform.

Equivalently, the nonlinear equation can be formulated as the compatibility condition of

the overdetermined linear system

$$\Psi_x = U(x,t,\lambda)\,\Psi, \tag{1.2}$$

$$\Psi_t = V(x,t,\lambda)\,\Psi, \tag{1.3}$$

where U and V are matrix-valued functions depending on the spectral parameter λ.

The compatibility condition $\Psi_{xt} = \Psi_{tx}$ yields the zero–curvature equation

$$U_t - V_x + [U,V] = 0. \tag{1.4}$$

From a differential geometric perspective, U and V define a connection on a principal bundle associated with a Lie algebra, and the above relation expresses the vanishing of its curvature tensor. The nonlinear partial differential equation thus appears as a flatness condition of this connection.

The algebraic interpretation of the zero–curvature representation, fully developed in the 1980s, revealed the intrinsic Lie algebraic structure underlying integrable systems. This framework enabled:

- the construction of recursion operators generating infinite hierarchies of symmetries and conserved quantities,
- the development of Bäcklund transformations linking distinct solutions of integrable equations,
- the formulation of Darboux transformations, which provide an explicit algebraic method for generating new solutions from known ones through gauge transformations of the Lax pair,
- and the systematic derivation of entire families of integrable equations via algebraic and spectral methods.

In particular, for the nonlinear Schrödinger equation (NLS), the Zakharov–Shabat spectral problem supplies the Lax representation. Within this framework, Darboux transformations constitute a powerful tool for constructing soliton, breather, and rogue-wave solutions in an explicit and recursive manner.

1.3 Soliton

Their remarkable property of maintaining their shape even after interacting with other particles is worthy of note. Due to the soliton's robustness and useful applicability in a variety of physical circumstances, mathematicians, physicists and engineers have been attracted to this unique behaviour. The soliton can be considered an answer to non-linear partial differential equations [41].

1.3.1 Historical background of soliton

In order to ascertain the most efficacious canal boat design, the Scottish naval architect John Scott Russell conducted a series of experiments in 1834. It was during the course of these experiments that he discovered an astonishing phenomenon that he termed the "translation wave". He subsequently published the first scientific description of solitons in an article entitled Report on Waves, in which he detailed his findings. The consequence of this event was the formation of a water wave with distinct and peculiar properties in a narrow channel. In contrast to ordinary waves, which gradually flatten or steepen, this wave remained stationary, maintaining its speed and shape. Russell was able to track the wave for several miles and developed an empirical formula for determining the speed of such waves by careful measurement. However, he was unable to derive the exact equation of motion that governed the phenomenon [42].

The solitary waves of John Scott Russell were mathematically verified in 1895 by Diederik Korteweg and his graduate student Hendrik de Vries, who derived a nonlinear partial differential equation now known as the Korteweg-de Vries (KdV) equation. Their investigation demonstrated that a balance between dispersive and nonlinear factors controls the evolution of the wave over time.However, they were unable to solve the equation in a general way.Their work was largely forgotten until 1965.

In 1955, Enrico Fermi, John Pasta and Stanislaw Ulam (FPU) conducted a study of energy equipartition in a weakly nonlinear mechanical system using the Los Alamos MANIAC computer. They hypothesised that, due to the weak nonlinearity of the system, energy added to one mode would gradually be redistributed to all modes. However, the energy occasionally returned to the first mode excited, which was an unexpected result. In 1965,

Norman Zabusky and Martin Kruskal approximated the FPU system in the continuum limit using the Korteweg-de Vries (KdV) equation in order to seek an explanation for this unexpected behaviour. Using numerical simulations, they found that individual waves in the system can pass through each other without changing their speed or shape, and exhibit only a slight phase shift after collisions. To emphasise the particle-like properties of these waves, Zabusky and Kruskal introduced the term "soliton" to describe them [43].

In 1967, Clifford Gardner, John Greene, Martin Kruskal and Robert Miura proposed a novel approach to the Korteweg-de Vries (KdV) problem (Gardner et al., 1967) that facilitated the discovery of exact solutions, including solitons. This method, which was subsequently termed the Inverse Scattering Method (ISM), proved to be effective. It was later discovered that the ISM is more general and can be applied to derive exact soliton solutions in many other integrable nonlinear systems (Zakharov, 1972). The ISM was extended by Alexei Borisovich Shabat and Vladimir Zakharov in 1972 to solve the Nonlinear Schrödinger Equation (NLSE). They proved the existence of soliton solutions and the integrability of the problem (Zakharov, 1972). Since then, the NLSE has become a key model in many fields, including Bose-Einstein condensates, plasma waves, nonlinear optics, hydrodynamics and nonlinear acoustics [43].

The concept of solitons manifesting in optical fibres, a phenomenon attributable to a harmonious equilibrium between anomalous dispersion and self-phase modulation, was initially postulated by Akira Hasegawa in 1973. Leveraging the Raman effect to engender optical gain within the fibre, Linn Mollenauer and his associates accomplished the transmission of soliton pulses over a span of 4,000 kilometres in 1988.

1.3.2 Different Types of Solitons

It is possible to classify solitons into several distinct categories based on their shape and properties in nonlinear systems.

1.3.2.1 Bright Solitons

Bright solitons are localised peaks that emerge in media with focusing nonlinearity. It has been demonstrated that these solitons are capable of preserving their shape and amplitude during propagation and subsequent interactions with other solitons. The existence of bright

Figure 1.1: Recreating Russells soliton in canal . (Photography Cliris Eilbeck and Heriot-Watt University. 1995 [43].

solitons has been observed in a variety of settings, including optical fibres, water waves, and Bose-Einstein condensates [44, 45, 46].

1.3.2.2 Dark Solitons

Dark solitons are defined as localized dips or notches in a continuous background wave. These phenomena manifest in media characterised by defocusing nonlinearity, exhibiting a phase jump across the notch. The subject of dark solitons has been the focus of extensive research in the fields of nonlinear optics and atomic systems [47, 48].

1.3.2.3 Breathers and Kinks

Breathers are defined as localised oscillatory wave packets that periodically exchange energy, while kinks represent transitions between different stable states of a system. These soliton types are of significance in a variety of physical models, including optical systems, condensed matter, and field theory [49].

These distinct soliton types offer insight into the intricate dynamics of nonlinear systems and are of central importance to contemporary research in integrable equations. The employment of analytical methodologies, including the Lax pair and Darboux transformation, facilitates the construction of explicit solutions for these solitons.

1.4 Breathers

In recent decades, the field of breathwork has attracted significant interest. The concept of a breather, alternatively referred to as the N-Soliton solution, can be conceptualised as a superposition of N distinct solitons with a coinciding centre. In essence, a breather can be defined as a spatially localized solution that exhibits a temporally periodic structure, a characteristic that distinguishes it as a Ma Breather. Alternatively, it can be understood as a spatially periodic structure, a property that identifies it as an Akhmediev breather. These breathers are of critical importance for the study of localised-type phenomena, which are prevalent in condensed matter physics, biophysics and optics. As a case in point, solitons in nematic liquid crystals â otherwise known as 'nematicons' â exhibit a propensity to undergo breathing phenomena when the parameters of the solution deviate from the ideal, shape-invariance of the nematicon [50]. In contradistinction to solitons, which traverse considerable distances without undergoing amplitude attenuation or shape change [51], breathers appear to be bound states and internal oscillations of nonlinear wave packets [52]. The regulation of breathers in an optical fibre is feasible even when the average dispersion falls within the typical range, as evidenced by analytical and numerical data [53, 54]. It has been demonstrated that strongly birefringent fibres have the capacity to facilitate stable breather propagation [55]. As is evident from the extant literature, discrete breathers have been employed in a number of fields. These include Bose-Einstein condensates (BECs) [56], photonic-crystal waveguides [57], macroscopic-mechanical systems [58], and low-dimensional materials [59]. For the extended Korteweg-de Vries (KdV) equation [60], Gardner's equation [61], the modified KdV equation [62], and the NLS equation [63], breather solutions have been obtained.

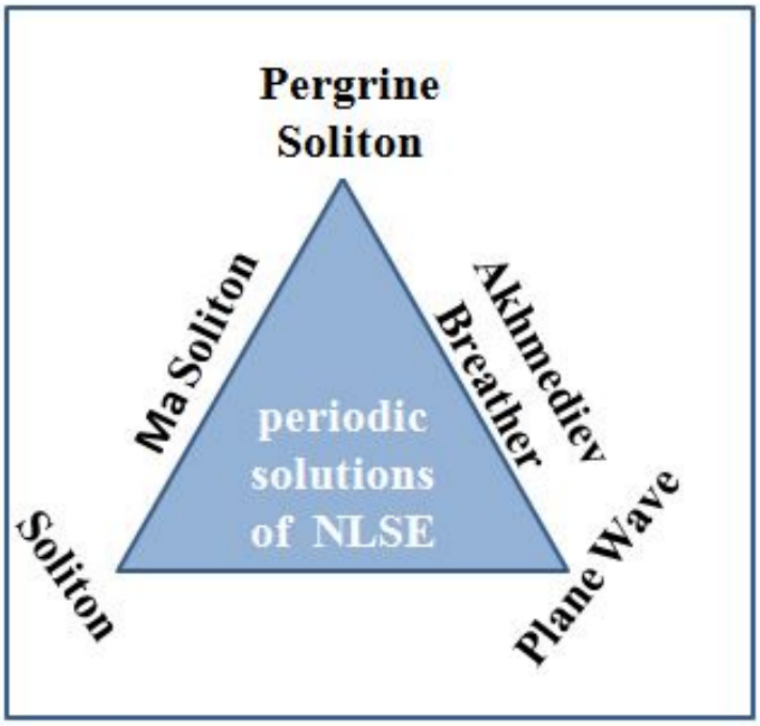

Figure 1.2: Diagram of periodic solutions of the NLSE

1.4.1 Different types of Breathers

1.4.1.1 Ma Breather

The first family of breathers, otherwise referred to as breathing solitons, can be considered a solution to this issue. The initial discovery was made in 1977 by Kusnetsov[64]. This was followed by further research by Kawata and Inoue [65]. In 1979, MA provided a comprehensive description of it. The latter is resolved ESNL by taking into account a slightly perturbed plane wave in relation to the starting state for boundary conditions; it gradually goes to infinity and returns to the initial state. He thereby proved that there is a family of journals. A breather is defined as a single wave in space that is encircled by tiny residual dispersive waves of amplitude. As asserted by [66], these solitons are characterised by continuous oscillation in a background state, characterised by cycles of compression and decompression. These waves are distinguished by their time-periodic nature and localisation in space.

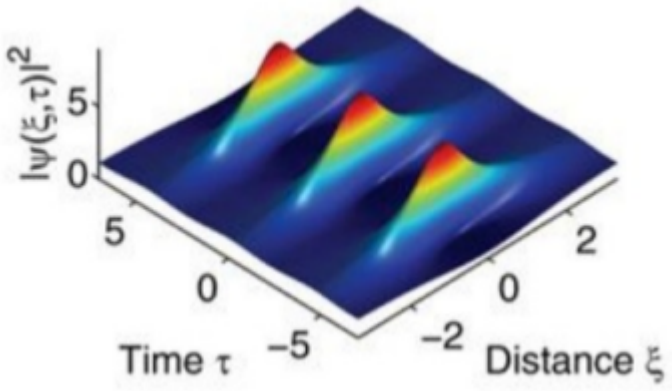

Figure 1.3: Ma Breather

1.4.1.2 Akhmediev Breather

Akhmediev et al [67, 68] identified a distinct family of solutions undergoing a compression-decompression phase that is analogous to that of the Modulation Instability (MI). The authors proposed a methodology for generating a plane wave with a periodic perturbation, with a view to elucidating modulation instability. The boundary condition stipulates that the solution must revert to its initial state as the distance approaches infinity. In contrast to the conventional usage of the term "breather," which evokes continuous oscillatory phenomena, the Akhmediev breather manifests a solitary oscillatory occurrence. Initially, the amplitude of this solution increases, reaching a peak before symmetrically decreasing and eventually diminishing entirely as the distance extends to infinity. This specific structure is now recognised as the Akhmediev breather [64]. These waves are characterised as space-periodic and localised by time.

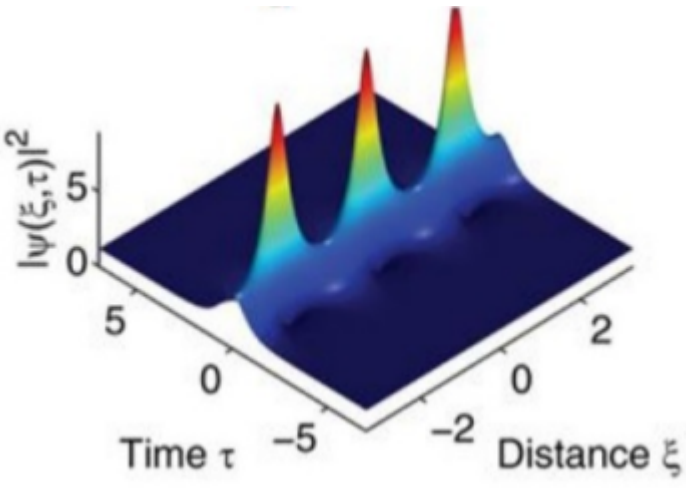

Figure 1.4: Akhmedeiv Breather

1.5 Rogue Waves

Rogue waves (RWs) are a type of wave that lacks a universal definition. However, they do share a fundamental characteristic in that they emerge suddenly and then disappear without a trace. In the field of oceanography, RWs are typically defined by their height. The height of a rogue wave is defined as being at least twice the significant wave height. The significant wave height is defined as the average height of the highest one third of waves over a given time period. The time period is typically 10-30 minutes [69, 70, 71, 72, 73, 74].The term "rogue wave" (or "freak wave") was first introduced to the scientific community by Draper in 1964 [75]. Such undulations are also designated as freak waves, monster waves, killer waves, abnormal waves, steep waves, giant waves, or extreme waves. More recently, the term "rogon" (or "freakon") has been proposed for waves that reappear with little change in size or shape after interactions [76]. The study of rogue waves in optics has been a rapidly expanding field for a period exceeding five years, attracting interest from researchers across a range of disciplines [77]. This field of research emerged following the seminal experiments of Solli et al [78], who analysed super continuum generation in optical fibres. Utilising a pioneering dispersive Fourier transform technique, they detected remarkably high amplitude peaks at specific wavelengths within chaotic spectra. In accordance with the analogy established with extreme ocean waves [79], these optical pulses were designated "optical rogue waves". This correlation between localised optical structures and extreme ocean waves has engendered novel opportunities for the study of extreme value dynamics through the utilisation of controlled laboratory experiments. In addition to the references cited in the seminal work of Key et al [78], recent research has investigated the interconnections between rogue waves and nonlinear breather propagation. A concerted global effort to investigate these extreme optical events is now underway, driven by both their fundamental interest and their potential to offer insights into large-amplitude ocean waves [80]. The concept of rogue waves has since been applied in various scientific domains [77]. It is submitted that small-scale experimental studies may provide a more profound understanding of rogue waves in the ocean, given that similar mathematical models describe these phenomena across different fields. However, it is important to note that certain laboratory-generated waves also introduce unique research directions, distinct from oceanic wave studies. The Peregrine soliton is a particularly pertinent structure. It was first described by D. H. Peregrine in 1983 while he was studying hydrodynamics at the University of Bristol [81]. In contradistinction to fundamental solitons, which are characterised

by their ability to preserve their shape during propagation, the Peregrine soliton manifests double localization in both time and space.

The Peregrine soliton is characterised by a small perturbation on a continuous background, which gradually increases in amplitude while shortening in duration. At its point of maximum compression, the amplitude of the Peregrine soliton reaches three times that of the surrounding background (or nine times higher in intensity, as typically measured in optics). After reaching this peak, the soliton expands and fades away. This behaviour closely matches the characteristics often used to define rogue waves, making the Peregrine soliton a compelling theoretical explanation for their formation. Mathematically, the Peregrine soliton can be regarded as the limiting case of the spatially periodic Akhmediev breather when the period approaches infinity. Similarly, it can also be seen as the limiting case of the temporally periodic Kuznetsov-Ma breather under the same conditions.

Figure 1.5: A Rogue Wave is a short-lived large-amplitude [82, 83]

1.6 Advanced Wave Structures and Mixed States

1.6.1 Multi-Akhmediev Breathers

The historical trajectory of breather solutions reached a significant milestone with the development of higher-order solutions. Subsequent to the seminal work of Akhmediev [84], researchers employed the Darboux transformation to derive multi-breather solutions. The Multi-Akhmediev Breathers (MAB) are a representation of the nonlinear superposition of multiple unstable modes. Historically, these solutions provided the first mathematical

framework for "super rogue waves," where the peak amplitude significantly exceeds the standard amplification factor of three [85].

1.6.2 Mixed Dark-Akhmediev Interactions

Although solitons are often studied in isolation, physical systems frequently exhibit mixed states. The interaction between dark solitons and Ahmediev breathers has become a focal point in the study of multi-component systems [36].

1.7 Numerical Methodology and Stability Framework

The transition from analytical theories to numerical validation represents a significant milestone in the study of nonlinear wave phenomena. While exact solutions provide the theoretical foundation, numerical simulations allow for the exploration of wave stability under real-world conditions, such as noise and structural perturbations.

1.7.1 Modulation Instability and G_{max} Dynamics

The initial phase of the stability assessment focuses on modulation instability (MI), which represents a specific form of linear spectral stability of a continuous-wave (CW) solution. The analysis is carried out by introducing a small random perturbation, denoted by ϵ, to the initial condition. This procedure has its origins in the seminal work of Benjamin and Feir [86], in which it was demonstrated that continuous wave trains are inherently unstable in the presence of infinitesimal fluctuations. In this framework, the maximum gain (G_{max}) is monitored as a primary evolutionary metric. Historically, the maximum group speed, G_{max}, has been utilised to quantify the intensity of rogue wave events by comparing peak amplitudes to the initial background[85, 84]. The growth rate within this MI regime is fundamentally determined by the eigenvalue, λ.

Numerical Integration via SSFM and L_2 Validation

Following the physical assessment of growth, the temporal evolution is computed using the split-step Fourier method (SSFM). In order to guarantee the reliability of the numerical evolution and to verify that the emergent wave structures are not numerical artefacts, the L_2 error norm is employed. The adoption of this norm as a benchmark for numerical fidelity

became standard following the development of the SSFM by Taha and Ablowitz [18]. The relative L_2 error norm is employed to furnish a standardised measure of the discrepancy between the perturbed numerical solution, denoted by $\Psi_{\text{perturbed}}(x,t)$, and the analytical solution, denoted by $\Psi_{\text{analytical}}(x,t)$:

$$L_2(t) = \frac{\|\Psi_{\text{perturbed}}(x,t) - \Psi_{\text{analytical}}(x,t)\|_2}{\|\Psi_{\text{analytical}}(x,t)\|_2} = \frac{\sqrt{\int_{-\infty}^{+\infty} \left|\Psi_{\text{perturbed}}(x,t) - \Psi_{\text{analytical}}(x,t)\right|^2 dx}}{\sqrt{\int_{-\infty}^{+\infty} \left|\Psi_{\text{analytical}}(x,t)\right|^2 dx}}$$

In this context, the L_2 norm functions as a **Fidelity Monitor** or a **Quality Check**. It measures the degree to which the numerical computation drifts away from the underlying physics. In contrast to absolute error measures, the relative L_2 norm provides an assessment that is amplitude-independent. For the nonlinear Schrödinger equation (NLSE), it serves as a proxy for the system's fundamental conservation laws. Following the seminal contributions of Zakharov and Shabat [37], it has been established that any substantial augmentation in the L_2 error norm indicates a contravention of mass or power conservation, typically attributed to numerical dissipation or artificial dispersion [87].

1.7.2 Center of Mass (x_{cm})

To track the spatial localization and trajectory of the pulse, the center of mass (x_{cm}) is defined. This metric, adapted from classical particle dynamics into soliton theory [88], is given by:

$$x_{cm} = \frac{\int_{-\infty}^{+\infty} x|\phi(x,t)|^2 dx}{\int_{-\infty}^{+\infty} |\phi(x,t)|^2 dx} \tag{1.5}$$

In this expression:

- $|\phi(x,t)|^2$ represents the **local intensity** (or probability density), indicating where the wave's energy is concentrated at time t.
- The denominator $\int_{-\infty}^{+\infty} |\phi|^2 dx$ corresponds to the **total energy** (or mass) of the solution, which is a conserved quantity for these breathers.
- The numerator $\int_{-\infty}^{+\infty} x|\phi|^2 dx$ is the **first-order moment**, calculating the average position weighted by the intensity.

This calculation is vital for observing how perturbations, denoted by the parameter ϵ, or

interactions in mixed states induce a spatial shift in the wave's path. This provides a quantitative measure of the soliton's particle-like behavior under external influence. Specifically, the mathematical framework for such mixed-coupled nonlinear Schrödinger solutions, which allow for the coexistence of diverse localized structures, was rigorously established by Baronio et al [36].

Chapter 2

The Methods: Darboux Transformation and Lax Pair

2.1 Introduction

A significant domain of research in nonlinear science pertains to the analysis of integrable nonlinear partial differential equations (PDEs) and their exact solutions, including solitons and breathers. These nonlinear wave structures emerge in a diverse array of physical systems, encompassing shallow water waves, plasma physics, and optical fibre communications [7, 46]. The construction of explicit solutions to such equations is essential for understanding the underlying physical mechanisms and has therefore attracted considerable interest from both mathematicians and physicists [19].

Nonlinear partial differential equations are challenging to solve exactly. In general, explicit analytical solutions are only available for a restricted class of such equations. Among these, integrable systems occupy a distinguished position due to their rich mathematical structure and physical relevance. A fundamental feature of integrable systems is the existence of a Lax pair, which provides a linear representation of the nonlinear equation through a compatibility condition [89].

The Lax Pair consists of two linear operators, L (which represents the physical state of the wave) and P (which represents the time-evolution of that wave), which are linked by the compatibility condition $\frac{dL}{dt} = [P, L]$ to prove that a complex nonlinear PDE (like the NLS equation)[40] is actually just a simpler system where the essential properties of the wave remain constant over time. This formulation reveals the integrable nature of the system,

facilitates the identification of conserved quantities, and provides a robust framework for the analysis of nonlinear evolution equations.

Once a Lax pair has been established, powerful solution-generating techniques can be employed. It is evident that the Darboux transformation occupies a pivotal position within this context. The method was originally introduced by G. Darboux in the context of linear differential equations [34]. This approach was later extended by V. B. Matveev and others to integrable nonlinear partial differential equations [90]. The Darboux transformation acts directly on the linear system associated with the Lax pair, thereby enabling the systematic construction of new solutions from known ones.

The Darboux transformation has been shown to offer an efficient and local procedure for generating exact solutions, including solitons, breathers and higher-order solutions [91]. This is in contrast to methods that require solving integral equations. The efficacy of the model has been demonstrated in a number of significant integrable models, including the Kortewegâde Vries equation, the sine-Gordon equation, and the nonlinear Schrödinger equation.

In this study, we apply the Lax pair formulation and the Darboux transformation to two specific integrable models: the Hirota equation and the Sasa–Satsuma equation. For each equation, we construct the corresponding Lax pair, implement the Darboux transformation, and obtain explicit analytical solutions, including soliton and breather waves. These applications illustrate the practical utility of the methods and demonstrate their power in analysing the dynamics of nonlinear waves in integrable systems. Thus, this chapter provides the theoretical foundation for the methods used to derive exact solutions, which are presented and analysed in detail in the subsequent sections.

$\mathrm{U}_{0t} - V_{0x} + [U_0, V_0] = 0$

2.2 Lax Pair Method

In the Lax pair method for solving nonlinear partial differential equations (PDEs), the primary step is to construct a pair of 2×2 matrices, U and V. These matrices define a linear system of equations for an auxiliary matrix field $\mathbf{\Phi}(x, t)$, given by:

$$\mathbf{\Phi}_x = U\mathbf{\Phi}, \quad \mathbf{\Phi}_t = V\mathbf{\Phi} \tag{2.1}$$

The compatibility condition of this system, $\mathbf{\Phi}_{xt} = \mathbf{\Phi}_{tx}$, leads to the **Zero-Curvature Condition**:

$$U_t - V_x + [U, V] = 0 \tag{2.2}$$

where $[U, V] = UV - VU$ is the matrix commutator. It is imperative that this matrix equation be identical to the target nonlinear PDE.

2.2.1 Mathematical Definitions

To clarify the nature of the variables involved:

- **The Scalar Field:** $Q(x, t)$ is the complex scalar function representing the physical solution to the PDE $F[Q, Q^*, \dots] = 0$.
- **The Auxiliary Field (Fundamental Matrix):** The symbol $\mathbf{\Phi}$ represents the fundamental solution matrix. It is composed of linearly independent solution vectors:

  $$\mathbf{\Phi}(x, t) = \begin{pmatrix} \psi_1(x, t) & \psi_2(x, t) \\ \phi_1(x, t) & \phi_2(x, t) \end{pmatrix}$$

  Each column of this matrix satisfies the linear system (2.1). The components ψ_i and ϕ_i act as auxiliary spectral variables that encode the evolution of the nonlinear field $Q(x, t)$.
- **The Lax Pair:** U and V are 2×2 matrices whose entries are functionals of Q, Q^*, and their derivatives.
- **The Spectral Parameter:** $\mathbf{\Lambda}$ is a constant diagonal matrix, typically defined as $\mathbf{\Lambda} = \text{diag}(\lambda, -\lambda)$ or:

  $$\mathbf{\Lambda} = \begin{pmatrix} \lambda_1 & 0 \\ 0 & \lambda_2 \end{pmatrix}$$

2.2.2 Expansion and Derivation

We expand the Lax operators in powers of the spectral parameter $\mathbf{\Lambda}$:

$$\mathbf{\Phi}_x = (U_0 + U_1\mathbf{\Lambda})\mathbf{\Phi} \tag{2.3}$$

$$\mathbf{\Phi}_t = (V_0 + V_1\mathbf{\Lambda} + V_2\mathbf{\Lambda}^2 + V_3\mathbf{\Lambda}^3)\mathbf{\Phi} \tag{2.4}$$

The expansion order of the temporal part $\mathbf{\Phi}_t$ is governed by the highest-order spatial derivative in the governing equation. For higher-order nonlinear Schrödinger (HNLS) systems, such as the Hirota or Sasa–Satsuma equations, a third-order expansion in $\mathbf{\Lambda}$ is necessary to account for third-order dispersive effects. By imposing the equality of mixed partial derivatives $\mathbf{\Phi}_{xt} = \mathbf{\Phi}_{tx}$ and equating the coefficients of $\mathbf{\Lambda}^k$, we obtain a hierarchy of consistency equations. The target nonlinear PDE is embedded within the $\mathbf{\Lambda}^0$ term:

$$U_{0t} - V_{0x} + [U_0, V_0] = \begin{pmatrix} 0 & F \\ -F^* & 0 \end{pmatrix} \tag{2.5}$$

The system is integrable if $F = 0$ satisfies the remaining higher-order matrix relations.

2.3 Darboux Transformation

The Darboux transformation (DT) is an algebraic "dressing" method used to generate a new solution $Q[1]$ from a known *seed solution* Q_0. Consider the following formulation:

$$\mathbf{\Phi}[1] = (\mathbf{\Lambda} - \sigma)\mathbf{\Phi} \tag{2.6}$$

where $\mathbf{\Phi}[1]$ is the transformed auxiliary field. The transformation matrix σ is constructed as $\sigma = \mathbf{\Phi}_0\mathbf{\Lambda}\mathbf{\Phi}_0^{-1}$, where $\mathbf{\Phi}_0$ is the fundamental solution of the linear system (2.3)–(2.4) evaluated at the seed solution Q_0. To ensure the new field $\mathbf{\Phi}[1]$ satisfies a linear system of the same form (covariance), the new Lax operator $U[1]$ must satisfy:

$$U_0[1] = U_0 + [U_1, \sigma] \tag{2.7}$$

Conceptual Clarification of the Transformation Law: The right-hand side of Equation (2.7) functions as a mathematical recipe:

- U_0, U_1**:** The original Lax matrices built from the simple **seed solution** (e.g., $Q_0 = 0$).

- σ**:** The "dressing" matrix that carries information about the eigenvalues and the auxiliary field Φ_0.

The transformation of the spatial Lax operator involves two physical contributions:

- **The Similarity Transformation:** Maps the background spectral data of the seed solution.
- **The Gauge Connection:** Responsible for the deformation of the potential, creating the localized "peaks" of the soliton solution in the 3D intensity profile.

In summary, the Darboux transformation establishes a direct algebraic link between a simple seed solution Q_0 and a complex solution $Q[1]$. In the following chapter, this method will be applied to solve the **Hirota** equation.

2.4 Aplication of Analytical solutions

2.4.1 The Hirota Equation with Time-Dependent Coefficients

In this study, we consider the generalized Hirota equation [92] where the physical parameters are non-static. Specifically, all coefficients are expressed as functions of time, $a_i = a_i(t)$, reflecting a system with varying dispersion and nonlinearity. The equation is given by:

$$i\psi_t + a_1(t)\psi_{xx} + a_2(t)|\psi|^2\psi + ia_3(t)\psi_{xxx} + ia_4(t)|\psi|^2\psi_x + i\Gamma(t)\psi + V_{ext}(x,t)\psi = 0 \quad (2.8)$$

Physical Significance of the Terms

The dynamics of the field $\psi(x,t)$ are governed by the following physical effects:

- **Group Velocity Dispersion (GVD):** Represented by $a_1(t)$, this term accounts for the chromatic dispersion of the wave pulse.
- **Kerr Nonlinearity:** Represented by $a_2(t)$, this term describes the self-phase modulation arising from the intensity-dependent refractive index.
- **Third-Order Dispersion (TOD):** Represented by $a_3(t)$, this higher-order term becomes significant for ultra-short pulses.

- **Dissipation and Potential:** The real-valued functions $\Gamma(t)$ and $V_{ext}(x,t)$ account for the system's gain/damping and the influence of an external spatial potential, respectively.

Transition to 3×3 Lax Representation

While a standard 2×2 Lax pair is sufficient for the basic Nonlinear Schrödinger equation, the inclusion of higher-order dispersion $a_3(t)$ and nonlinear gradients $a_4(t)$ introduces additional complexity.During the derivation of the integrability conditions, it becomes evident that the 2×2 matrices U_0 and V_0 cannot satisfy the zero-curvature condition for all time-dependent parameters simultaneously. Consequently, the utilization of 3×3 matrices is essential. This expanded dimensionality provides the necessary degrees of freedom to maintain the covariance of the system and to rigorously apply the Darboux transformation method to find exact soliton solutions.

2.4.2 Lax pair

To establish the integrability of the higher-order Hirota equation with time-dependent coefficients, we construct the associated Lax pair $(\mathbf{U}, \mathbf{V})$. The spatial evolution of the auxiliary field is governed by the operator $\mathbf{U} = \mathbf{U}_0 + \mathbf{\Lambda U}_1$, where the matrices are defined as:

$$\mathbf{U_0} = \begin{pmatrix} C_1 & -ic_2(t)\ exp[G(x,t)]\ \psi_0(x,t) \\ c_2(t)\ exp[G(x,t)]\ \psi_0^*(x,t) & C_1 \end{pmatrix} \tag{2.9}$$

$$\mathbf{U_1} = \begin{pmatrix} -\sqrt{6}\ c_{315} + cf_{411}(x,t) & 0 \\ 0 & cf_{411}(x,t) \end{pmatrix} \tag{2.10}$$

and

$$\mathbf{V_0} = \begin{pmatrix} Y(x,t) & L(x,t) \\ \\ k(x,t) & P(x,t) \end{pmatrix} \tag{2.11}$$

$$\mathbf{V_1} = \begin{pmatrix} \mathrm{c}g_{411}(x,t) + \dfrac{1}{\sqrt{6}}\, c_{315}\, a_4(t)\, \psi_0(x,t)\, \psi_0^*(x,t) & Z(x,t) \\ \\ Z(x,t)^* & T(x,t) \end{pmatrix} \tag{2.12}$$

$$\mathbf{V_2} = \begin{pmatrix} cg_{21}(t) & -\sqrt{\dfrac{6\, a_4(t)}{a_3(t)}}\, c_{315}^2\, a_3(t)\, \psi_0(x,t) \\ \\ \sqrt{\dfrac{6\ a_4(t)}{a_3(t)}}\ c_{315}^2\, a_3(t)\, \psi_0^*(x,t) & -6\, i\, c_{315}^2\, a_1(t) + cg_{21}(t) \end{pmatrix} \tag{2.13}$$

$$\mathbf{V_3} = \begin{pmatrix} 6\,\sqrt{6}\, c_{315}^3\, a_3(t) + cg_{219}(t) & 0 \\ 0 & cg_{219}(t) \end{pmatrix} \tag{2.14}$$

"The detailed components of the 3×3 Lax matrices and the full algebraic expansions are provided in Appendix A for brevity."

2.4.3 Derivation and Structure of the Lax Operators

The determination of the Lax operators U and V is rooted in the **consistency condition** (or zero-curvature condition) of the linear system. To ensure that the auxiliary system is integrable and corresponds exactly to the higher-order nonlinear Schrödinger (HNLS) equation, the following mathematical framework is employed:

1. **The Compatibility Condition:** For the linear system to be consistent, the mixed partial derivatives of the auxiliary function ϕ must commute, such that $\phi_{xt} = \phi_{tx}$. This requirement leads to the **zero-curvature equation**:

$$U_t - V_x + [U, V] = 0, \tag{2.15}$$

where $[U, V] = UV - VU$ denotes the commutator. Solving this equation allows us to *find* the required functional forms of the operators and their internal functions.

2. **Functional Terms (e.g., $G(x,t)$):** The specific functions within the operators are not arbitrary. Their structures are strictly defined by the consistency condition as functions of the field $\phi(x,t)$ and its spatial derivatives. These terms are essential for maintaining the integrability of the model; if these functions were modified randomly, the zero-curvature equation would no longer vanish, and the Darboux transformation would fail.

3. **Free Parameters and Constants (e.g., C_1, λ):** While the functional *form* is fixed by the zero-curvature condition, the operators contain integration constants and the spectral parameter λ. These represent the degrees of freedom in the solution. Once the operators are derived, we can **assign any specific value** to these constants to investigate different physical regimes, such as adjusting the soliton velocity, the background intensity, or the phase shift during interaction.

This distinction is fundamental: the consistency condition *finds* the necessary mathematical structure, while the choice of parameter values *defines* the specific physical characteristics of the resulting breather or soliton solutions.

2.4.4 Linear Evolution of the Auxiliary Field

The auxiliary field (or wave function) $\psi(x,t)$ is represented as a matrix of basis solutions. For the system under consideration, the field is defined as

$$\psi(x,t) = \begin{pmatrix} \psi_1(x,t) & \psi_2(x,t) \\ \phi_1(x,t) & \phi_2(x,t) \end{pmatrix}. \tag{2.16}$$

The dynamics of this field are governed by a linear system of equations associated with a Lax pair formulation. These equations are expressed in terms of a constant spectral matrix $\mathbf{\Lambda}$, defined as

$$\mathbf{\Lambda} = \begin{pmatrix} \lambda_1 & 0 \\ 0 & \lambda_2 \end{pmatrix}. \tag{2.17}$$

The spatial and temporal evolutions of the auxiliary field are given by

$$D[\psi, x] = \partial_x \psi = \mathbf{U}_0 \psi + \mathbf{U}_1 \psi \mathbf{\Lambda}, \tag{2.18}$$

$$D[\psi, t] = \partial_t \psi = \mathbf{V}_0 \psi + \mathbf{V}_1 \psi \mathbf{\Lambda} + \mathbf{V}_2 \psi \mathbf{\Lambda}^2 + \mathbf{V}_3 \psi \mathbf{\Lambda}^3. \tag{2.19}$$

To verify the consistency of these relations, we define the residual expressions

$$eq_x = \partial_x \psi - (\mathbf{U}_0 + \mathbf{U}_1 \mathbf{\Lambda})\, \psi = D[\psi, x] - \psi_x = 0, \tag{2.20}$$

$$eq_t = \partial_t \psi - \left(\mathbf{V}_0 + \mathbf{V}_1 \mathbf{\Lambda} + \mathbf{V}_2 \mathbf{\Lambda}^2 + \mathbf{V}_3 \mathbf{\Lambda}^3\right) \psi = D[\psi, t] - \psi_t = 0. \tag{2.21}$$

Where D the differential operator ∂_x or ∂_t. Imposing the conditions $eq_x = 0$ and $eq_t = 0$ ensures that the auxiliary field satisfies the associated linear spectral problem. The compatibility condition between these equations yields the zero-curvature condition

$$\partial_t \mathbf{U} - \partial_x \mathbf{V} + [\mathbf{U}, \mathbf{V}] = 0,$$

which constitutes the necessary and sufficient condition for the integrability of the Hirota equation.

2.4.4.1 Solitonic solution

In this case we consider the hirota equation in presence of damping or gain,the equation can be written as :

$$\begin{aligned} i\psi_t(x,t) + a_1(t)\psi_{xx}(x,t) + a_2(t)|\psi(x,t)|^2\psi(x,t) + ia_3(t)\ \psi_{xxx}(x,t) + ia_4(t)|\psi(x,t)|^2\psi_x(x,t) \\ + i\Gamma(t)\psi(x,t) + V_{ext}(t)\psi(x,t) = 0 \end{aligned} \tag{2.22}$$

Where the equation is integrable only if $V_{ext} = 0$, $\Gamma(t) = \frac{a_{4t}(t)}{2a_4(t)} - \frac{a_{3t}(t)}{2a_3(t)}$ and $a_4(t) = \frac{2a_2(t)a_3(t)}{a_1(t)}$

$a_{it}(t) = \frac{da_i(t)}{dt}, \quad (i = 3, 4)$

To construct explicit solutions via the Darboux transformation, we consider the trivial (zero) seed solution defined by

$$\psi_0(x,t) = 0. \tag{2.23}$$

This choice satisfies the Hirota equation identically and represents the simplest possible background. The use of the zero seed significantly simplifies the associated linear spectral problem and allows the construction of fundamental localized solutions. The selection of the seed solution follows standard criteria: (i) The seed must be an exact solution of the governing equation. (ii) It should simplify the Lax pair structure and the spectral problem. (iii) It serves as a reference state from which more complex solutions are generated through the Darboux transformation. In this case, the zero background leads naturally to the construction of bright soliton-type solutions. The detailed components of the full algebraic expansions are provided in Appendix A for brevity.
The Hirota equation admits the soliton solution:

$$\psi(x,t) = \frac{A(t)}{2\cosh\left(\sqrt{6}\,x - b(t)\right)} \exp\left[6i \int a_1(t)\,dt\right]. \tag{2.24}$$

where

$$A(t) = -12\sqrt{\frac{a_3(t)}{a_4(t)}}, \tag{2.25}$$

$$b(t) = 6\sqrt{6} \int a_3(t)\,dt. \tag{2.26}$$

Figure 2.1 illustrates the dynamical evolution of the squared modulus $|\psi(x,t)|^2$ for the Hirota equation under the autonomous regime. The consistent behavior observed across the three panels the linear trajectory in the contour plot (a), the invariant localized peak in the three dimensional evolution (b), and the symmetric high intensity profile in the two dimensional cross section (c) demonstrates that the derived solution corresponds to a stable, non dispersive bright soliton. From a physical perspective, this stability indicates that the third-order dispersion and nonlinear effects are exactly balanced by the lower-order contributions within the Hirota framework. From a mathematical viewpoint, these results confirm the effectiveness of the 3×3 Darboux transformation in constructing exact analytical solutions. This stable configuration provides a fundamental reference case for investigating

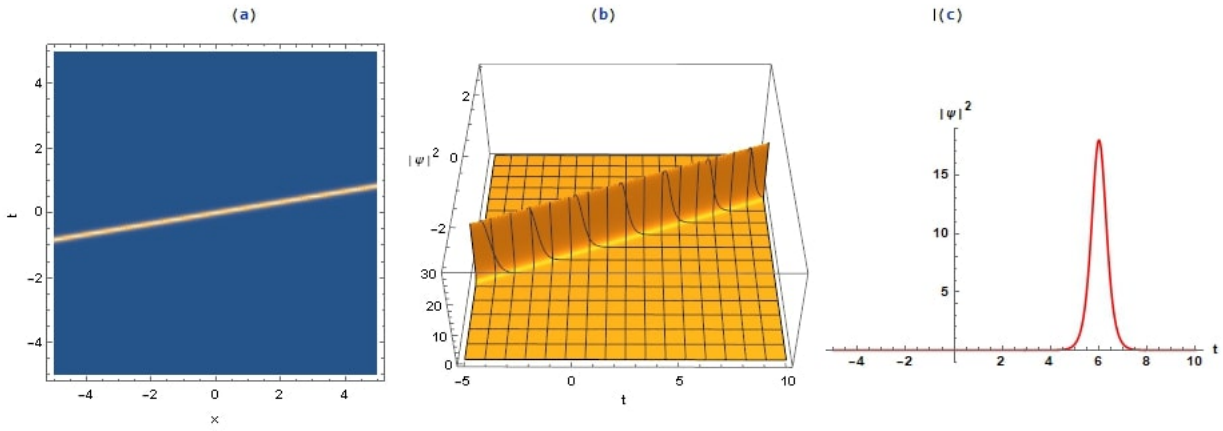

Figure 2.1: Spatiotemporal evolution of the soliton solution $|\psi|^2$ for the Hirota Equation (HE) with parameters $a_1(t) = 1, a_3(t) = 1, a_4(t) = 2$. (a) Contour plot, (b) 3D evolution, and (c) temporal profile of the solution.

more complex pulse dynamics arising from time-dependent coefficients $a_i(t)$ and external potentials.

2.4.4.2 Breather solution

First case: In this case : damping $\Gamma = 0$, potential $V_{ext} = 0$, $a_4(t) = -a_3(t)$,$a_2(t) = -\frac{a_3(t)}{2}$ and, $a_1(t) = \frac{6\ (a_3(t)^2\ a_4(t) - a_3(t)\ a_4(t)^2) + 3\ i\ (a_4(t)\ a_{3t}(t) - a_3(t)\ a_{4t}(t))}{2\ a_4(t)\ (3\ a_3(t) - a_4(t))}$ Substituting these conditions integrable into equation (2.22), we obtain a new reduced form of the equation, which is simpler and explicitly integrable.

$$i\,\psi_t(x,t) - \frac{a_3(t)}{2}\Big(2i\,|\psi(x,t)|^2\psi_x(x,t) + |\psi(x,t)|^2\psi(x,t) - 3\,\psi_{xx}(x,t) - 2i\,\psi_{xxx}(x,t)\Big) = 0 \tag{2.27}$$

Starting from the plane wave seed solution: $\psi_0(x,t) = \exp(ix)$, the Darboux transformation allows the construction of more complex localized structures. In particular, breather-type solutions can be obtained, which describe localized waves exhibiting periodic oscillations either in time or in space. These solutions represent a modulation of the constant background and are of significant interest in nonlinear wave dynamics.

and After some simplifications using the method discussed before the HE supports breather solution ,one such solutions is given by :

$$\psi(x,t) = -\frac{\exp(\,ix)\,Q(x,t)}{Q_1(x,t)} \tag{2.28}$$

The detailed components of the full algebraic expansions are provided in Appendix A for brevity.

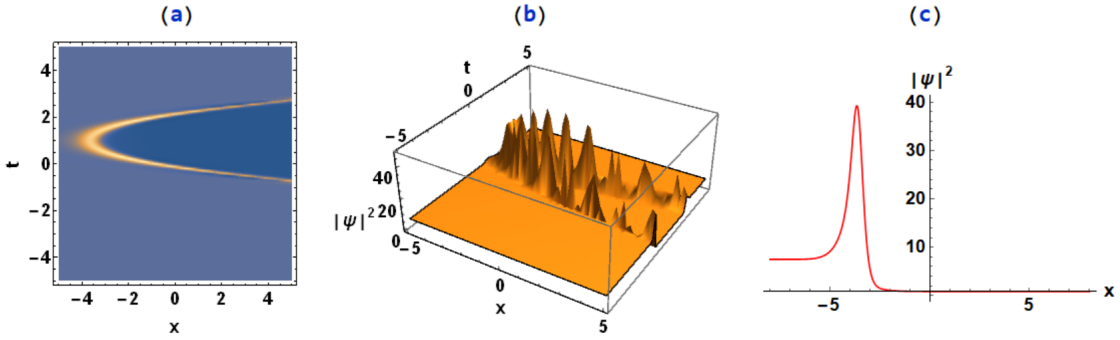

Figure 2.2: **General breather solution** $|\psi|^2$ of the Hirota Equation (HE) with parameters $\lambda_2 = 1, c_{315} = 1, a_3(t) = t - 1$. (a) Contour plot of the solution, (b) 3D evolution of the general breather, and (c) temporal profile of the general breather solution.

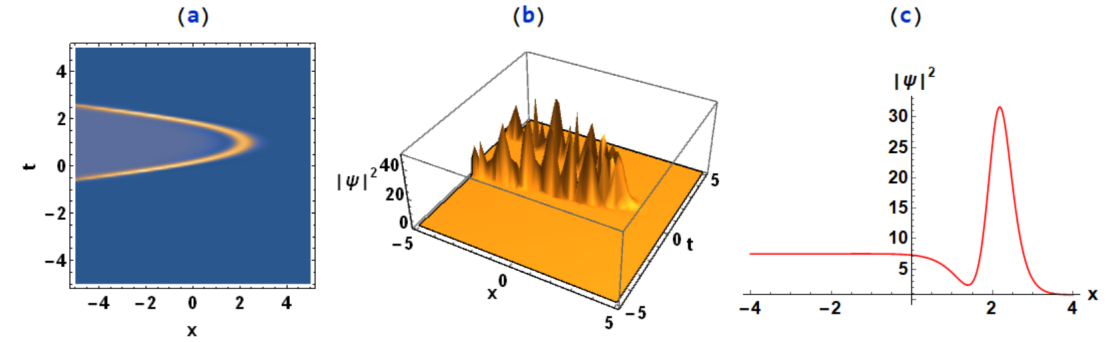

Figure 2.3: **General breather solution** $|\psi|^2$ of the Hirota Equation (HE) with parameters $\lambda_2 = 1, c_{315} = 1, a_3(t) = -t + 1$. (a) Contour plot of the solution, (b) 3D evolution of the general breather, and (c) temporal profile of the general breather solution.

Second case: In this case, we move from the higher order hirota equation or hnls to the standard hirota equation by setting $a_1(t) = 0$ in equation (2.22) :

$$\psi_t(x,t) + a_3(t)\;\psi_{xxx}(x,t) + a_4(t)\;|\psi(x,t)|^2\;\psi_x(x,t) + V_{ext}\;\psi(x,t) = 0 \tag{2.29}$$

We find that the equation is integrable only if $V_{ext} = -\frac{a_{3t}(t)}{2\,a_3(t)} + \frac{a_{4t}(t)}{2\,a_4(t)}$,This relation ensures the necessary balance between dispersion and nonlinearity, permitting the reduction of the system to its standard integrable form and the subsequent derivation of exact multi solutions.

The seed solution is changed according to the type of nonlinear strcteure we aim to generate and to remain compatible with the considered from of equation,we choosing the seed $\psi_0(x,t) = \sqrt{\frac{a_3(t)}{a_4(t)}}\exp(\,ix)$ and

using the same method chapter 2 , the standard Hirota equation supports breather solution , one such solutions is given by :

$$\psi(x,t) = \frac{-(\lambda_1-\lambda_2)\,e^{\frac{1}{6}x(A+3M_2)}\,B(x,t)\,P(x,t) + e^{ix}Y_2(x,t)}{\sqrt{\frac{a_4(t)}{a_3(t)}}\,Y_2(x,t)} \tag{2.30}$$

The detailed components of the full algebraic expansions are provided in Appendix A for brevity.

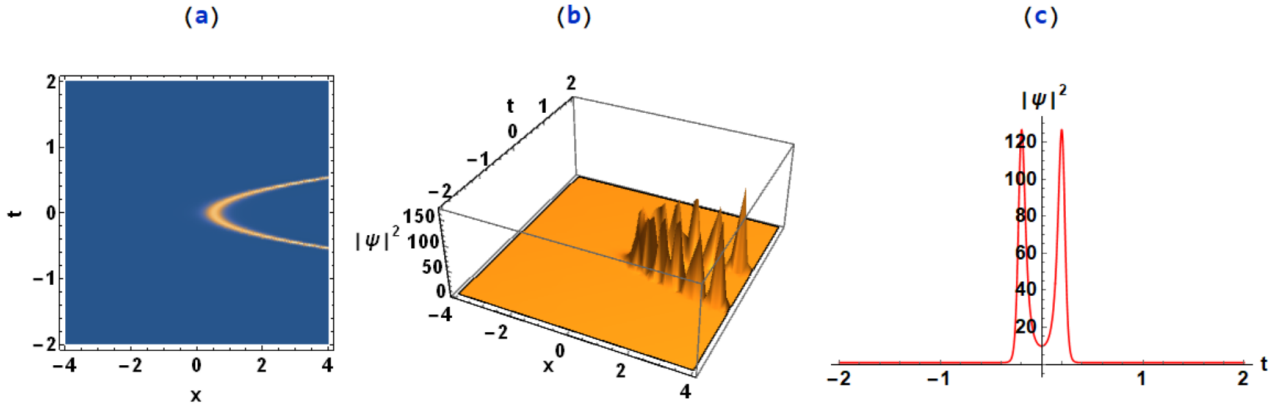

Figure 2.4: **General breather solution** $|\psi|^2$ of the Hirota Equation (HE) with parameters $\lambda_2 = -2, \lambda_1 = 2, c_{315} = 1, a_4(t) = t, a_3(t) = t, c_{111} = c_{222} = 1, cg_{219}(t) = cg_{21}(t) = 1$. (a) Contour plot of the solution, (b) 3D evolution of the general breather, and (c) temporal profile of the general breather solution.

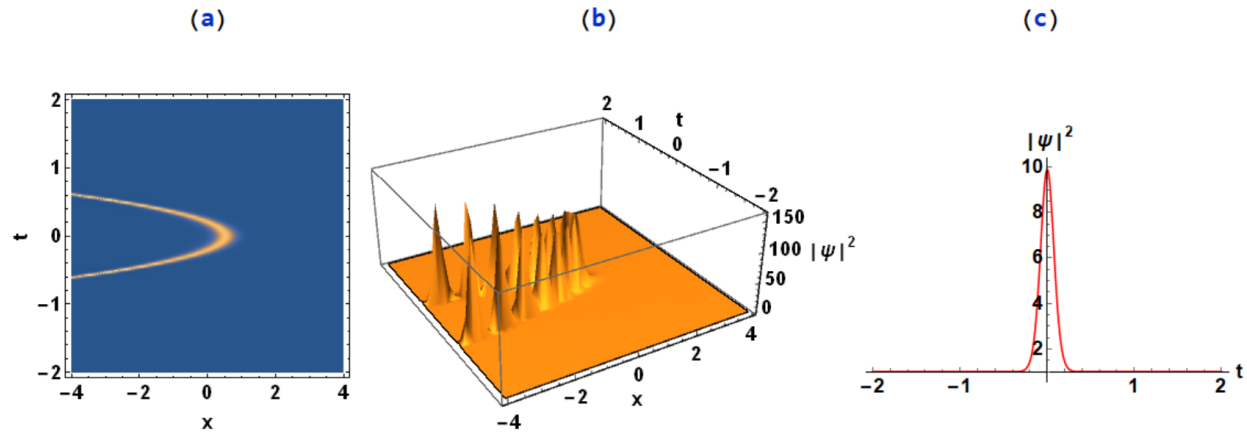

Figure 2.5: **General breather solution** $|\psi|^2$ of the Hirota Equation (HE) with parameters $\lambda_2 = -2, \lambda_1 = 2, c_{315} = 1, a_4(t) = -t, a_3(t) = -t, c_{111} = c_{222} = 1, cg_{219}(t) = cg_{21}(t) = 1$. (a) Contour plot of the solution, (b) 3D evolution of the general breather, and (c) temporal profile of the general breather solution.

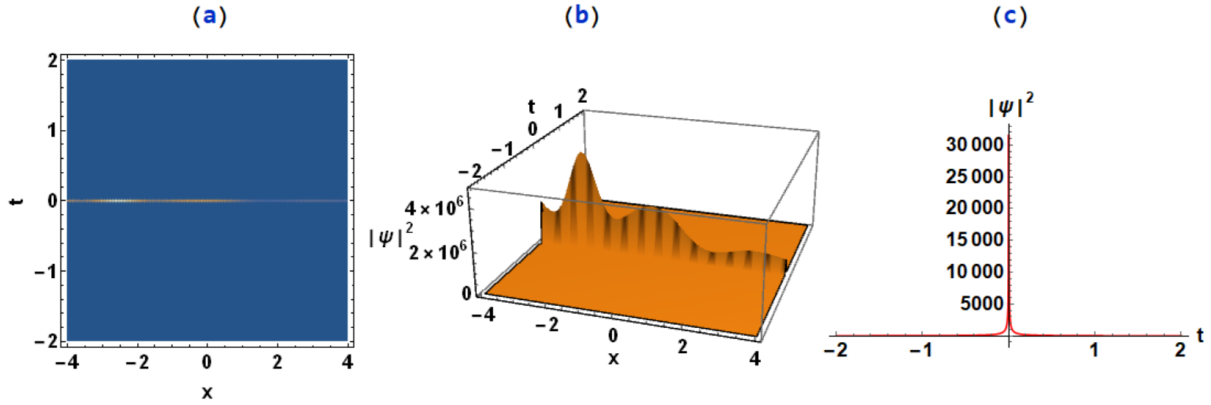

Figure 2.6: **Akhmediev breather solution** $|\psi|^2$ of the Hirota Equation (HE) with parameters $\lambda_2 = -2, \lambda_1 = 2, c_{315} = 1, a_4(t) = t, a_3(t) = 1, c_{111} = c_{222} = 1, cg_{219}(t) = cg_{21}(t) = 1$. (a) Contour plot of the solution, (b) 3D evolution of the Akhmediev breather, and (c) temporal profile of the Akhmediev solution.

2.4.4.3 Conclusions and Outlook

In this work, we have investigated the dynamical behavior of the non-autonomous higher order Hirota equation (HE) within the context of complex physical media. While nonlinear evolutionary equations are fundamental to modeling diverse natural phenomena, the introduction of time-dependent coefficients typically breaks the integrability of the system, leading to soliton decay or radiation.Our analysis rigorously demonstrates that the Hirota equation, when subjected to damping and a linear potential, preserves its integrability only under a specific balancing condition between the third order dispersion $a_3(t)$ and the self-steepening coefficient $a_4(t)$. Physically, this implies that for a stable wave

structure to persist in a non uniform medium, the rate of change of the higher order dispersion must be perfectly compensated by the evolution of the nonlinear self-steepening effect.Key physical insights derived from this study include:Symmetry Induced Stability: The identified integrability condition acts as a "physical tuning" mechanism. It ensures that the external potential effectively cancels the dynamical chirping induced by the time varying medium, maintaining the infinite set of conserved quantities required for soliton existence.Breather Dynamics and Control: We have shown that the transition from a general breather to an Akhmediev breather a localized structure often associated with the precursor to rogue waves is fundamentally governed by the self-steepening coefficient.Passive Motion Control: Most significantly, our results indicate that the center of mass motion of the breather can be precisely controlled by manipulating the third-order dispersion $a_3(t)$. This suggests a method for steering pulses in optical fibers through "dispersion engineering" alone, without the requirement of an external trapping potential.These findings provide a theoretical framework for managing high-power pulse compression and signal routing in advanced nonlinear optical systems, where higher order effects and medium inhomogeneities cannot be neglected.

2.4.5 Sasa-satsuma equation

The transition from the higher-order Hirota equation to the Sasa–Satsuma equation (SSE) is motivated by the fact that the SSE constitutes a specifically constrained manifold where parameters such as a_1 and a_2 are no longer free [93]. This constraint ensures the integrability of the system, enabling a structured analytical study of complex nonlinear wave solutions, including solitons and breathers.Unlike lower-order models, the inclusion of the higher-order terms a_3, a_4, and a_5 necessitates to 3×3 Matrix Formulation rather than a 2×2 one. In this framework, a_3 accounts for third-order dispersion, a_4 represents self-steepening, and a_5 describes the self-frequency shift (Raman effect). This 3×3 representation is essential for capturing the full dynamics of the system while preserving its analytical tractability. The Sasa–Satsuma equation is expressed as:

$$i\psi_t(x,t) + ia_3\psi_{xxx}(x,t) + 3ia_4|\psi(x,t)|^2\psi_x(x,t) + ia_5\ |\psi(x,t)|^2\psi_x^*(x,t) = 0 \tag{2.31}$$

2.4.5.1 Lax pair

To establish the integrability of the higher-order Hirota equation with time-dependent coefficients, we construct the associated Lax pair $(\mathbf{U}, \mathbf{V})$, where the matrices are defined as:

$$\mathbf{U_0} = \begin{pmatrix} 0 & -\frac{ia_5\psi(x,t)}{3a_3} & \frac{ia_5\psi^*(x,t)}{3a_3} \\ -i\psi^*(x,t) & 0 & 0 \\ i\psi(x,t) & 0 & 0 \end{pmatrix}$$

$$\mathbf{V_0} = \begin{bmatrix} 0 & \frac{ia_5}{9a_3}\left(4a_5\psi^2\psi^* + 3a_3\psi_{xx}\right) & -\frac{ia_5}{9a_3}\left(4a_5\psi\psi^{2*} + 3a_3\psi^*_{xx}\right) \\ \frac{i}{3}\left(4a_5\psi\psi^{2*} + 3a_3\psi^*_{xx}\right) & \frac{a_5}{3}\left(\psi^*\psi_x - \psi\psi^*_x\right) & 0 \\ -\frac{i}{3}\left(4a_5\psi^2\psi^* + 3a_3\psi_{xx}\right) & 0 & -\frac{a_5}{3}\left(\psi^*\psi_x - \psi\psi^*_x\right) \end{bmatrix}$$

and

$$\mathbf{U_1} = \begin{pmatrix} u_{111} & 0 & 0 \\ 0 & u_{133} & 0 \\ 0 & 0 & u_{133} \end{pmatrix}$$

$$\mathbf{V_1} = \begin{pmatrix} -\frac{2}{3}a_5A\psi(x,t)\psi^*(x,t) & \frac{1}{3}ia_5A\psi_x(x,t) & -\frac{1}{3}ia_5A\psi^*_x(x,t) \\ -ia_3A\psi^*_x(x,t) & \frac{1}{3}a_5A\psi(x,t)\psi^*(x,t) & -\frac{1}{3}a_5A(\psi^*)^2 \\ ia_3A\psi_x(x,t) & -\frac{1}{3}a_5A\psi^2 & \frac{1}{3}a_5A\psi(x,t)\psi^*(x,t) \end{pmatrix}$$

$$\mathbf{V_2} = \begin{pmatrix} v_{233}(t) & \frac{1}{3}ia_5A^2\psi(x,t) & -\frac{1}{3}ia_5A^2\psi^*(x,t) \\ ia_3A^2\psi^*(x,t) & v_{233}(t) & 0 \\ -ia_3A^2\psi(x,t) & 0 & v_{233}(t) \end{pmatrix}$$

$$\mathbf{V_3} = \begin{pmatrix} v_{333}(t) - a_3A^3 & 0 & 0 \\ 0 & v_{333}(t) & 0 \\ 0 & 0 & v_{333}(t) \end{pmatrix}$$

where: $A = u_{111} - u_{133}$

To apply the Lax pair method to more complex integrable systems, such as the Sasa–Satsuma equation, we extend the auxiliary field to a 3×3 fundamental matrix $\mathbf{\Psi}(x,t)$. In this

framework, the Lax operators U and V are expanded in powers of the spectral parameter λ (or the diagonal matrix $\mathbf{\Lambda}$).

Substituting the expansions:

$$U = U_0 + \lambda U_1 \tag{2.32}$$

$$V = V_0 + \lambda V_1 + \lambda^2 V_2 + \lambda^3 V_3 \tag{2.33}$$

into the Zero-Curvature Condition $U_t - V_x + [U, V] = 0$, and collecting the coefficients for each power of λ, we obtain the following set of matrix equations:

$$\text{eq1} = \frac{\partial U_0}{\partial t} + U_0 V_0 - V_0 U_0 - \frac{\partial V_0}{\partial x} = \begin{pmatrix} 0 & 0 & 0 \\ 0 & 0 & 0 \\ 0 & 0 & 0 \end{pmatrix} \tag{2.34}$$

$$\text{eq2} = \frac{\partial U_1}{\partial t} + U_0.V_1 - V_1.U_0 + U_1.V_0 - V_0.U_1 - \frac{\partial V_1}{\partial x} = \begin{pmatrix} 0 & 0 & 0 \\ 0 & 0 & 0 \\ 0 & 0 & 0 \end{pmatrix} \tag{2.35}$$

$$\text{eq3} = -U_0.V_2 + V_2.U_0 - U_1.V_1 + V_1.U_1 + \frac{\partial V_2}{\partial x} = \begin{pmatrix} 0 & 0 & 0 \\ 0 & 0 & 0 \\ 0 & 0 & 0 \end{pmatrix} \tag{2.36}$$

$$\text{eq4} = -U_0.V_3 + V_3.U_0 - U_1.V_2 + V_2.U_1 + \frac{\partial V_3}{\partial x} = \begin{pmatrix} 0 & 0 & 0 \\ 0 & 0 & 0 \\ 0 & 0 & 0 \end{pmatrix} \tag{2.37}$$

$$eq5 = V_3.U_1 - U_1.V_3 = \begin{pmatrix} 0 & 0 & 0 \\ 0 & 0 & 0 \\ 0 & 0 & 0 \end{pmatrix} \tag{2.38}$$

Also: $\Psi = \begin{pmatrix} \psi_1(x,t) & \psi_2(x,t) & \psi_3(x,t) \\ \phi_1(x,t) & \phi_2(x,t) & \phi_3(x,t) \\ \chi_1(x,t) & \chi_2(x,t) & \chi_3(x,t) \end{pmatrix}$

Where $\psi_{1,2,3}(x,t)$, $\phi_{1,2,3}(x,t)$ and $\chi_{1,2,3}(x,t)$are the components that make it up. The linear system of equations for the auxiliary field is formalized as an expansion in powers of the matrix of constant eigenvalues.

$$\Lambda = \begin{pmatrix} \lambda_1 & 0 & 0 \\ 0 & \lambda_2 & 0 \\ 0 & 0 & \lambda_3 \end{pmatrix}$$

$as\ follows$

$\Psi_x = U_0.\Psi + U_1.\Psi.\Lambda$

$\Psi_t = V_0.\Psi + V_1.\Psi.\Lambda + V_2.\Psi.\Lambda.\Lambda + V_3.\Psi.\Lambda.\Lambda.\Lambda$

and

$$eqx = D[\psi, x] - \psi_x \tag{2.39}$$

$$eqt = D[\psi, t] - \psi_t \tag{2.40}$$

Where D the differential operator ∂_x or ∂_t . The seed selection follows the same criteria introduced in the Hirota analysis.

2.4.5.2 Solitonic solution

Applying the seed: $\psi(x,t) = 0$, $\psi_s(x,t) = 0$, The detailed components of the full algebraic expansions are provided in Appendix A for brevity.
The solution of SSE is:

$$\psi(x,t) = \frac{144\, a_3^2\, c_{1110}^2\, c_{1140}^2\, \lambda_3^2\ \exp\left[4\lambda_3\left(4a_3\lambda_3^2(t-1)+x\right)\right]}{\left(2a_5 c_{1140}^2\, \exp\left(16a_3\lambda_3^3(t-1)\right) + 3a_3 c_{1110}^2\, \exp(4\lambda_3 x)\right)^2} \tag{2.41}$$

Analysis of the Solitonic Wave

In Figure 2.7: The results reveal the fundamental solitonic solution obtained by setting the vacuum seed $\psi(x,t) = 0$. The figure illustrates a localized energy distribution and stable propagation characteristics, demonstrating the classic non-dispersive behavior of the Sasa-Satsuma soliton.

2.4.5.3 Breather solution

We now construct breather-type solutions of the Sasa Satsuma equation. In this case, we consider the reduced form:

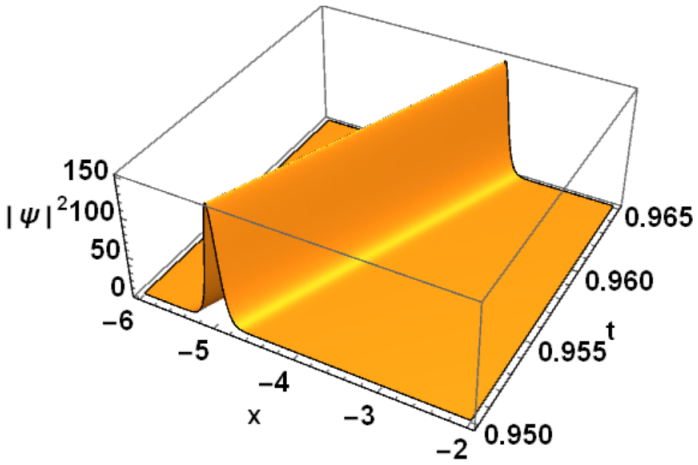

Figure 2.7: **Soliton solution** $|\psi|^2$ of the Sasa-Satsuma Equation (SSE) with parameters $c_{1110} = 1, c_{1140} = 1, \lambda_3 = 5, a_3(t) = 1, a_5(t) = 1$. (a) Contour plot of the solution, (b) 3D evolution of the soliton solution, and (c) temporal profile of the soliton solution.

$$i\psi_t(x,t) + ia_5(3|\psi(x,t)|^2\psi_x(x,t) + |\psi(x,t)|^2\psi_x^*(x,t) + 2\psi_{xxx}(x,t)) = 0 \tag{2.42}$$

To generate breather solutions, we choose a non-zero constant seed:

$\psi_0(x,t) = i$ with the constraints: $u_{111} = 0, \quad a_3 = 2a_5., \quad \mathrm{a}_1 = a_2 = 0.$

Unlike the soliton case, this non-trivial seed leads to oscillatory solutions in time. Following the same Darboux transformation procedure introduced in the Hirota analysis, and using the associated eigenfunctions of the Lax pair, we obtain breather-type solutions.

For brevity, we present the final form of the solution:

$$\psi(x,t) = \frac{i\left(H(x,t) + G(x)M(x,t) - L(x,t)\right)}{H(x,t)L(x,t)} \tag{2.43}$$

The detailed components of the full algebraic expansions are provided in Appendix A for brevity.

Remark: The breather solution exhibits a localized structure in space combined with periodic oscillations in time. This behavior arises from the interplay between exponential decay and hyperbolic/trigonometric oscillations, which is a characteristic feature of breathers in integrable nonlinear systems. For specific parameter choices, these solutions reduce to

periodic or quasi-periodic wave packets, demonstrating the rich dynamics supported by the Sasa Satsuma equation.

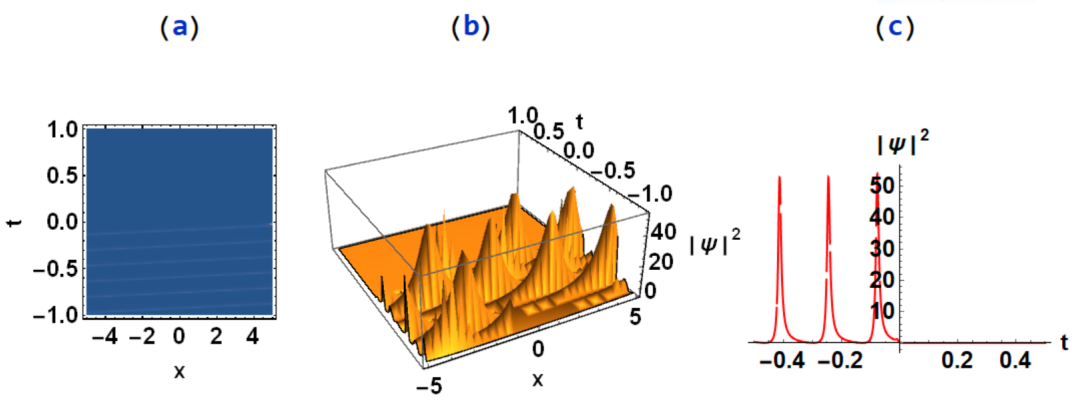

Figure 2.8: **Multi-general breather solution** $|\psi|^2$ of the Sasa-Satsuma Equation (SSE) with parameters $\lambda_1 = 1+i, \lambda_3 = 1+i, \lambda_2 = 1-i, u_{133} = -1, u_{111} = 0, a_5 = 50, v_{333}(t) = 5t, v_{233}(t) = -8t, c_1 = c_2 = 1, c_3 = 1, c_5 = c_6 = -c_4, c_7 = c_8 = 0$. (a) Contour plot of the solution, (b) 3D evolution of the multi-general solution, and (c) temporal profile of the multi-general solution.

Analysis of the Breather Wave

In Figure 2.8: The results demonstrate the transition to complex wave morphologies using the non-zero constant seed $\psi_0(x,t) = i$. By systematically varying the governing parameter-sâspecifically $\lambda_i, u_{133}, a_5, v_{233}(t)$, and the integration constantsâthe figure provides a concise visualization of breather-type structures and their periodic amplitude modulations.

2.4.5.4 Conclusions and Outlook

In the present study, the Lax pair and the Darboux transformation were successfully employed to solve the Sasa-Satsuma equation (SSE) with time-dependent coefficients. This approach enabled the derivation of exact analytical solutions, confirming the integrability of the system under non-autonomous conditions.

The parametric study indicates that the constants λ, u_{133}, and a_5 function as the principal control mechanisms for the wave onset, peak height, and amplitude modulation. In summary, the combination of the Lax pair and Darboux transformation provides a powerful analytical framework for addressing nonlinear equations with time-varying coefficients. This methodology effectively captures the rich dynamics of the Sasa-Satsuma model, offering a robust path for exploring high-order nonlinear phenomena in non-autonomous systems.

Chapter 3

The Higher-Order Nonlinear Schrödinger Equation (HNLS) with Time-Independent Coefficients

3.1 Introduction

Based on the progression of this study, the evolution of nonlinear wave models was analyzed starting from the higher-order Hirota (HNLSE) equation **without external potential and damping** to the comprehensive Higher-order Nonlinear Schrödinger Equation (HNLSE) **including potential and damping factors**, as structured below:

- **Fundamental Higher-order Hirota Model:** The analysis begins with the Hirota equation in its simplest form, studied specifically in the absence of an external potential (V_{ext}) and damping ($\Gamma = 0$).
- **Standard Hirota Transition:** The model was then transitioned toward the standard Hirota form. In this context, the group velocity and the standard Kerr nonlinearity coefficients are null ($a_1 = a_2 = 0$). This phase introduced the influence of the external potential (V_{ext}) while focusing on higher-order effects.
- **Sasa–Satsuma Equation (SSE):** The study extended to the Sasa–Satsuma equation,

which maintains the $a_1 = a_2 = 0$ constraints but incorporates the **Self-frequency shift** (the **Raman effect**). This model describes the dynamics of the wave when the Raman effect becomes a dominant factor in pulse evolution.

Finally, we reach the HNLSE, which integrates all the previously mentioned physical parameters (higher-order dispersion, Raman effect, and nonlinearities) into a single, unified framework. For constant coefficients, the equation is represented as:

$$\begin{aligned} i\psi_t(x,t) + a_1\psi_{xx}(x,t) + a_2|\psi(x,t)|^2\psi(x,t) + ia_3\psi_{xxx}(x,t) \\ + ia_4|\psi(x,t)|^2\psi_x(x,t) + i\Gamma\psi(x,t) + V_{ext}\psi(x,t) = 0 \end{aligned} \tag{3.1}$$

The complexity of the solutions is explored through two primary analytical techniques: the **Lax Pair formulation**, which confirms the system's integrability, and the **Darboux Transformation (DT)** [94, 95, 96], utilized to construct complex multi-soliton solutions from simpler seed solutions. The study focuses specifically on five key classes of localized structures: fundamental solitons [97], general and specific breathers (including the Akhmediev [98] and Kuznetsov–Ma [99] types), extreme Rogue Waves (RW) [100, 101], and unique hybrid states. The formation and stability of these waves are fundamentally determined by the interplay between dispersion (a_1) and Kerr nonlinearity (a_2) [102]. This balance governs the process of energy localization, whereby power is concentrated from the continuous-wave background into high-intensity peaks. Furthermore, the evolution of these solutions is quantified through a detailed growth rate analysis, in which $\mathrm{Re}(\lambda)$ characterizes instability and $\mathrm{Im}(\lambda)$ governs the oscillation frequency [103]. Additionally, the tracking of the center of mass (x_{cm}) facilitates the monitoring of the spatial drift induced by third-order dispersion (a_3) [104]. It is imperative to analyze these energy-concentrated structures within the framework of the HNLSE to comprehend wave dynamics and power stability in advanced nonlinear media [105, 106].

3.2 Lax pair

This chapter presents the Lax pair formulation for the (HNLSE):

$$\mathbf{U}_0 = \frac{1}{2}i\sqrt{\frac{-3a_2(t)}{2a_1(t)}} \times \begin{pmatrix} 0 & e^{-i\frac{a_1(t)}{3a_3(t)}x}\Psi(x,t) & -e^{i\frac{a_1(t)}{3a_3(t)}x}\Psi^*(x,t) \\ -e^{i\frac{a_1(t)}{3a_3(t)}x}\Psi^*(x,t) & 0 & 0 \\ e^{-i\frac{a_1(t)}{3a_3(t)}x}\Psi(x,t) & 0 & 0 \end{pmatrix},$$

$$\mathbf{V}_0 = \begin{pmatrix} 0 & G(x,t) & G^*(x,t) \\ G^*(x,t) & Z(x,t) & 0 \\ G(x,t) & 0 & Z^*(x,t) \end{pmatrix}, \mathbf{V}_1 = \begin{pmatrix} A(x,t) & C(x,t) & C^*(x,t) \\ -C^*(x,t) & B(x,t) & D^*(x,t) \\ -C(x,t) & D(x,t) & B(x,t) \end{pmatrix},$$

$$\psi(\mathbf{x},\mathbf{t}) = \begin{pmatrix} \psi_1(x,t) & \psi_2(x,t) & \psi_3(x,t) \\ \phi_1(x,t) & \phi_2(x,t) & \phi_3(x,t) \\ \chi_1(x,t) & \chi_2(x,t) & \chi_3(x,t) \end{pmatrix}, \quad \mathbf{\Lambda} = \begin{pmatrix} \lambda_1 & 0 & 0 \\ 0 & \lambda_2 & 0 \\ 0 & 0 & \lambda_3 \end{pmatrix} \tag{3.2}$$

$$\mathbf{V}_3 = \begin{pmatrix} v_{311}(t) & 0 & 0 \\ 0 & a_3(t).h + v_{311}(t) & 0 \\ 0 & 0 & a_3(t).h + v_{311}(t) \end{pmatrix}. \mathbf{U}_1 = \begin{pmatrix} u_{111} & 0 & 0 \\ 0 & u_{133} & 0 \\ 0 & 0 & u_{133} \end{pmatrix},$$

The detailed components of the 3×3 Lax matrices and the full algebraic expansions are provided in Appendix B for brevity.

3.3 Solitonic solution

In this case, we consider the seed solution $\psi_0(x,t) = 0$. The detailed components of the full algebraic expansions are provided in Appendix B for brevity Following algebraic simplifications, the HNLS equation admits solitonic solutions; one such solution is expressed

as:

$$\psi(x,t) = -\frac{8i\sqrt{\frac{2}{3}}\, c_{1110}c_{1170}\lambda_3\, e^{z(x,t)}}{\sqrt{-\frac{a_2(t)}{a_1(t)}}\left(c_{1110}^2 e^{f(x,t)} - 2c_{1170}^2 e^{h(x,t)}\right)} \tag{3.3}$$

The detailed components of the full algebraic expansions are provided in Appendix B for brevity

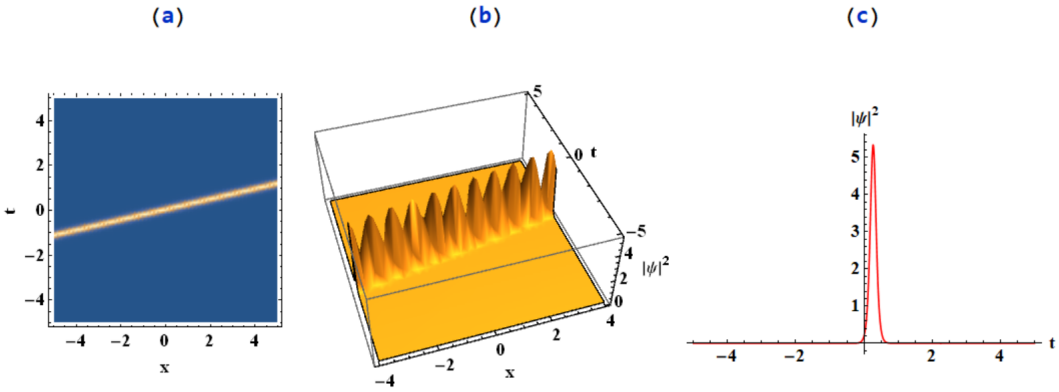

Figure 3.1: **Soliton solution** of the Higher-Order Nonlinear Schrödinger (HNLS) equation for parameters $\lambda_3 = 1, a_1 = 1, a_2 = 1, a_3 = 1, c_{111} = 1, c_{117} = i, v_{133}(t) = t, v_{311}(t) = t$, as depicted by its (a) contour plot, (b) three-dimensional evolution, and (c) temporal profile for a fixed position x.

3.4 The Role of the Spectral Parameter (λ)

3.4.1 General Breather Regime

The general breather solution is characterised by the presence of a pulsating, localized wave that evolves on a non-zero constant background [107]. In contradistinction to conventional solutions, which preserve a static configuration [108], breathers demonstrate periodic fluctuations in their amplitude and width as they propagate [109]. Within the framework of the HNLS equation, the general breather functions as the primary parent solution for a variety of localized states. By precisely tuning the spectral parameter λ, the solution can be specialized into distinct structures: it may manifest as a **spatial breather** (Kuznetsov–Ma type), which is periodic in time and localized in space, or a **temporal breather** (Akhmediev type), which is periodic in space and localized in time. Essentially, the spectral parameter governs the orientation and periodicity of the wave's pulsations within the (x,t) plane. The seed selection follows the same criteria introduced in the Hirota analysis, ensuring consis-

tency in the construction of the non-zero [110]. We consider the plane-wave seed solution (background field) defined by:

$$\psi_0(x,t) = \frac{\exp\left(i\frac{a_1}{3a_3}x\right)}{\sqrt{-\frac{a_2}{a_1}}} \tag{3.4}$$

By applying the Darboux transformation (or the specific calculation procedure previously established for the soliton case) and assuming a Lax pair with constant coefficients, $a_i(t) = a_i$, we obtain a class of solutions for the following Higher-order Nonlinear Schrödinger Equation (HNLS):

$$i\Psi_t + a_1\Psi_{xx} + \frac{3}{4}a_2|\Psi|^2\Psi + ia_3\Psi_{xxx} + ia_4|\Psi|^2\Psi_x + ia_5\Psi^2\Psi_x^* + a_6\Psi = 0. \tag{3.5}$$

Physical Significance of the Terms In the context of nonlinear optics or fluid dynamics, the parameters in this model represent:
a_1: The Group Velocity Dispersion (GVD) coefficient.
a_2: The cubic nonlinearity responsible for Self-Phase Modulation (SPM).
a_3: The Third-Order Dispersion (TOD) term, critical for ultra-short pulse propagation.
a_4, a_5: Nonlinear dispersion terms, often associated with self-steepening and the delayed Raman response.
a_6: A linear phase shift or potential term.
$a_4 = \frac{27\,i\,a_2\,a_3}{8\,a_1}$, $a_5 = \frac{9\,i\,a_2\,a_3}{8\,a_1}$, $a_6 = \frac{1}{54\,a_3^2}$. The application of the Darboux transformation (DT) leads to the breather solution of the HNLS equation. For completeness, the full expressions are presented in Appendix B.The breather solution of HNLS :

$$\Psi(x,t) = \Psi_0(x,t)\,\frac{f\lambda_3 z(u-v)\left(\sinh(fx)\,m_1(x,t) - \cosh(fx)\,m_2(x,t)\right) + f_1}{-f\lambda_3 z(u-v)\left(\sinh(fx)\,m_1(x,t) - \cosh(fx)\,m_2(x,t)\right) + f_2}, \tag{3.6}$$

It is evident that both u and v are constants, as are c_2 and c_3. The detailed expressions for f_1 and f_2 are also provided,these parameters represent the complex algebraic weighting factors derived from the Darboux Transformation. These terms ensure the synchronization between the nonlinear pulse and the continuous-wave background Ψ_0. By substituting the specific parameters $u_{111} = -8i$ and $u_{133} = 8$, the expressions are simplified to define the specific phase and amplitude of the breather. The spectral parameters are selected in such a manner that $\lambda_1 = \lambda_2 = -\lambda_3$. We assume the values of u_{111} and u_{133} are $-8i$ and 8, respectively, and substitute these values into Equation (3.69). The corresponding solution is shown in Figure 3.2

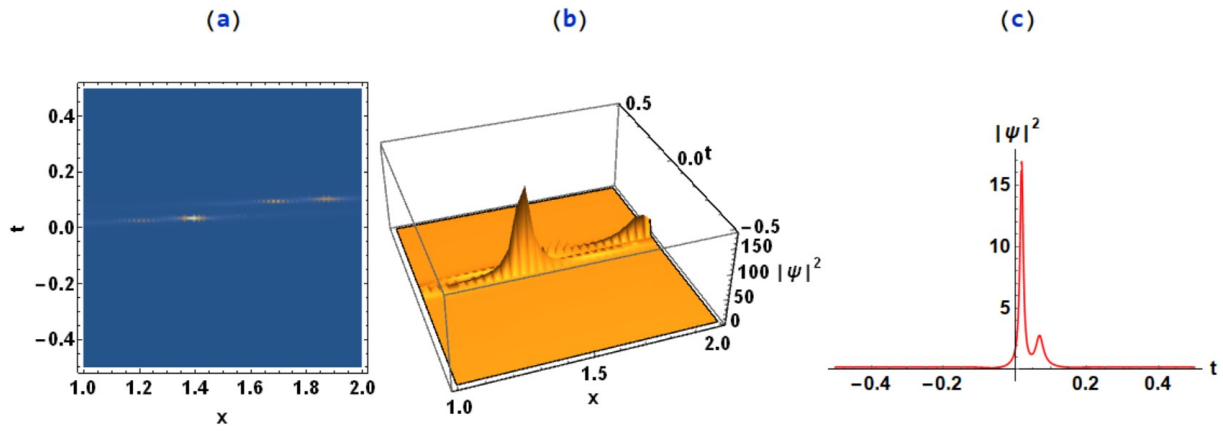

Figure 3.2: **General breather solution** of the Higher-Order Nonlinear Schrödinger (HNLS) equation for parameters $\lambda_3 = -i/6, a_1 = 2i, a_2 = -10i, a_3 = 6i, a_4 = 101.25, a_5 = 33.75, a_6 = -0.0005144.$, as depicted by its (a) contour plot, (b) three-dimensional plot, and (c) temporal profile for a fixed position x.

3.4.2 Akhmediev Breather (Spatial periodicity)

The Akhmediev Breather (AB) is a solution that is periodic in the spatial coordinate x but localized in time t[111]. Physically, it describes the growth and decay of a modulated carrier wave, making it a primary model for studying Modulational Instability (MI)[98]. In the field of nonlinear optics, the AB represents a pulse that emerges from a weakly modulated continuous wave, attains a peak intensity, and subsequently returns to its initial state [112], thereby exhibiting what can be termed "breathing" behaviour once across the temporal domain. We assume the values of u_{111} and u_{133} are -8 and 8, respectively, and substitute these values into Equation (3.69). The corresponding solution is shown in Figure 3.3

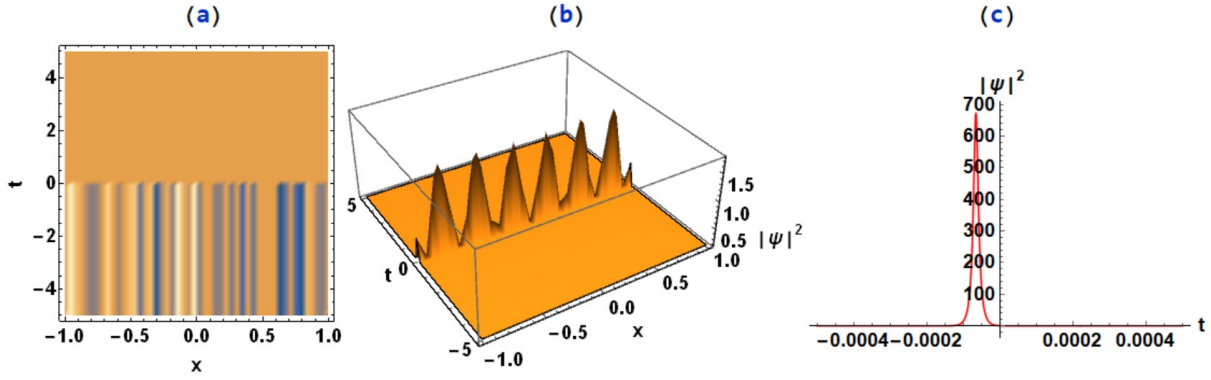

Figure 3.3: **Akhmediev breather solution** of the Higher-Order Nonlinear Schrödinger (HNLS) equation for parameters $\lambda_1 = 2i, a_1 = 2i, a_2 = -10i, a_3 = 6i, a_4 = 101.25, a_5 = 33.75, a_6 = -0.0005144$, as depicted by its (a) contour plot, (b) three-dimensional evolution, and (c) temporal profile for a fixed position x.

3.4.3 Kuznetsov-Ma Breather (Temporal periodicity)

The Kuznetsov-Ma (KM) breather has been shown to be the mathematical "dual" of the Akhmediev breather[113]. It is localised in the spatial direction x, but exhibits strict periodicity in time t. This solution represents a high-intensity peak that stays fixed at a spatial position (or travels at a constant velocity) while its amplitude oscillates indefinitely. The model is frequently employed to simulate stable, recurring energy localisations in fibre optics and deep-water waves. We assume the values of u_{111} and u_{133} are -10 and 8, respectively, and substitute these values into Equation (3.69). The corresponding solution is shown in Figure 3.4

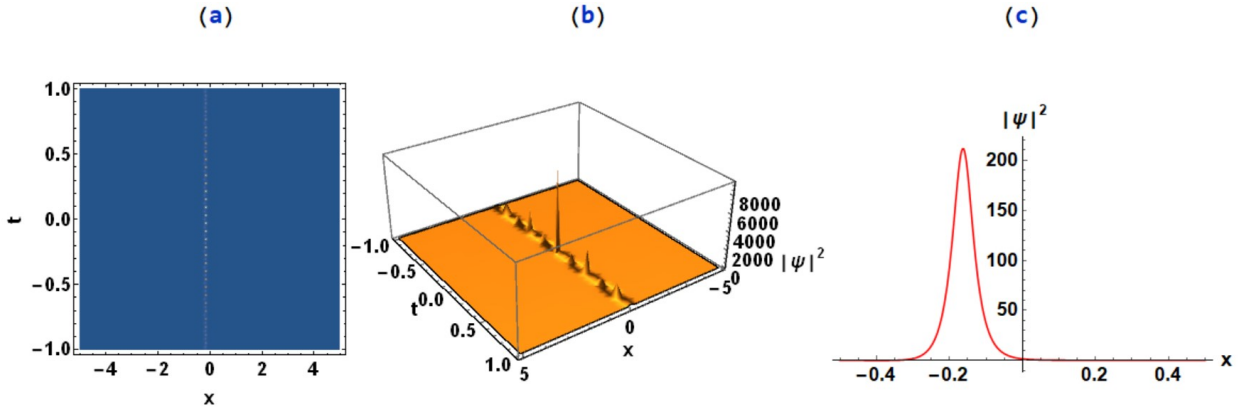

Figure 3.4: **Ma breather solution** of the Higher-Order Nonlinear Schrödinger (HNLS) equation for parameters $\lambda_1 = -1, a_1 = 2i, a_2 = -10i, a_3 = 6i, a_4 = 101.25, a_5 = 33.75, a_6 = -0.0005144$, as depicted by its (a) contour plot, (b) three-dimensional evolution, and (c) temporal profile for a fixed position x.

3.4.4 Mixed Dark Soliton and Akhmediev Breather (The hybrid interaction)

In complex nonlinear systems, different classes of solutions have been shown to coexist and interact. This hybrid regime is characterised by the superposition of a dark soliton[114, 115], which is defined as a localised "dip" or "hole" in a constant intensity background, and an Akhmediev breather. This interaction is of particular significance in the study of multi-component signals in optical fibres, wherein the background field carries both a topological defect (the dark soliton) and a pulsating instability (the breather)[116]. We assume the values of u_{111} and u_{133} are -8 and 8, respectively, and substitute these values into Equation (3.69). The corresponding solution is shown in Figure 3.5

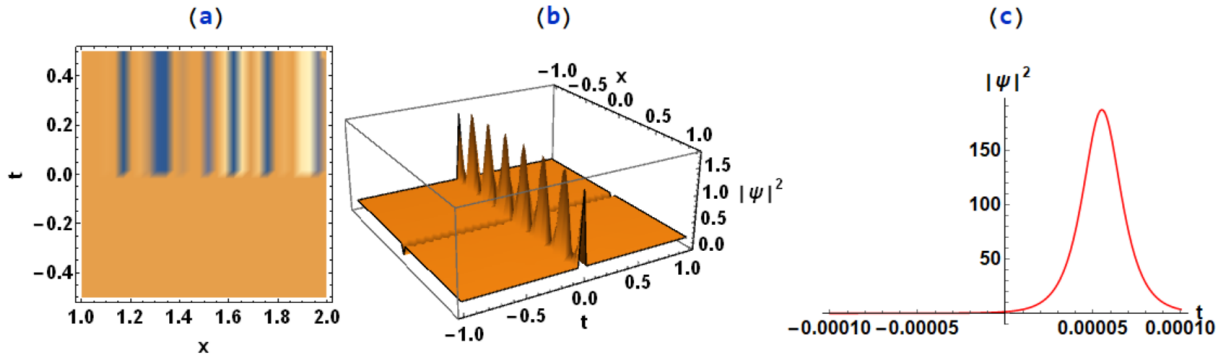

Figure 3.5: **Mixed dark soliton and Akhmediev breather solution** of the Higher-Order Nonlinear Schrödinger (HNLS) equation for parameters $\lambda_1 = -\frac{4i}{3}, a_1 = 2i, a_2 = -10i, a_3 = 6i, a_4 = 101.25, a_5 = 33.75, a_6 = -0.0005144$, as depicted by its (a) contour plot, (b) three-dimensional evolution, and (c) temporal profile for a fixed position x.

3.4.5 Multi-Akhmediev Breathers (Higher-order complexity)

Multi-Akhmediev breathers are defined by higher-order nonlinear interactions, whereby multiple fundamental breathers overlap[117]. This regime is characterised by a higher level of complexity, as evidenced by the presence of multiple peaks and intricate interference patterns on the plane-wave seed. Mathematically, these are constructed using higher-order Darboux transformations[96], and they are crucial for understanding the transition from simple periodic waves to the turbulent "sea" of nonlinear oscillations [118]. We assume the values of u_{111} and u_{133} are -8 and 8, respectively, and substitute these values into Equation (3.69). The corresponding solution is shown in Figure 3.6

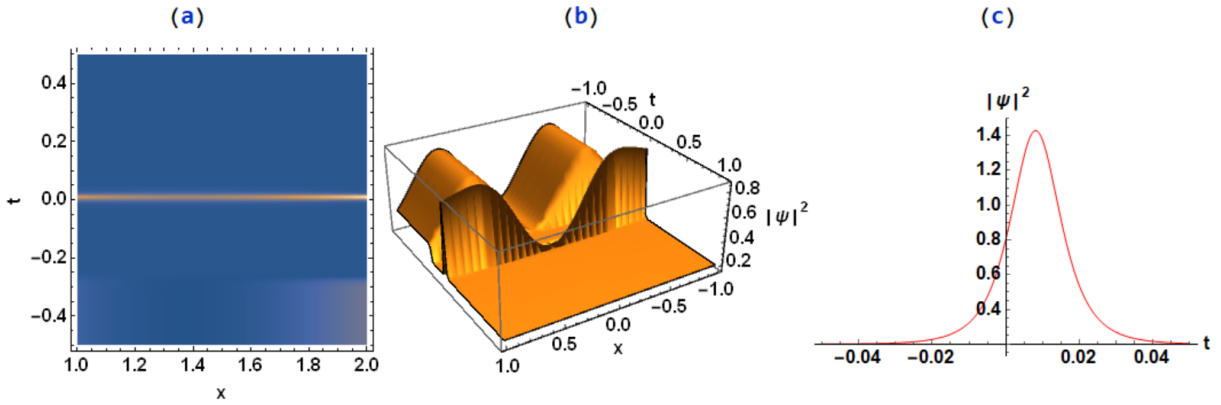

Figure 3.6: **Multi-Akhmediev breather solution** of the Higher-Order Nonlinear Schrödinger (HNLS) equation for parameters $\lambda_1 = -0.18i, a_1 = 2i, a_2 = -10i, a_3 = 6i, a_4 = 101.25, a_5 = 33.75, a_6 = -0.0005144$, as depicted by its (a) contour plot, (b) three-dimensional evolution, and (c) temporal profile for a fixed position x.

3.4.6 Rogue Wave (Peregrine Soliton:The limiting case)

The Peregrine soliton is frequently regarded as the limiting case of both the Akhmediev and Kuznetsov-Ma breathers when the period approaches infinity [119]. This model is regarded as the simplest mathematical representation of a rogue wave [120, 121], which is characterised by its solitary, isolated peak. Such an occurrence is aptly described as "appearing from nowhere and disappearing without a trace [101]." The amplitude of the oscillating field is such that it is precisely three times the amplitude of the background field. This results in a substantial accumulation of energy within a minuscule spatial and temporal window. We assume the values of u_{111} and u_{133} are -2 and 2, respectively, and substitute these values into Equation (3.69). The corresponding solution is shown in Figure 3.7

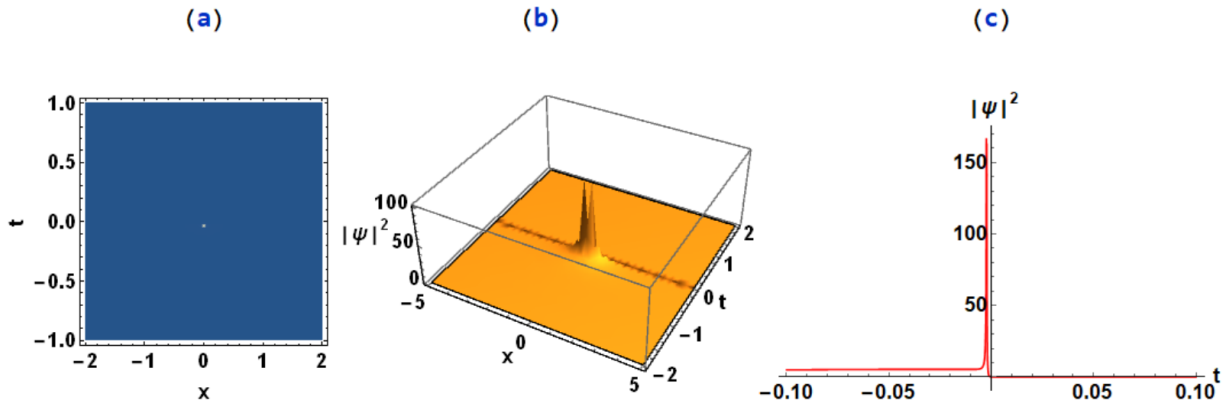

Figure 3.7: **Rogue wave solution** of the Higher-Order Nonlinear Schrödinger (HNLS) equation for parameters $\lambda_1 = -2i, a_1 = 2i, a_2 = -10i, a_3 = 6i, a_4 = 101.25, a_5 = 33.75, a_6 = -0.0005144$, as depicted by its (a) contour plot, (b) three-dimensional evolution, and (c) temporal profile for a fixed position x.

3.5 Influence of Constant Physical Coefficients and Stability Analysis

3.5.1 Stability Analysis and Coherence Preservation

The stabilizing effect of the spectral parameter λ is central to the integrity of the waveforms [122]. We evaluate this by examining the maximum growth rate g_{max} as a function of the spectral parameter λ [123].

- **Stability Regimes (g_{max}):** As illustrated in the g_{max} vs. λ plots, the system enters

a stable regime when the imaginary part of λ is sufficiently large. In these regions, $g_{max} = 0$, indicating that the waveforms are immune to modulation instability and sideband perturbations [124] (Figure 3.10).

- **Compensatory Role of λ_1:** As illustrated in Figure 3.8, various scenarios where a_1 and a_2 are either comparable or significantly different (e.g., $a_2 = -5a_1$, $a_2 = -a_1$, and $a_2 = -a_1/5$) remain stable. This underscores the notion that λ_1 compensates for any imbalances, guaranteeing that the waveforms remain stable and coherent [125].

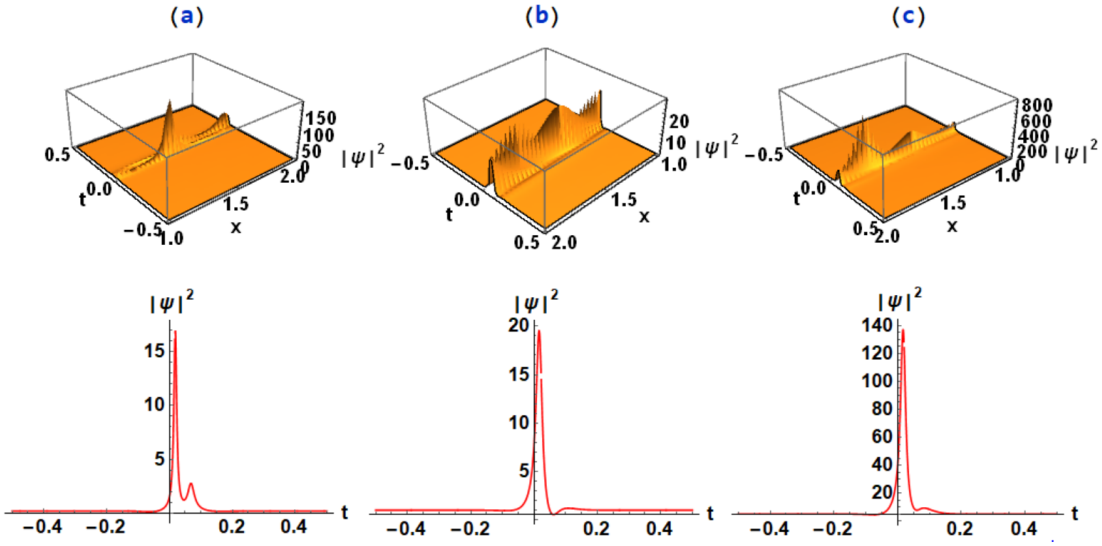

Figure 3.8: **General breather solution** of the Higher-Order Nonlinear Schrödinger (HNLS) equation with parameters $\lambda_1 = -i/6$ and $a_3 = 6i$ for varying values of a_2: (a) $a_2 = -5a_1 = -12i$, (b) $a_2 = -a_1 = -12i$, and (c) $a_2 = -a_1/5 = -2i$. The upper panels display the three-dimensional evolution, while the lower panels show the temporal profile for a fixed position x.

- **Destabilization:** This role is further elucidated in Figure 3.9, where modification of the spectral parameter λ leads to a state of destabilization [126], even when the coefficients a_1 and a_2 remain constant. This confirms that the stability of the breather is fundamentally ensured by the spectral tuning of λ_1.

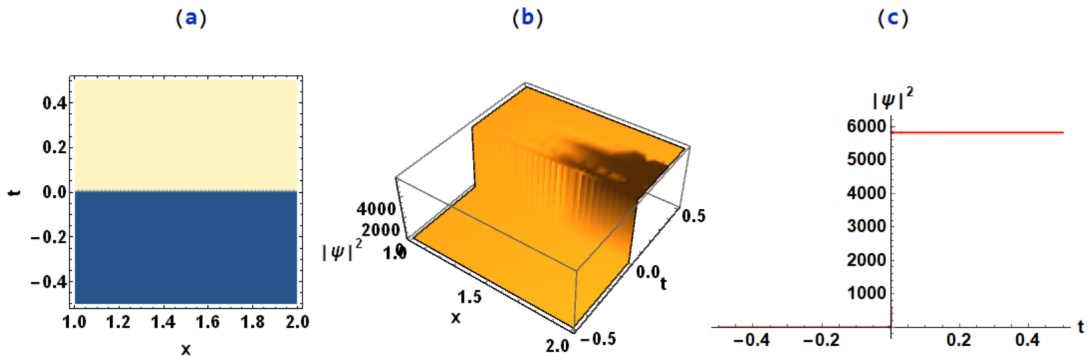

Figure 3.9: **Onset of instability** for the solution with spectral parameter $\lambda_1 = e^{-2i}$, where a_1, a_2 and a_3 are the same as those in Fig. 3.8. (a) Contour plot of the solution, (b) three-dimensional evolution, and (c) temporal profile for a fixed position x.

Justification of the Onset of Instability: The identification of the onset of instability in Fig. 3.9 is based on the qualitative and dynamical transitions observed in the evolution of the field. First, the solution initially exhibits a nearly uniform plane-wave profile, characteristic of the stable background. As evolution progresses, a localized deformation emerges in the wave amplitude. This growth in $|\Psi|^2$ provides a direct manifestation of the gain relation derived in Eq. (X), where small perturbations are amplified by the nonlinear medium rather than being damped. Second, the temporal profile at a fixed spatial coordinate reveals a loss of stationarity. In the stable regime, the amplitude is time-invariant; however, the observed modulation signifies that the system has entered the unstable regime where the background energy is transferred into the perturbation modes. Third, the instability is marked by the breaking of spatial uniformity. The emergence of localized structures (breathers or solitons) indicates that energy is no longer equidistributed but has focused into specific regions. This spatial symmetry breaking is a primary signature of modulational instability in higher-order nonlinear systems. Consequently, the onset of instability is defined as the transition point from a uniform stationary state to a dynamical regime characterized by perturbation growth, symmetry breaking, and the loss of temporal invariance.

3.5.2 Physical Interpretation of the Spectral Parameters Re(λ) and Im(λ)

In the context of the Higher-Order Nonlinear Schrödinger (HNLS) equation, the complex spectral parameter $\lambda = \text{Re}(\lambda) + i\text{Im}(\lambda)$ functions as a fundamental control mechanism for the dynamical stability and energy distribution of the wave field. Its components correspond to specific physical processes that balance dispersive and nonlinear effects [127].

The Real Part Re(λ): Dispersive Energy Spreading

The real component is physically associated with *dispersive energy spreading*, dictating how power is spatially and temporally distributed across the system. Numerical analysis in Table 3.1 confirms that the absence of this mechanism ($\mathrm{Re}(\lambda) = 0$) results in localized instability [128, 129].

The Imaginary Part Im(λ): Localization and Stability

The imaginary component regulates *energy localization*. A larger magnitude $|\mathrm{Im}(\lambda)|$ enhances the nonlinear self-focusing effect, favoring nonlinearity (a_2) over dispersive broadening (a_1). This results in the confinement of energy into high-intensity peaks.

$\mathrm{Re}(\lambda)$	$\mathrm{Im}(\lambda)$	$g_{\max}(\lambda)$
0	-60	0
0	-48	0
0	-30	$3.24486 + 0\,i$
1	0	3.16471
0	0.18	$3.46889 + 0\,i$
-1	0	3.65137
0	-0.18	$3.6268 + 0\,i$
0	$\frac{4}{3}$	$2.74433 + 0\,i$
0	$\frac{1}{6}$	$3.47518 + 0\,i$
0	$-\frac{4}{3}$	$4.00516 + 0\,i$
0	$-\frac{1}{6}$	$3.62136 + 0\,i$
0	2	$2.84227 + 0\,i$
0	-2	$4.16197 + 0\,i$
0	48	0
0	60	0

Table 3.1: Values of $\mathrm{Re}(\lambda)$, $\mathrm{Im}(\lambda)$ and $g_{\max}(\lambda)$.

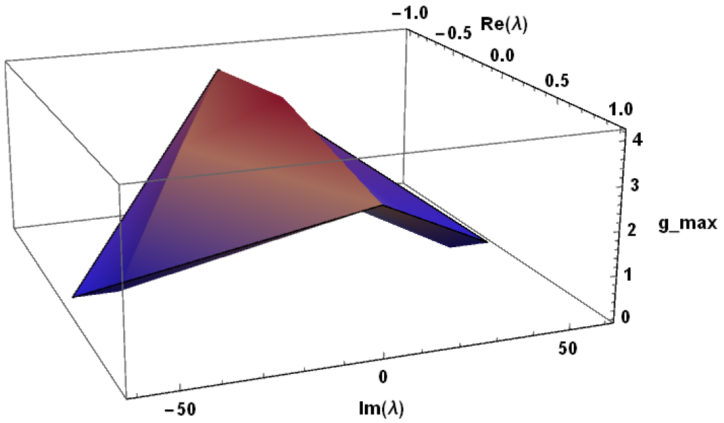

Figure 3.10: **Maximum growth rate** $g_{\max}$ as a function of the complex eigenvalue λ. The surface illustrates the variation of $g_{\max}$ over the complex plane, demonstrating how the real and imaginary components of λ influence the system stability.

3.5.2.1 Quantitative Interpretation and Experimental Application

The numerical data in Table 3.1 quantifies the transition from instability to steady-state equilibrium. For the purely imaginary case, a definitive stability threshold is observed at $|\text{Im}(\lambda)| = 48$, where the growth rate vanishes ($g_{\max} = 0$). This signifies that the nonlinear gain exactly compensates for dissipative losses. Conversely, the real case ($\lambda = \pm 1$) remains unstable ($g_{\max} \approx 3.16$), as frequency-detuned pulses cannot achieve this dissipative balance.

3.5.2.2 Experimental Realization in Active Media

The use of imaginary coefficients (a_n) and spectral parameters (λ) indicates a **dissipative stability** regime, typically realized in active systems like Erbium-doped fiber lasers. In a laboratory setting, these parameters are mapped to specific "knobs":

- **Gain Control (a_1, a_2):** Managed by the **pumping intensity** of the laser diodes. Higher pump currents increase the magnitude of the imaginary gain coefficients.
- **Power Tuning (Im(λ)):** Managed by an **optical attenuator** to control input peak power. The threshold $|\text{Im}(\lambda)| = 48$ defines the specific power required to "freeze" the wave into a stable dissipative breather [130, 131, 132, 133, 134].
- **Frequency Tuning (Re(λ)):** Managed by the **center wavelength** of the seed laser (frequency detuning).

This mapping allows the experimentalist to tune the system to the exact 'Fixed Point' where dissipative structures propagate without decay.

3.5.2.3 Mathematical Derivation of the Gain Relation

A. Plane–wave background: We consider a continuousâwave (CW) solution of the form:

$$\Psi_0 = Ae^{i\Omega t}, \quad A > 0, \tag{3.7}$$

which, after substitution into Eq. (3.5), yields the frequency relation:

$$\Omega = \tfrac{3}{4}a_2|A|^2 + a_6. \tag{3.8}$$

B. Small perturbation: Following the standard linearâstability approach [103, 106], a weak modulation is introduced as:

$$\Psi(x,t) = \Big[A + \varepsilon(ue^{iKx+\Omega(K;\lambda)\,t} + v^*e^{-iKx+\Omega(K;\lambda)\,t})\Big]e^{i\Omega t}, \tag{3.9}$$

where K is the perturbation wavenumber, and $\Omega(K;\lambda)$ is the growth rate of the perturbation for a given breather spectral parameter λ.

C. Linearization: Substituting the perturbed solution into Eq. (3.5) and linearizing with respect to the small parameter ε yields the matrix system:

$$\begin{pmatrix} L_+(K,\lambda) & C(K) \\ -C(K) & L_-(K,\lambda) \end{pmatrix} \begin{pmatrix} u \\ v \end{pmatrix} = 0, \tag{3.10}$$

with

$$L_\pm(K,\lambda) = \Omega(K;\lambda) + a_6 + a_1K^2 \pm ia_3K^3, \tag{3.11}$$

$$C(K) = \tfrac{3}{4}a_2|A|^2 - (a_4+a_5)|A|^2K. \tag{3.12}$$

D. Dispersion relation and Gain function: A nontrivial solution requires the determinant of the matrix to vanish, giving the dispersion relation:

$$\left|\Omega(K;\lambda) + a_1K^2 + ia_3K^3 + a_6\right|^2 - [C(K)]^2 = 0. \tag{3.13}$$

Consequently, the gain function is defined as:

$$\Omega(K;\lambda) = \left|\lambda_s + a_1K^2 + ia_3K^3 + a_6\right|^2 - [C(K)]^2 \tag{3.14}$$

3.5.2.4 Numerical Evaluation and Stability Regimes

The maximum gain for a given breather,

$$g_{\max}(\mathrm{Re}\lambda, \mathrm{Im}\lambda) = \max_{K\in[-10,10]} \Re\big[\Omega(K;\lambda)\big],$$

was computed through numerical maximization techniques, utilizing the following physical coefficients:

$$a_1 = 2,\ a_2 = -10,\ a_3 = 6,\ a_4 = -101.25,\ a_5 = -33.75,\ a_6 = 0.01646,\ A = \sqrt{0.2}.$$

The calculation was performed for the spectral values:

$$\lambda = \{-60i, -48i, -30i, 1, 0.18i, -1, -0.18i, \tfrac{4i}{3}, \tfrac{i}{6}, -\tfrac{4i}{3}, -\tfrac{i}{6}, 2i, -2i, 48i, 60i\}.$$

3.5.2.5 Physical Interpretation

The numerical results, visualized in the 3D spectra (Figure. 3.10) and summarized in Table 3.1, reveal the following stability characteristics:

- **Stability Indicator:** The maximum growth rate $g_{\max}(\lambda)$ functions as a quantitative metric for system stability. When $g_{\max} = 0$, the system remains stable and the energy distribution remains uniform across the CW background.
- **Stability Threshold:** The system enters an absolutely stable regime when the imaginary part $|\mathrm{Im}(\lambda)|$ is sufficiently large (e.g., $|\mathrm{Im}(\lambda)| \geq 48$). In this state, the waveforms are immune to modulation instability (MI).
- **Energy Regulation:** The spectral parameter λ effectively delineates the boundary between stability and instability, acting as a control mechanism that regulates the flow of energy to maintain the coherence of localized structures against dispersive degradation.

3.5.3 Influence of Constant Physical Coefficients (a_1, a_2, a_3)

The HNLS framework allows for a detailed investigation into how the medium's inherent physical properties dictate wave propagation. To isolate the specific roles of the coefficients

a_1 and a_2, the general breather solution is examined while maintaining a constant third-order dispersion coefficient, $a_3 = 6i$.

3.5.3.1 Spectral Filtering (a_1) and Spatial Stretching

As illustrated in Figure 3.11, the coefficient a_1 acts as a primary regulator of the breather's spatial width. An increase in the magnitude of the imaginary coefficient from $a_1 = 2i$ to $12i$ induces a pronounced spatial stretching, broadening the wave profile while the peak amplitude remains relatively invariant. Conversely, smaller values of a_1 yield a highly compressed and localized structure. Physically, while a_1 is associated with the Group Velocity Dispersion (GVD) position in the HNLS equation, its purely imaginary nature in this model characterizes it as **spectral filtering** or **gain dispersion**. In dissipative systems, such as fiber lasers or active amplifiers, an imaginary a_1 represents the finite bandwidth of the gain medium. The observed spatial stretching is a direct consequence of this filtering mechanism: a larger $|a_1|$ corresponds to a broader spectral "window" that allows a wider range of frequencies to experience gain, thus supporting a spatially wider breather. This representation arises from the requirements of the Darboux transformation and integrability, mapping the mathematical dissipative parameters to the physical energy-balancing mechanisms of the active medium.

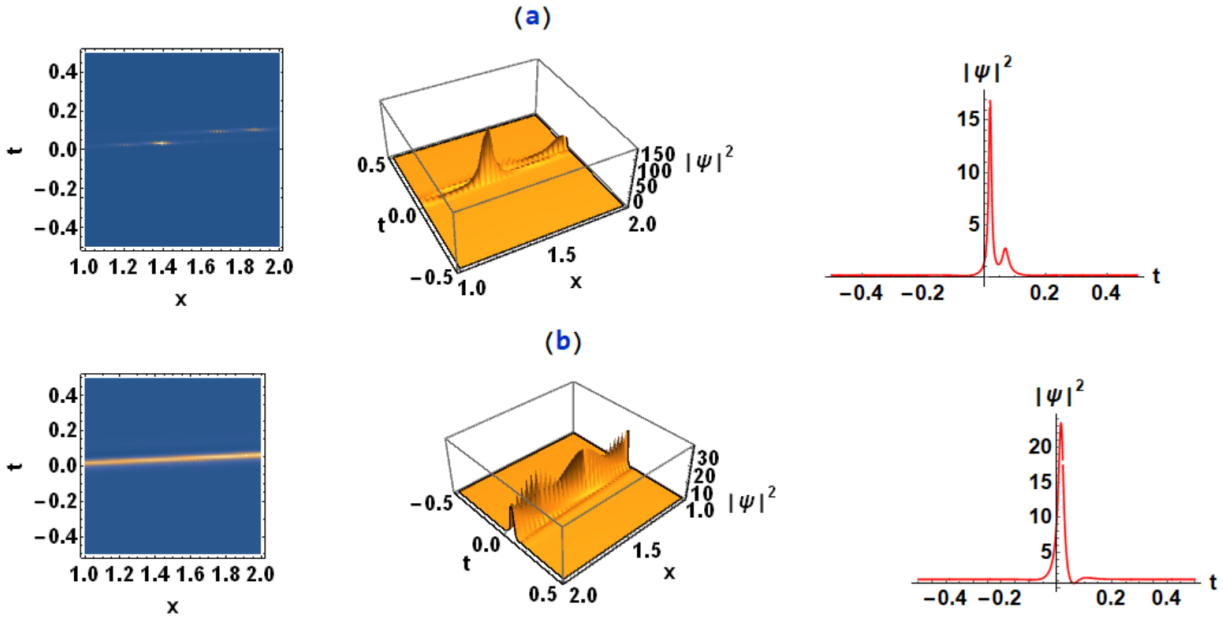

Figure 3.11: **Profile of the general breather solution** $|\psi|^2$ for parameter $a_2 = -10i$. (a) Evolution with $a_1 = 2i$ and (b) evolution with $a_1 = 12i$. Each panel illustrates the transition of the wave profile under the influence of the higher-order terms.

3.5.3.2 Nonlinear Gain Saturation (a_2) and Energy Redistribution

As illustrated in Figure 3.12, the role of the nonlinearity coefficient a_2 is fundamental in regulating the breather's intensity profile. Under conditions of stronger imaginary nonlinearity ($|a_2| = 10$), the breather exhibits a narrower spectral bandwidth and a lower peak amplitude. Conversely, weaker nonlinearity ($|a_2| = 3$) results in a wider bandwidth and higher amplitude. While this behavior appears counter-intuitive relative to standard real-valued self-focusing, it is consistent with the physics of dissipative systems where a_2 represents **nonlinear gain**. This phenomenon is quantified by the redistribution of energy required to satisfy the stability conditions ($g_{\max} = 0$) found in Table 3.1. Specifically, as $|a_2|$ increases from 3 to 10, the system experiences a higher rate of nonlinear energy injection. To prevent a singularity or 'blow-up,' the breather redistributes this energy by narrowing its spectral width, thereby increasing the effective dissipation from the spectral filter a_1. This energy-balancing mechanism forces the peak amplitude to saturate at a lower level ($|a_2| = 10$) compared to the lower-gain regime ($|a_2| = 3$), ensuring that the total integrated power remains finite and stable.

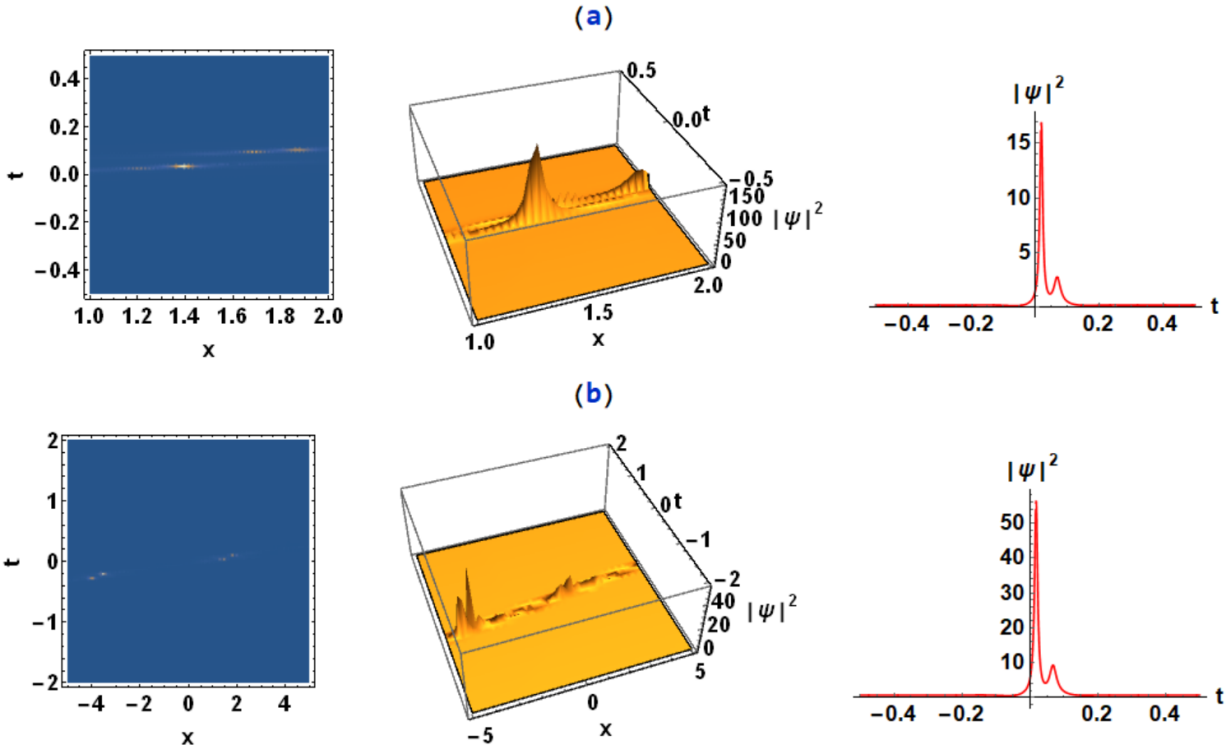

Figure 3.12: **Profile of the general breather solution** $|\psi|^2$ for parameter $a_1 = 2i$. (a) Evolution with $a_2 = -10i$ and (b) evolution with $a_2 = -3i$. The plots demonstrate the structural changes in the breather profile as the higher-order parameter a_2 varies.

3.5.3.3 Third-Order Dispersion (a_3) and the Shift of the Center of Mass

The third-order dispersion coefficient a_3 exerts a direct influence on the spatial dynamics and symmetry of the wave. To quantify this effect, the breather's center-of-mass position x_{cm} is calculated through numerical integration of the intensity $I(x,t) = |\Psi(x,t)|^2$ according to the standard definition used in nonlinear optical fiber dynamics [102]:

$$x_{cm}(t) = \frac{\int_{-6}^{6} xI(x,t)dx}{\int_{-6}^{6} I(x,t)dx} \tag{3.15}$$

From the results presented in Figure 3.14, it is evident that at $a_3 = \pm 6$, the center of mass $x_{cm} = 0$, indicating a nearly symmetrical mass distribution (see Figure 3.13). However, as shown in Figure 3.14, when $a_3 = -2$, x_{cm} drops sharply to a minimum of -4.7, representing the maximum spatial displacement of the pulse center. As a_3 increases toward positive values, x_{cm} rises and gradually returns toward zero [105]. This coordinate-dependent velocity shift causes the localized wave to lean or translate during propagation without compromising its overall structural integrity.

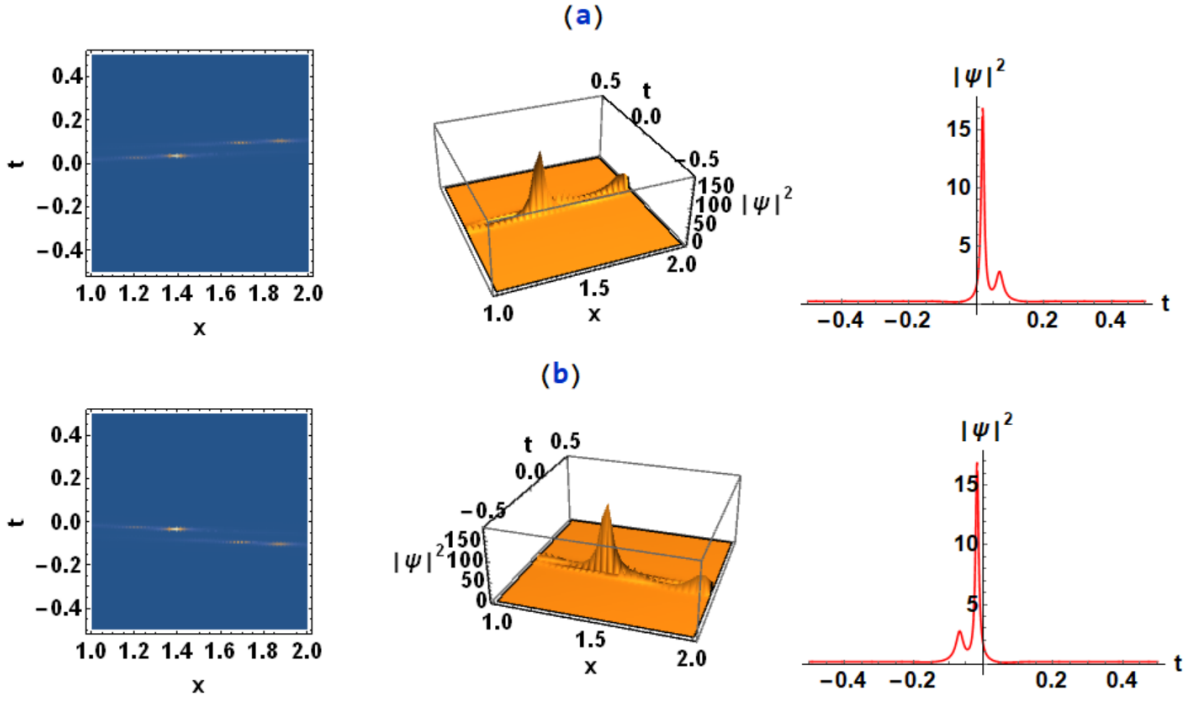

Figure 3.13: **Profile of the general breather solution** $|\psi|^2$ for parameters $a_1 = 2i$ and $a_2 = -10i$. (a) Evolution with $a_3 = 6i$ and (b) evolution with $a_3 = -6i$. The comparison illustrates the effect of the higher-order parameter a_3 on the symmetry of the breather profile.

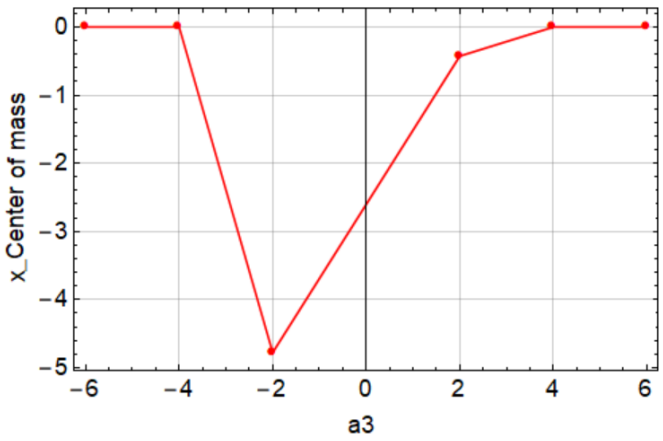

Figure 3.14: **Center-of-mass position** x_{cm} as a function of the parameter a_3. The plot illustrates how the spatial shift of the solution is influenced by the higher-order coefficient.

3.6 Chapter Summary

In this chapter, we have provided a rigorous investigation into the Higher-Order Nonlinear Schrödinger (HNLS) equation characterized by time-independent coefficients within a conservative framework. The theoretical foundation of the system's integrability was established through the formulation of the Lax pair, which enabled the systematic construction of exact analytical solutions via the Darboux transformation (DT) method. By employing both zero and plane-wave seed solutions, a diverse spectrum of localized nonlinear structures was derived and categorized. This inventory includes fundamental solitons and general breather regimes, specifically Akhmediev breathers exhibiting spatial periodicity and Kuznetsov-Ma breathers characterized by temporal periodicity. Furthermore, higher-order complexities such as multi-Akhmediev breathers and hybrid interaction states-specifically the coexistence of dark solitons and breathers-were analyzed. The rogue wave solution was identified as the rational limiting case of the breather regime, underscoring its unique property of extreme energy localization on a non-vanishing background. Beyond the construction of solutions, this chapter presented a detailed parametric study of the spectral parameter λ and higher-order dispersion terms. Through linear stability analysis, the gain function and the maximum spectral growth rate $g_{\max}$ were derived, revealing a stability threshold that ensures the preservation of wave coherence. We specifically isolated the physical contributions of the coefficients: a_1 and a_2 were found to govern the balance between spatial stretching and nonlinear self-focusing, while a_3 (third-order dispersion) was identified as the primary factor inducing center-of-mass shifts and group velocity modi-

fications. In conclusion, the analytical framework established in this chapter provides a fundamental benchmark for understanding nonlinear wave dynamics in homogeneous media. These results serve as the necessary prerequisite for the transition to the generalized HNLS model featuring time-dependent coefficients, which will be the focus of the subsequent chapter.

Chapter 4

The Higher-Order Nonlinear Schrödinger Equation (HNLS) with Time-Dependent Coefficients

4.1 Introduction

The theoretical investigation conducted in Chapter 3 established a fundamental understanding of localized structures in homogeneous media. However, as noted by J. Scott Russell in his seminal observations, localized waves in nonlinear media are characterized by their stability and ability to persist without dissipation due to the balance between dispersion and nonlinearity [116, 124]. Although the aforementioned results established a foundational framework, the practical applications of nonlinear optics in contemporary settingsâsuch as pulse propagation in tapered fibers or matter-wave solitons in BoseâEinstein condensates (BECs)âfrequently involve media in which physical parameters are inhomogeneous in both space and time [125, 107]. In this chapter, we expand our analysis to the non-autonomous HNLS equation, where the coefficients governing dispersion, nonlinearity, and higher-order effects are explicitly defined as functions of time. This generalization is not merely a mathematical extension; it represents a shift toward dispersion and nonlinearity management. The mounting demand for nonlinear wave phenomena in contemporary applications necessitates the extension of the classical NLSE to encompass complex dynamical features

through time-dependent coefficients representing dispersion, nonlinearity, and higher-order corrections [109]. The incorporation of time-dependency into the coefficients $a_1(t), a_2(t),$ and $a_3(t)$ signifies a transition from static wave translation to the active engineering of waveforms, as evidenced in the extant literature [125, 120]. The Darboux transformation (DT), adapted for non-autonomous systems [110], is employed to derive a wide spectrum of localized nonlinear structures. The present investigation focuses on the modulation of these coefficients, a process that has been demonstrated to facilitate transitions between distinct localized states. This includes the conversion of a general breather into Akhmediev or Kuznetsov-Ma regimes, as evidenced in the literature [98, 99]. The DT's inherent incorporation of the spectral parameter functions as a "control switch," thereby enabling the deliberate manipulation of dispersion and nonlinearity effects, thus facilitating the intentional reshaping of waveforms [96, 135]. In conclusion, the objective of this study is to establish a connection between analytical theory and practical reliability. To this end, the search for precise and stable solutions is addressed [136, 111]. In this study, we present a numerical validation using the split-step fast Fourier transform (SFFT) method. This analysis demonstrates that these structures maintain their integrity even under small perturbations ($\epsilon = 0.001$). This finding is supported by previous research from [113, 119, 137]. This comprehensive approach provides the mathematical rigor and numerical proof necessary for advancing the use of nonlinear wave phenomena across various fields of physics.

4.2 Derivation of General Solutions for the Non-autonomous HNLS Equation

In this section, we embark on an investigation of the generalized Higher-order Nonlinear Schrödinger (HNLS) equation. This equation functions as a robust model for optical soliton propagation in non-homogeneous and advanced fiber systems [138, 117]. The evolution of the complex wave envelope, denoted by the symbol $\Psi(x,t)$, is governed by the following non-autonomous equation:

$$i\Psi_t + a_1(t)\Psi_{xx} + \frac{3}{4}a_2(t)|\Psi|^2\Psi + ia_3(t)\Psi_{xxx} + ia_4(t)|\Psi|^2\Psi_x + ia_5(t)|\Psi|^2\Psi_x^* + V(t,x)\Psi + i\Gamma(t)\Psi = 0. \tag{4.1}$$

The time-dependent coefficients are known to represent the second-order dispersion $a_1(t)$, Kerr nonlinearity $a_2(t)$, third-order dispersion $a_3(t)$, and derivative nonlinearities $a_4(t), a_5(t)$. In addition, the potential $V(t,x)$ and gain/loss $\Gamma(t)$ must be considered. In order to ensure integrability, the following constraints must be imposed:

$$a_4(t) = 3a_5(t), \quad a_5(t) = \frac{9a_2(t)a_3(t)}{8a_1(t)}, \tag{4.2}$$

$$V(t,x) = \frac{1}{54}\left(\frac{18x\dot{a}_1(t)}{a_3(t)} - \frac{18xa_1(t)\dot{a}_3(t)}{a_3^2(t)} + \frac{4a_1^3(t)}{a_3^2(t)}\right), \quad \Gamma(t) = \frac{1}{54}\left(-\frac{27\dot{a}_1(t)}{a_1(t)} + \frac{27\dot{a}_2(t)}{a_2(t)}\right). \tag{4.3}$$

4.2.1 Breather Solutions via the Darboux Transformation

In accordance with the calculation procedure previously applied to the soliton case, and employing the same Lax pair formalism with the same structural coefficients, explicit breather solutions are derived. These are derived by selecting a non-trivial plane wave seed solution , The seed selection follows the same criteria introduced in the Hirota analysis, ensuring consistency in the construction of the non-zero background. We consider the plane-wave seed solution (background field) defined by:

$$\Psi_0(x,t) = \frac{\exp\left(i\frac{a_1(t)}{3a_3(t)}x\right)}{\sqrt{-\frac{a_2(t)}{a_1(t)}}}, \tag{4.4}$$

In order to satisfy the background dynamics of equation HNLS (4.1), the Darboux transformation (DT) is applied iteratively. For completeness, the full expressions are presented in Appendix B. This procedure yields the following generalized breather solution:

$$\Psi(x,t) = \Psi_0 \frac{2Be^{F(x,t)}\cosh[H(x,t)] + 4\lambda_3 u_{111}e^{Z(x,t)}\sinh[M(x,t)] - T(x)}{2Be^{F(x,t)}\cosh[H(x,t)] + 4\lambda_3 u_{133}e^{Z(x,t)}\sinh[M(x,t)]}. \tag{4.5}$$

The functions $M(x,t)$, $H(x,t)$, $Z(x,t)$ and $F(x,t)$, which encode the complex spatiotemporal dynamics. The components of the 3×1 eigenfunction vector (ζ_i) are the explicit closed-form solutions of the underlying Lax pair, providing the necessary phase and am-

plitude modulation dictated by the time-varying coefficients $a_1(t), a_2(t)$, and $a_3(t)$. This emphasises the role of non-autonomous systems in shaping wave profiles [121].

4.2.2 General Breather Regime

For generic values of the spectral parameter λ_3 and the system parameters $a_1(t)$, $a_2(t)$, and $a_3(t)$, the derived solution exhibits extended, smoothly varying breather dynamics. Figure 4.1 illustrates the spatiotemporal surface profile of the intensity $|\Psi|^2$ as a function of x and t. The temporal evolution at a fixed spatial coordinate confirms the presence of parabolic amplitude modulation, while magnified views of the peak regions reveal persistent regularity and structural stability within this regime. To demonstrate the specific behaviour of these solutions, we consider an explicit instance which simplifies to:

$$\Psi(x,t) = -\frac{2e^{\frac{2ix}{3}}\left[-4\sqrt{2}e^{\zeta_1(t,x)} - \beta e^{\zeta_2(t,x)} + 4\sqrt{2}e^{\zeta_3(t)} - \sqrt{35}e^{\zeta_4(x)}\right]}{(\sqrt{70}-8)e^{\zeta_2(t,x)} + 8e^{\zeta_3(t)} + \sqrt{70}e^{\zeta_4(x)}}, \tag{4.6}$$

where $\beta = 4\sqrt{2} + \sqrt{35}$. The functions ζ_j represent linear combinations of the spatial coordinate x and the quadratic temporal term t^2, providing the necessary modulation for non-autonomous dynamics. These auxiliary functions are defined as follows:

$$\zeta_1(t,x) = \frac{1}{24}\left(800\sqrt{2} + 191\sqrt{35}\right)t^2 + \frac{1}{2}\left(4\sqrt{2} + \sqrt{35}\right)x, \tag{4.7}$$

$$\zeta_2(t,x) = \frac{200\sqrt{2}}{3}t^2 + \sqrt{35}x, \tag{4.8}$$

$$\zeta_3(t) = \frac{1}{12}\left(800\sqrt{2} + 191\sqrt{35}\right)t^2, \tag{4.9}$$

$$\zeta_4(x) = \left(4\sqrt{2} + \sqrt{35}\right)x. \tag{4.10}$$

This analytical structure confirms the presence of temporal modulations and spatial localization under the influence of non-autonomous system parameters. The precise interplay between the exponential arguments, designated as ζ_j, dictates the evolution of the breather peaks and their trajectories. This highlights the complexity of wave propagation in advanced optical fibres.

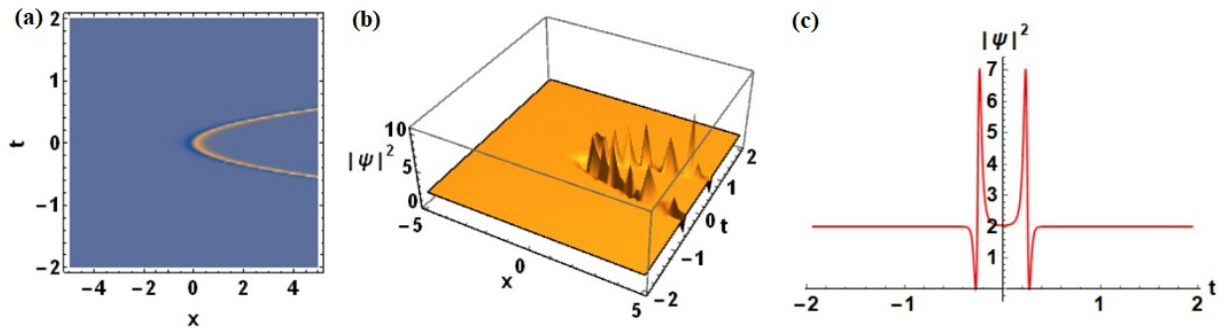

Figure 4.1: **General breather profile** of the Higher-Order Nonlinear Schrödinger (HNLS) equation for parameter $\lambda_3 = \frac{\sqrt{2}i}{2}$. (a) Contour plot of the solution demonstrating an extended smoothly varying breather regime, (b) 3D evolution of $|\psi|^2$ revealing the general breather structure, and (c) temporal profile of $|\psi|^2$ at fixed x showing a parabolic evolution.

4.2.3 Kuznetsov–Ma Breather Regime

The dynamical behaviour of the derived solutions is highly sensitive to the spectral parameter, denoted here by λ_3, and the functional forms of the non-autonomous coefficients. By selecting the time-dependent coefficients as $a_1(t) = 2t$, $a_2(t) = -t$ and $a_3(t) = t$, the solution exhibits distinct transitions between different breather typologies. As illustrated in Figure 4.2, the spectral parameter, denoted here by λ_3, acts as a control mechanism for the morphological deformation of the wave profile. Specifically, as λ_3 increases, the solution evolves from a broad, general breather state toward a more spatially periodic Ma-type breather. This transition is characterised by a significant enhancement in spatial periodicity and a stronger degree of amplitude localization.

The capacity to manipulate these transitions by tuning the spectral parameter, particularly under the influence of time-varying dispersion and nonlinearity, provides an essential theoretical framework for engineering targeted nonlinear waveforms in advanced optical systems. These results emphasise the unique degrees of freedom offered by non-autonomous systems in the precise control of pulse shaping and wave dynamics[139].

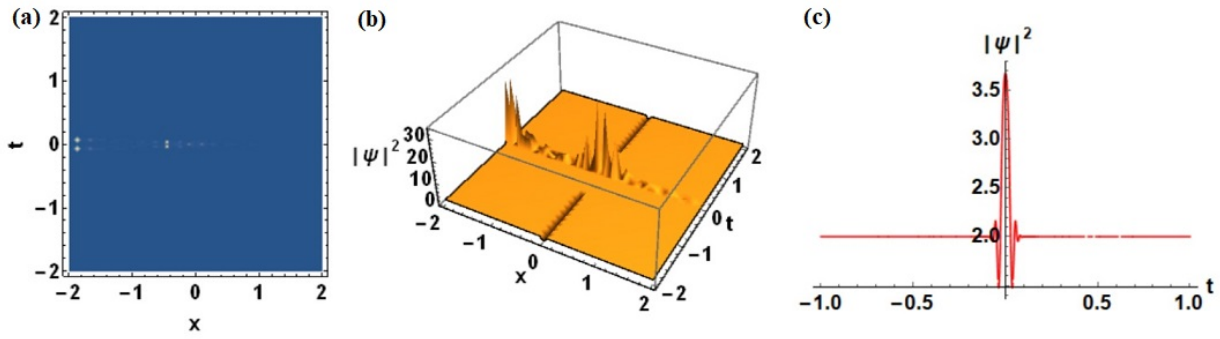

Figure 4.2: **Transition from a general breather to a Ma breather** for spectral parameter $\lambda_3 = 2i$. (a) Contour plot of the solution, (b) 3D evolution of $|\psi|^2$ showing the morphological shift from a general state to a Ma-type breather with increasing spatial periodicity and amplitude localization, and (c) temporal profile of $|\psi|^2$ at fixed x.

4.2.4 Akhmediev Breather Regime

The solution undergoes a morphological transformation into the Akhmediev breather (AB) regime when the spectral parameter is set to $\lambda_3 = 8i$. The state under consideration is characterised by two fundamental properties. Firstly, it displays periodicity in the spatial coordinate, x. Secondly, it exhibits pronounced localization along the temporal axis, t. As illustrated in Figure 4.3, the 3D spatiotemporal evolution of the intensity profile $|\Psi(x,t)|^2$ is presented. The surface plot reveals a characteristic arrangement where intensity maxima are distributed periodically across the spatial domain, while remaining strictly confined within a finite temporal window on the continuous-wave background. In the context of non-autonomous fiber systems, the Akhmediev breather regime is of significant theoretical and practical importance. The framework provides a robust basis for the investigation of modulation instability and serves as a critical mechanism for high-repetition-rate pulse generation and advanced optical pulse shaping[140, 141]. The stability of these localised peaks under time-varying coefficients further highlights the potential for the deterministic control of high-power waveforms in non-homogeneous dispersive media.

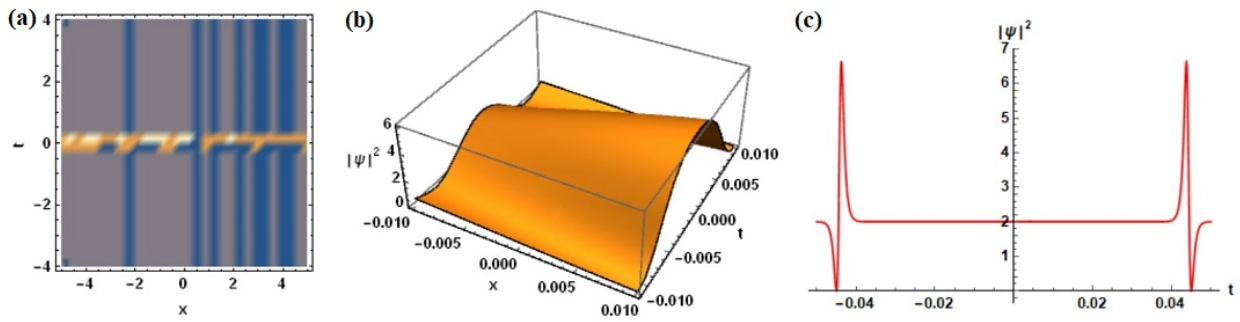

Figure 4.3: **Akhmediev breather solution** of the HNLS equation for spectral parameter $\lambda_3 = 8i$. (a) Contour plot of the solution, (b) 3D evolution of $|\psi|^2$ revealing the hallmark periodic structure in space with localized amplitude maxima and background modulation, and (c) temporal profile of $|\psi|^2$ at fixed position x.

4.2.5 Ma-type and Rogue Wave Breather Regime

As demonstrated in Figure 4.4, for the specific spectral parameter value of $\lambda_3 = -2i$, the system transitions into a mixed regime. This phenomenon highlights the significant sensitivity of breather dynamics to spectral detuning. Within this parametric configuration, even a narrow variation in the spectral domain can trigger extreme localization events, characterised by an exceptional concentration of wave energy. This regime is primarily associated with the formation of Ma-type breathers, which exhibit distinct temporal periodicity and rigorous spatial localization. The interaction between the time-dependent coefficients and the spectral parameters facilitates a transition towards rogue wave-like structures, where the wave amplitude undergoes a substantial, localised intensification. The emergence of these high-energy states demonstrates that the deterministic control of spectral detuning, coupled with the system's inherent non-autonomous variability, provides a robust framework for engineering targeted extreme waveforms in advanced nonlinear optical media[142].

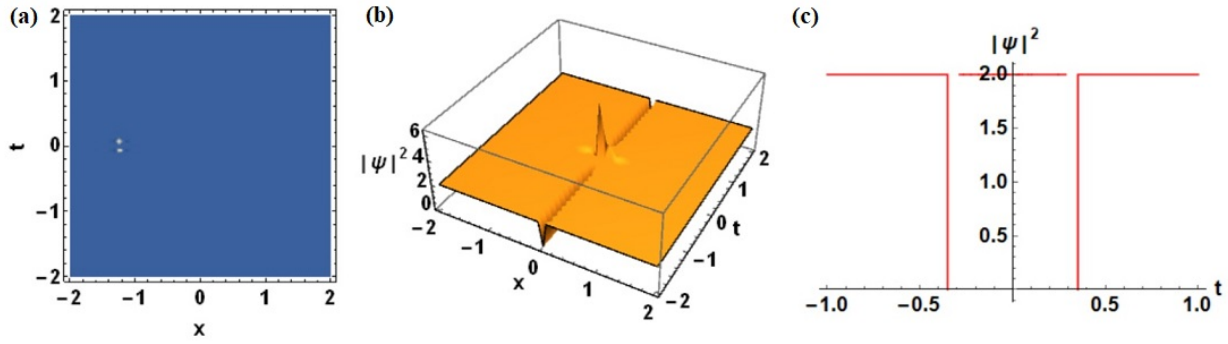

Figure 4.4: **Ma breather and rogue wave solution** of the HNLS equation for spectral parameter $\lambda_3 = -2i$. (a) Contour plot of the solution, (b) 3D evolution of $|\psi|^2$ revealing the hallmark periodic structure in space with localized amplitude maxima and background modulation, and (c) temporal profile of $|\psi|^2$ at fixed position x.

4.2.6 Rogue Wave (Peregrine Soliton) Regime

The solution is reduced to the Peregrine soliton when the spectral parameter is set to a specific critical value. The Peregrine soliton serves as the fundamental prototype for rogue wave phenomena. As demonstrated in Figure 4.5, these rational solutions are distinguished by a singular, high-intensity amplitude peak that is strictly localised in both the spatial and temporal domains, eventually decaying to a constant background. From a physical perspective, these characteristics are indicative of extreme nonlinear events that have been observed in a variety of media, including non-homogeneous optical fibres, hydrodynamic systems, and Bose-Einstein condensates (BECs)[139]. The emergence of such structures is of significant fundamental interest, as they signify the ultimate limit of sudden energy localization driven by modulation instability [100, 101, 112]. In the context of the non-autonomous HNLS equation, the stability and peak intensity of the Peregrine soliton are directly modulated by the time-dependent coefficients. This offers a potential mechanism for the deterministic excitation of extreme waves. In order to facilitate a clear comparison of the dynamical regimes discussed thus far, the specific choices of spectral parameters and time-dependent dispersion coefficients for Figures 4.1 through 4.5 are consolidated in Table 4.1.

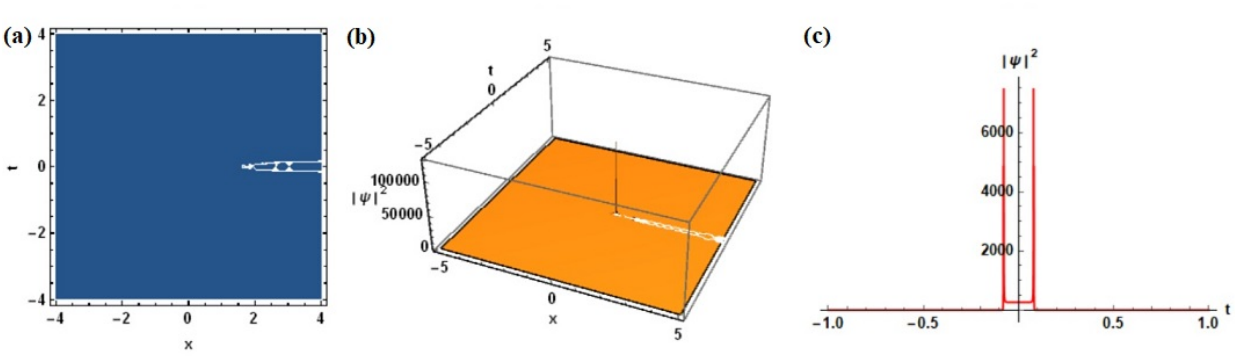

Figure 4.5: **Rogue wave (Peregrine soliton) solution** of the HNLS equation for spectral parameter $\lambda_3 = 1$. (a) Contour plot of the solution, (b) 3D evolution of $|\psi|^2$ displaying the sudden, steep amplitude peak localized in both x and t, and (c) temporal profile of $|\psi|^2$ at fixed position x.

Table 4.1: Summary of Breather Parameter Sets Used for Graphical Analysis in Figures 4.1â4.5.

Figure No(s).	**Wave Type**	$\boldsymbol{\lambda_3}$	$\boldsymbol{a_1(t)}$	$\boldsymbol{a_2(t)}$	$\boldsymbol{a_3(t)}$	$\boldsymbol{u_{111}}$	$\boldsymbol{u_{133}}$
Figure 4.1	General Breather	$\frac{\sqrt{2}}{2}i$	$2t$	$-t$	t	$-4i$	$4i$
Figure4.2	general to Ma breather	$2i$	$2t$	$-t$	t	i	-8
Figure 4.3	Akhmediev Breather	$8i$	$2t$	$-t$	t	$-2i$	$2i$
Figure 4.4	Ma + RW Mixed Case	$-2i$	$2t$	$-t$	t	$-8i$	8
Figure 4.5	Rogue Wave (Peregrine)	1	$2t$	$-t$	t	8	-8

4.2.7 Parameter Engineering: Dispersion and Nonlinearity Management

In order to elucidate the physical implications of the dynamical parameters presented in Figures 4.6–4.8, the distinct roles of the time-dependent coefficients are analysed as follows. The third-order dispersion (TOD) term, denoted by $a_3(t)$, governs the temporal drift and structural asymmetry of the breather, thereby providing a deterministic mechanism for trajectory control. The coefficient $a_1(t)$, representing group velocity dispersion (GVD), dictates the fundamental balance between dispersive broadening and nonlinear compression, thereby effectively determining the spatiotemporal scaling of the wave. Conversely, the nonlinearity coefficient $a_2(t)$ modulates the peak amplitude and self-focusing strength, facilitating the regulation of wave intensity and the suppression of inherent instabilities. It is evident that the variables $a_1(t)$, $a_2(t)$, and $a_3(t)$ are associated with quantifiable physi-

cal quantities, specifically GVD (ps^2/km), the Kerr nonlinear coefficient ($W^{-1}km^{-1}$), and TOD (ps^3/km), respectively. The concurrent modulation of these variables provides a physically consistent framework for the control of the localization, path, and robustness of nonlinear wave packets. As demonstrated in Figure 4.6, the transition of $a_3(t)$ from $10t$ to $-10t$ leads to a substantial attenuation of the degree of localization, resulting in a significant decrease in amplitude. Furthermore, the sign reversal of $a_3(t)$ induces a shift in the breather trajectory toward the opposite direction, confirming its dominant influence on propagation dynamics. The results obtained demonstrate that variations in TOD introduce controllable spatial drift, thereby allowing for the positioning of breathers or rogue waves without compromising their intrinsic morphology. The stable localisation of solitons within optical media is contingent upon an exact equilibrium between dispersive and nonlinear effects. By systematically adjusting the parameters $a_1(t)$ and $a_2(t)$, we seek to ascertain the manner in which this delicate equilibrium governs the stability of the wave. As illustrated

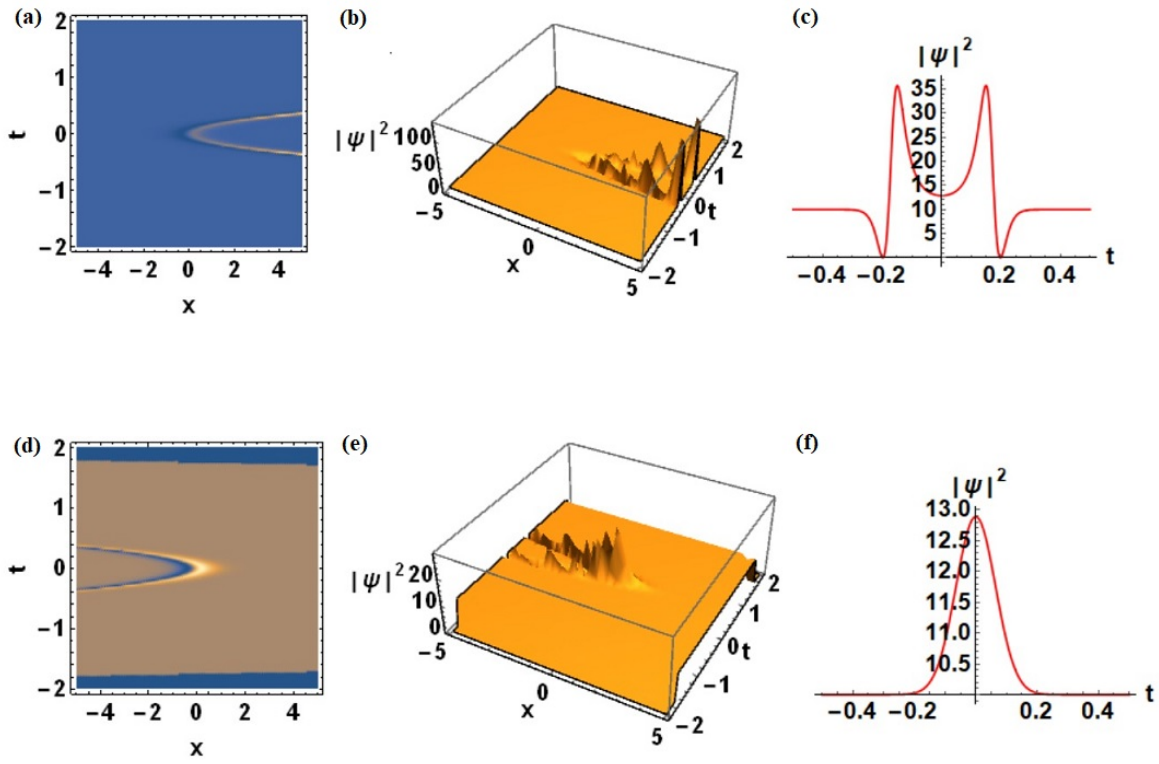

Figure 4.6: **Effect of time-dependent coefficients** on the evolution of breathers for a fixed spectral parameter $\lambda_3 = \frac{\sqrt{2}i}{2}$. The varying coefficients are defined as $a_1(t) = 10t$ and $a_2(t) = -t$ for: **(a–c)** $a_3(t) = 10t$, and **(d–f)** $a_3(t) = -10t$.

in Figures 4.7 and 4.8, the theoretical engineering of soliton dynamics can be achieved through the modulation of the relative strengths of these coefficients. As illustrated in

Figure 4.7, a significant enhancement in amplitude denotes the initiation of modulation instability. Conversely, Figure 4.8 demonstrates that amplitude suppression results in a more stable propagation regime. These findings suggest that by tailoring the non-autonomous coefficients, instabilities can be suppressed and robust, high-energy nonlinear wave packets can be generated. In the ensuing analysis, the time-dependent coefficients are adjusted while maintaining a fixed spectral parameter at $\lambda_3 = \frac{\sqrt{2}i}{2}$.

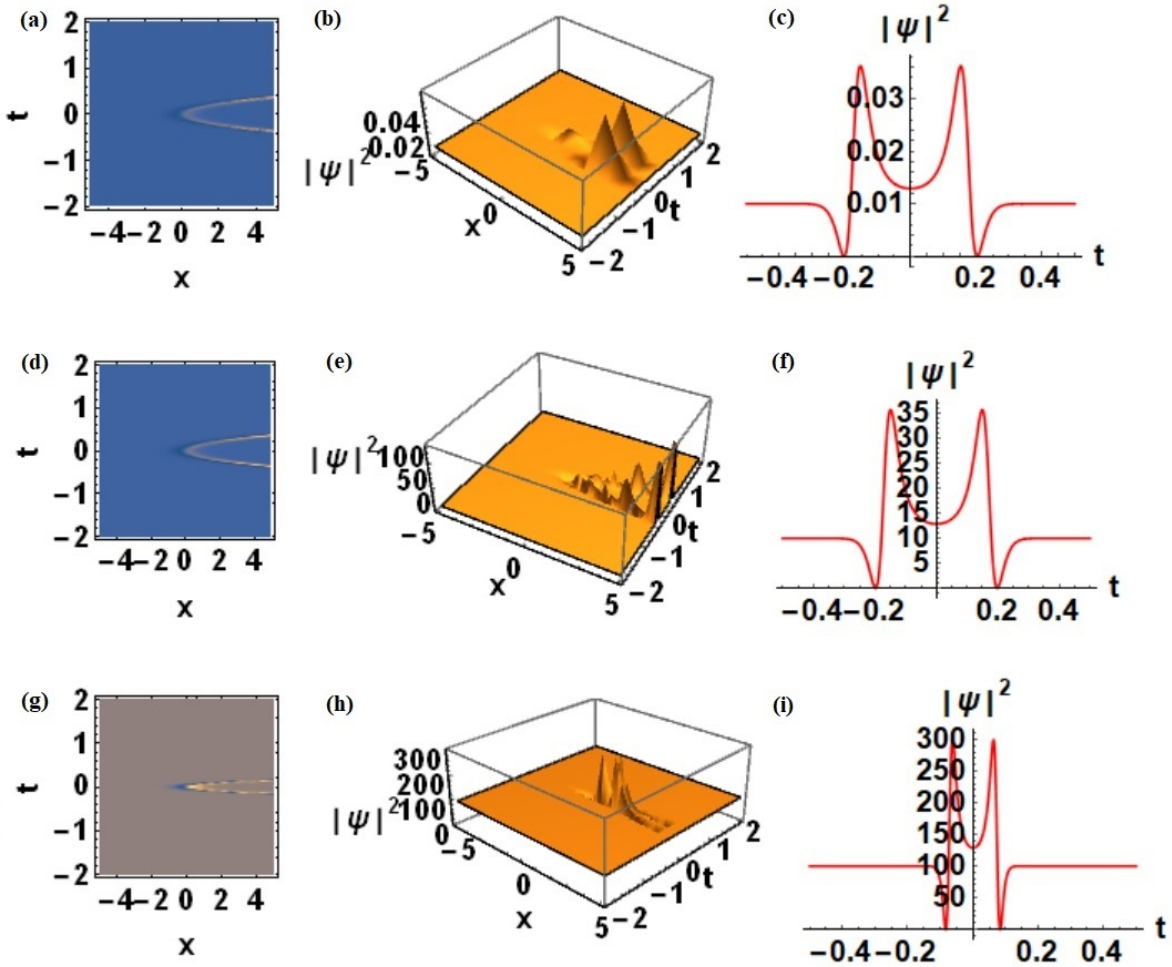

Figure 4.7: **Influence of the time-dependent coefficient** $a_1(t)$ on breather evolution. For a fixed spectral parameter $\lambda_3 = \frac{\sqrt{2}i}{2}$ with $a_3(t) = 10t$ and $a_2(t) = -t$, the cases shown are: **(a–c)** $a_1(t) = 0.01t$, **(d–f)** $a_1(t) = 10t$, and **(g–h)** $a_1(t) = 100t$.

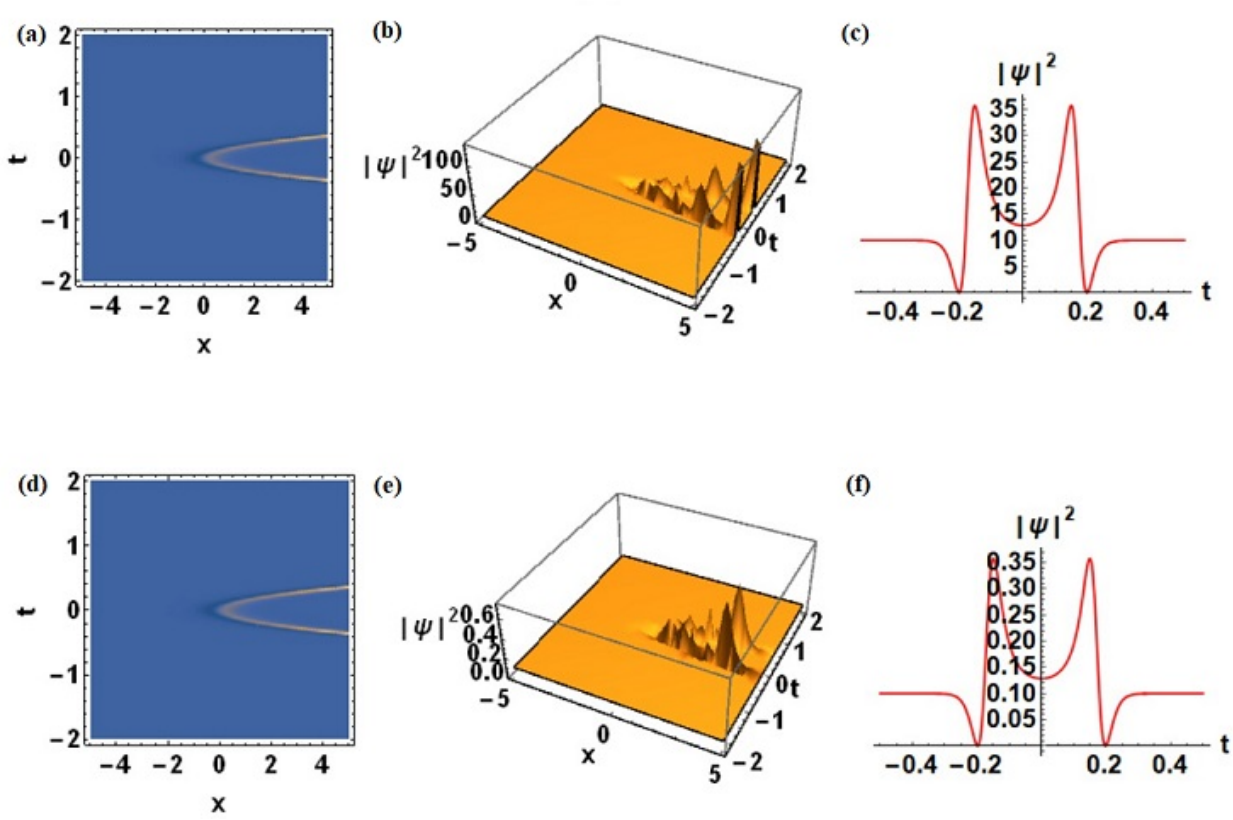

Figure 4.8: **Influence of the time-dependent coefficient** $a_2(t)$ on the breather evolution. For parameters $\lambda_3 = \frac{\sqrt{2}i}{2}$, $a_3(t) = 10t$, and $a_1(t) = 10t$, the effect of $a_2(t)$ is illustrated for: **(a–c)** $a_2(t) = -t$, and **(d–f)** $a_2(t) = -100t$.

4.2.8 Individual Parametric Influence of Time-Dependent Coefficients $a_i(t)$

In this subsection, a detailed interpretation of the results displayed in Figures 4.9–4.11 is presented. These figures illustrate the influence of different functional forms of the time-dependent coefficients, $a_1(t)$, $a_2(t)$, and $a_3(t)$, on the spatiotemporal evolution of breather-type localized waves. The significance of dispersion and nonlinearity management in stabilising or destabilising the nonlinear structures generated by the generalized HNLS equation is emphasised by these plots.

As illustrated in Figure 4.9, the selected parameters, namely $a_1(t) = cosh(2t)$, $a_2(t) = t$ and $a_3(t) = -t$, establish a highly non-autonomous environment, wherein the dispersion exhibits exponential growth over time, while the nonlinearity undergoes a linear evolution. This combination leads to a gradual broadening of the localized pulse, accompanied by a controlled reduction of its amplitude. This is indicative of enhanced temporal stability and reduced intensity fluctuations. The hyperbolic dependence of $a_1(t)$ has been demonstrated

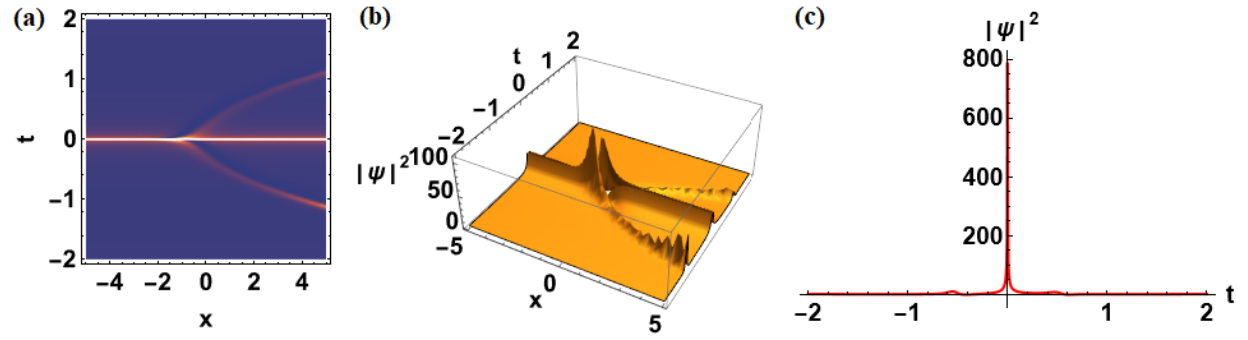

Figure 4.9: **Evolution of the rogue wave solution** with time-dependent coefficients $a_1(t) = \cosh(2t)$, $a_2(t) = t$, and $a_3(t) = -t$. All other parameters are identical to those in Fig. 4.8. (a) Contour plot of the solution, (b) three-dimensional evolution, and (c) temporal profile for a fixed position x.

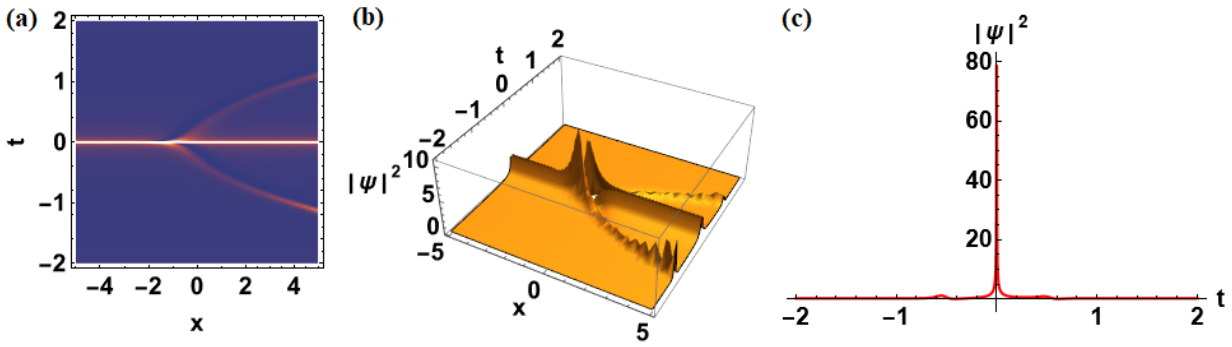

Figure 4.10: **Effect of the time-dependent coefficient** $a_2(t) = 10t$ on the breather evolution, with $a_1(t)$ and all other parameters identical to those in Fig. 4.9. (a) Contour plot of the solution, (b) three-dimensional evolution, and (c) temporal profile for a fixed position x.

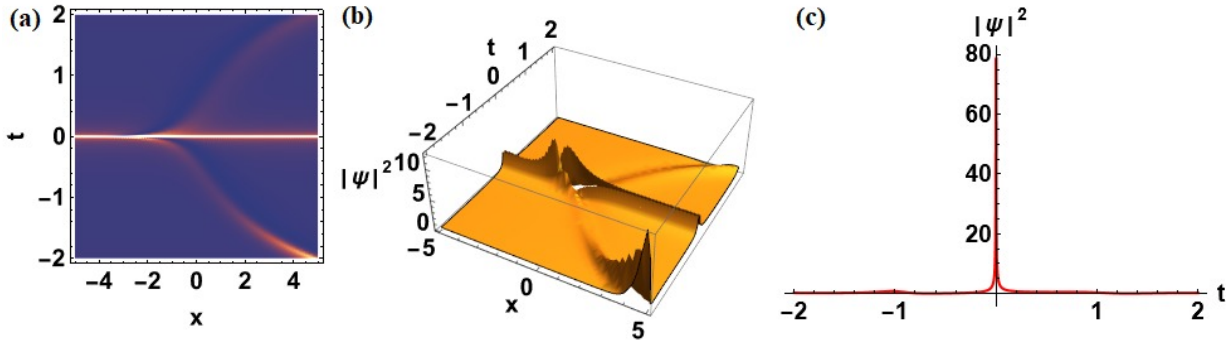

Figure 4.11: **Effect of the time-dependent coefficient** $a_3(t) = 2t$ on the evolution of the solution, with $a_1(t)$, $a_2(t)$, and all other parameters identical to those in Fig. 4.10. (a) Contour plot of the solution, (b) three-dimensional evolution, and (c) temporal profile for a fixed position x.

to effectively suppress excessive modulation instability, thereby ensuring a smoother energy distribution and stable wave confinement.

Figure 4.10 examines the effect of increasing the nonlinearity coefficient to $a_2(t) = 10t$ while maintaining the same $a_1(t)$ and $a_3(t)$ as in Figure 4.9. The enhanced nonlinear contribution has been shown to significantly amplify the breather's peak intensity and compress its width, thereby revealing the strong sensitivity of the localized amplitude to the nonlinear modulation strength. The corresponding contour and surface plots demonstrate a discernible increase in localization concomitant with a temporal narrowing, a hallmark of energy focusing driven by nonlinearity. This finding indicates that the nonlinearity term exerts a direct influence on the rate of energy accumulation and the formation of strongly confined breather structures. In Figure 4.11, the variation of the third-order dispersion coefficient to $a_3(t) = 2t$, with $a_1(t)$ and $a_2(t)$ fixed as in Figure 4.10, highlights the asymmetric deformation and drift of the breather envelope. The increase in $a_3(t)$ introduces a discernible spatial shift of the localization centre and modifies the temporal phase of the waveform without significantly altering its peak amplitude. This shift can be considered a physical manifestation of third-order dispersion-induced temporal drift, a phenomenon of particular relevance in the context of the control of pulse propagation in optical fibres and ultrafast systems. It is important to note that, despite this drift, the waveform retains its structural integrity, thereby emphasising the robustness of the system against higher-order dispersive perturbations.

4.2.9 Numerical Verification: L_2 Error and Spectral Analysis

The numerical stability of the analytical breather solution, denoted by $\Psi_{\text{analytical}}(x,t)$, was subjected to a rigorous examination. This was achieved by introducing a small-scale random perturbation with an amplitude of $\epsilon = 0.001$to the initial condition. The resulting evolution, denoted as $\Psi_{\text{perturbed}}(x,t)$, was evaluated against the exact analytical solution. The relative L_2 error, which serves as a metric for numerical fidelity, is defined as:

$$L_2 = \frac{\|\Psi_{\text{perturbed}}(x,t) - \Psi_{\text{analytical}}(x,t)\|_2}{\|\Psi_{\text{analytical}}(x,t)\|_2} \tag{4.11}$$

The simulations yielded an L_2 error of 6×10^{-4}, thereby confirming the high degree of fidelity and robustness of the initial breather state. Furthermore, spectral analysis con-

ducted via Fast Fourier Transformation (FFT) verified that the characteristic modes were strictly preserved throughout the propagation, with no evidence of spurious high-frequency components or numerical divergence. As demonstrated in Figure 4.12, the strong similarity between the analytical and perturbed states highlights the reliability of the numerical propagation for this nonautonomous system.

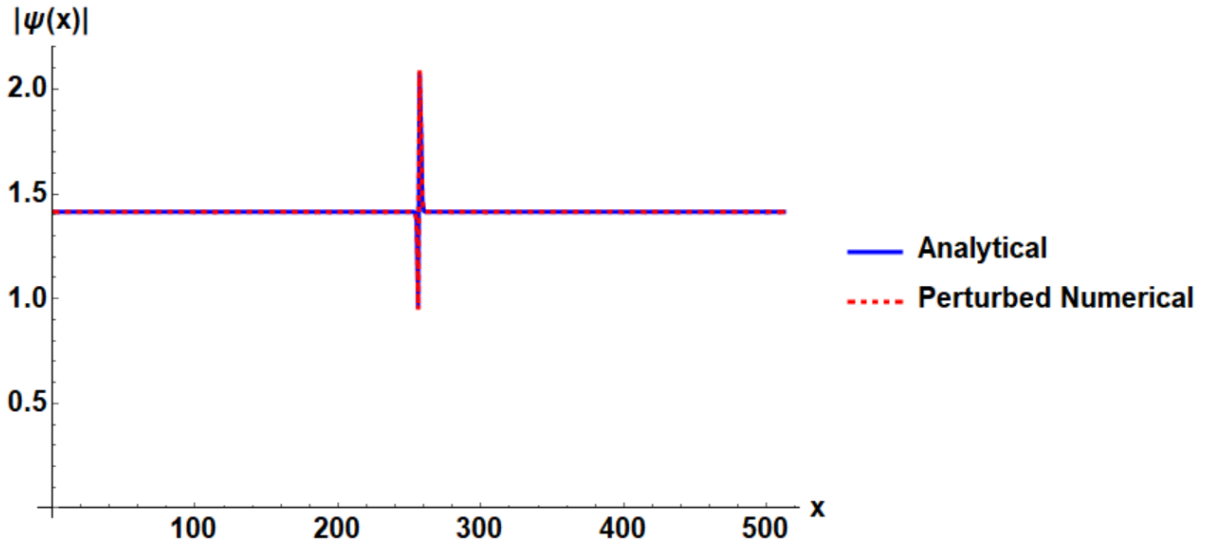

Figure 4.12: **Numerical validation of the breather solution.** Comparison of the analytical breather profile (solid blue line) against the numerically computed profile with a small initial perturbation ($\epsilon = 0.001$, solid red line). The plot demonstrates minimal deviation between the two profiles, confirming the accuracy and stability of the analytical solution for numerical propagation. The L_2 error for this initial profile is 6×10^{-4}.

4.2.10 Physical Insights and Applications

The results obtained through analytical and graphical investigations highlight the significant physical consequences of managing dispersion and nonlinearity in non-autonomous higher-order nonlinear Schrödinger (HNLS) systems. The dynamic interplay between the time-dependent coefficients, namely $a_1(t)$, $a_2(t)$, and $a_3(t)$, is represented by the group-velocity dispersion (GVD), the Kerr nonlinearity, and the third-order dispersion (TOD), respectively. This interplay functions as an effective control mechanism for tailoring localized waveforms, including breathers, rogue waves, and solitons. The modulation of these coefficients enables precise control over the amplitude, width, and localization of nonlinear excitations, thereby facilitating either stable propagation or the intentional induction of destabilized regimes. The physical roles of these parameters are summarised as follows:

- **Dispersion Management** $a_1(t)$**:** This coefficient is instrumental in regulating the broadening and compression of optical pulses. It has been demonstrated that a gradual increase in $a_1(t)$ results in enhanced pulse broadening and a reduction in peak intensity. This, in turn, fosters a stable regime with minimal modulation instability. Conversely, a rapid modulation or a sign change in $a_1(t)$ can trigger focusing behaviour, resulting in wave collapse or strong temporal compression.

- **Nonlinearity Control** $a_2(t)$**:** The function $a_2(t)$ has been demonstrated to act as a gain-like mechanism, thereby amplifying the local field energy. The findings demonstrate that increasing $a_2(t)$ enhances breather amplitude while simultaneously reducing its spatial extent, confirming that nonlinearity directly dictates energy concentration.

- **Higher-Order Effects** $a_3(t)$**:** The incorporation of TOD gives rise to phenomena such as asymmetry, spectral broadening, and envelope drift. The physical phenomenon under discussion can be considered to correspond to higher-order kinetic corrections in BoseâEinstein condensates (BEC) or third-order dispersion in fibre optics. This mechanism provides a means for "drift control," thereby enabling precise temporal synchronisation and routing of pulses.

The capacity to transition between typical breathers and extreme events, such as Peregrine rogue waves, is of practical significance in the field of fibre optics, where it contributes to the maintenance of signal integrity or the generation of high-intensity pulses. Beyond optics, these findings provide a theoretical roadmap for managing energy localization in plasma oscillations and BEC systems, where temporal tuning can be achieved via Feshbach resonances. It is evident that the integrated framework under consideration provides evidence to support the hypothesis that non-autonomous management of dispersion and nonlinearity serve as a universal mechanism for reconfigurable wave propagation across diverse physical media.

4.3 Comparative Advantages and Scientific Contributions

In order to delineate the specific contributions of the present study, a comparative analysis is provided with the author's previous research, as reported in reference [104] In the aforementioned investigation, the Higher-Order Nonlinear Schrödinger (HNLS) equation was analysed under the assumption of constant coefficients and a zero-background seed ($\Psi_0 = 0$). Consequently, the resulting wave structures were predominantly solitonic in na-

ture, characterised by stationary or linear translational dynamics. In contrast, the present study investigates the HNLS framework under the influence of time-dependent coefficients, $a_i(t)$, and employs a non-zero continuous-wave (CW) seed. This strategic modification gives rise to fundamentally novel dynamical behaviours, thereby facilitating the emergence of breather-type localized structures and rogue waves. It is mathematically feasible to obtain breathers in constant-coefficient models with a non-zero seed. However, the incorporation of temporal variability in $a_1(t), a_2(t),$ and $a_3(t)$ provides an additional degree of freedom for "parameter engineering". This enables the active control of pulse compression, peak intensity, and accelerated drift, features that are strictly inaccessible in static models. As illustrated in Table 4.2, the two models are distinguished by a number of key differences, particularly with regard to the integrability conditions, the selection of seed, and the subsequent analytical solutions.

Table 4.2: Comparative analysis of integrability, seed, and solutions between constant and time-dependent HNLS models.

Feature	**HNLS (Constant Coeff.)**	**HNLS (Time-Dependent Coeff.)**
Integrability	$a_4 = \frac{9a_2a_3}{2a_1}$ $a_5 = \frac{3a_2a_3}{2a_1}$	$a_4(t) = 3a_5(t)$ $a_5(t) = \frac{9a_2(t)a_3(t)}{8a_1(t)}$
Seed	0	$\Psi_0(x,t) = \frac{\exp\left(i\frac{a_1(t)}{3a_3(t)}x\right)}{\sqrt{-\frac{a_2(t)}{a_1(t)}}}$
Solution	$\Psi = \frac{A\exp\left(i\frac{a_1}{3a_3}\left(x+\frac{\pi}{2}\right)\right)}{\cosh(2x-b)}$	$\Psi = \Psi_0 \frac{2Be^F\cosh(H)+4\lambda_3 u_{111}e^Z\sinh(M)-T(x)}{2Be^F\cosh(H)+4\lambda_3 u_{133}e^Z\sinh(M)}$

The present study makes a significant extension to the analytical framework of the HNLS equation. By integrating temporal variability with a nonzero background seed, a more general class of solutions is revealed that reflects the non-homogeneous nature of real-world physical systems, such as non-uniform optical fibres and Bose-Einstein condensates.

4.4 Chapter Summary

In this chapter, we have presented a thorough analytical and numerical investigation into the dynamics of a generalized non-autonomous Higher-Order Nonlinear Schrödinger (HNLS) equation. By incorporating time-dependent coefficients for group-velocity dispersion $a_1(t)$, Kerr nonlinearity $a_2(t)$, and third-order dispersion $a_3(t)$, we have successfully demonstrated a framework for the active management of nonlinear wave structures. The primary findings

and contributions of this research are summarised as follows:

- **Analytical Framework:**The utilisation of a constructed 3×3 Lax pair in conjunction with the Darboux transformation resulted in the derivation of explicit breather and rogue-wave solutions. This methodological approach facilitated the investigation of wave dynamics under non-autonomous conditions, thereby extending the classical theory to more realistic, non-homogeneous media.

- **Parametric Control and Tuning:** The spectral parameter, designated as λ_3, was identified as a pivotal tuning variable that governs the seamless transition between diverse wave morphologies, including generalized breathers, Ma solitons, Akhmediev breathers, and Peregrine-type rogue waves.

- **Waveform Engineering:**The present study corroborates the hypothesis that temporal modulation of $a_1(t)$ and $a_2(t)$ provides a robust mechanism for regulating amplitude and localization width. Furthermore, the third-order dispersion term $a_3(t)$ was found to introduce structural asymmetry and a controlled trajectory drift without compromising the wave's peak intensity, serving as an effective "control switch" for pulse synchronization.

- **Numerical Validation:** The robustness of the analytical solutions was substantiated through numerical simulations using the split-step Fourier method. The calculated relative L_2 error norm, recorded at a high-fidelity value of 6×10^{-4}, confirms the inherent stability of the derived solutions against small perturbations. Crucially, the observed dynamics â such as targeted amplitude growth â were verified to be a result of intentional parametric modulation rather than numerical instability.

Notwithstanding the limitations of the present study, including the restriction to integrable regimes and the exclusion of stochastic or dissipative effects, the results provide a solid foundation for future research. The ability to engineer reconfigurable nonlinear states through time-dependent management offers significant prospects for the development of ultrafast photonic devices, coherent matter-wave engineering in Bose-Einstein condensates, and the prediction of extreme events in plasma physics. In conclusion, this integrated analytical and numerical approach demonstrates that the interplay of dispersion, nonlinearity, and higher-order effects is an efficient tool for regulating instability and achieving the controlled generation of localized nonlinear excitations across diverse physical systems.

General conclusion

The research presented in this thesis constitutes a rigorous investigation into the integrability, solution construction, and parametric control of higher-order nonlinear evolutionary equations. By systematically analysing the Hirota equation (HE), the Sasa-Satsuma equation (SSE), and the higher-order nonlinear Schrödinger equation (HNLS), a unified analytical framework has been established based on the Lax pair and Darboux transformation (DT). This work successfully bridges the gap between static theoretical models and dynamic, non-autonomous systems, providing a blueprint for the active management of localized wave structures. The key contributions of this research are detailed as follows:

- **Integrability and Structural Control:**It has been established that the HE with damping and linear potential remains integrable specifically under the influence of third-order dispersion $a_3(t)$ and self-steepening $a_4(t)$. A significant finding is that the $a_4(t)$ coefficient acts as the primary governor for the transition from general breathers to Akhmediev breathers, while $a_3(t)$ controls the centre-of-mass motion in optical fibres without requiring an external potential.

- **Seed Solution Dynamics:** Utilising the SSE as a paradigm, it was demonstrated that the nature of the derived solution is fundamentally dictated by the initial seed. A vacuum seed, i.e. a seed of zero value, yields localized solitonic pulses, whereas a non-zero constant seed, i.e. a seed of a non-zero value, triggers complex wave structures. In this context, parameters such as the spectral variable, denoted by the letter "lambda", and higher-order constants serve as the primary mechanisms for wave emergence and peak modulation.

- **Waveform Engineering via Time-Dependency:** The transition to time-dependent coefficients ($a_1(t), a_2(t), a_3(t)$) in the HNLS model enables the "engineering" of wave morphologies. It has been identified that temporal modulation of dispersion and nonlinearity regulate amplitude and width, while $a_3(t)$ functions as a "control switch" for pulse synchronisation by introducing structural asymmetry and trajectory drift.

- **Stability and Numerical Validation:**The robustness of these analytical solutions was confirmed through the use of the split-step Fourier method. With a calculated relative L_2 error norm of 6×10^{-4}, it was demonstrated that the observed dynamics â including targeted amplitude growth â are the result of intentional parametric management, rather than numerical instability or stochastic noise.

In conclusion, the present research demonstrates that the interplay between time-varying dispersion, nonlinearity, and higher-order effects is an efficient tool for achieving the controlled generation of nonlinear excitations. The analytical benchmarks established for breathers, rogue waves, and hybrid interaction states provide a solid foundation for future applications in ultrafast photonics, plasma physics, and Bose-Einstein condensates.

Appendix A

2-4-4-1 Solitonic solution

we derive the compatibility equations, we found 4 equations :2 equations for time and 2 equations for space :

$$eqt1x = -\sqrt{\frac{a_4(t)}{6a_3(t)}}\,\psi_0(x,t)\,\phi_2(x,t) + \lambda_2\left(\sqrt{6}\,c_{315} - cf_{411}(x,t)\right)\psi_2(x,t) + \psi_2^{(1,0)}(x,t). \tag{4.12}$$

$$eqt2x = -\lambda_2\,cf_{411}(x,t)\,\phi_2(x,t) + \sqrt{\frac{a_4(t)}{6a_3(t)}}\,\psi_0^*(x,t)\,\psi_2(x,t) + \phi_2^{(1,0)}(x,t). \tag{4.13}$$

$$\begin{aligned} eqt1t = &-\lambda_1^3\left(6\sqrt{6}\,c_{315}^3 a_3(t) + cg_{219}(t)\right)\psi_2(x,t) \\ &+ \lambda_1^2\left(\sqrt{\frac{6a_4(t)}{a_3(t)}}c_{315}^2 a_3(t)\,\psi_0(x,t)\phi_2(x,t) - cg_{21}(t)\psi_2(x,t)\right) \\ &+ \psi_2^{(0,1)}(x,t) - \lambda_2\left(cg_{411}(x,t) + \frac{1}{\sqrt{6}}c_{315}a_4(t)\psi_0\psi_0^*\right)\psi_2(x,t). \end{aligned} \tag{4.14}$$

$$\begin{aligned} eqt2t = &-\lambda_1^3 cg_{219}(t)\phi_2(x,t) - \lambda_1^2\left((-6ic_{315}^2 a_1(t) + cg_{21}(t))\phi_2(x,t)\right) \\ &+ \phi_2^{(0,1)}(x,t) - \lambda_2 cg_{411}(x,t)\phi_2(x,t). \end{aligned} \tag{4.15}$$

Applying the seed solution $\psi_0(x,t) = 0$ (and thus $\psi_0^*(x,t) = 0$), the system simplifies to:

$$eqt1x = -\lambda_2\left(-\sqrt{6}c_{315} + cg_{411}(x,t)\right)\psi_2(x,t) + \psi_2^{(1,0)}(x,t). \tag{4.16}$$

$$eqt2x = -\lambda_2 cg_{411}(x,t)\phi_2(x,t) + \phi_2^{(1,0)}(x,t). \tag{4.17}$$

$$\begin{aligned} eqt1t = &-\lambda_1^2 cg_{21}(t)\psi_2(x,t) - \lambda_1^3(6\sqrt{6}c_{315}^3 a_3(t) + cg_{219}(t))\psi_2(x,t) \\ &- \lambda_2 cg_{411}(x,t)\psi_2(x,t) + \psi_2^{(0,1)}(x,t). \end{aligned} \tag{4.18}$$

$$eqt2t = -\lambda_2^2(-6ic_{315}^2 a_1(t) + cg_{21}(t))\phi_2(x,t) - \lambda_2^3 cg_{219}(t)\phi_2(x,t) - \lambda_2 cg_{411}(x,t)\phi_2(x,t) + \phi_2^{(0,1)}(x,t). \tag{4.19}$$

$\psi^{(0,n)}(x,t) = \frac{d^n\psi(x,t)}{d\,t^n}$
$\psi^{(n,t)}(x,t) = \frac{d^n\psi(x,t)}{d\,x^n}$

Thus, the linear system admits the solutions:

$$\psi_2(x,t) = c_{111}(t)\,\exp\left[\int \left(\lambda_2 cg_{411}(x,t) - \sqrt{6}c_{315}\lambda_2\right) dx\right], \tag{4.20}$$

$$\phi_2(x,t) = c_{112}(t)\,\exp\left[\int \lambda_2 cg_{411}(x,t)\,dx\right]. \tag{4.21}$$

where $c_{111}(t)$ and $c_{112}(t)$ are given by:

$$c_{111}(t) = c_{1110}\exp\left[\int \frac{g(t) - 2a_4(t)(U(x,t)+L(x,t)) + h(x,t)}{2a_4(t)^{3/2}}\,dt\right], \tag{4.22}$$

$$c_{112}(t) = c_{1120}\exp\left[-i\lambda_2^2\int \left(6c_{315}^2 a_1(t) + cg_{21}(t) + cg_{219}(t)\right) dt\right]. \tag{4.23}$$

- **Definition of functions:**

$$g(t) = 12\,\sqrt{6}\,c_{315}^3\,\lambda_2^3\,a_3(t)\,a_4(t)^{3/2} + 2\,\lambda_2^2\,a_4(t)^{3/2}cg_{21}(t) + 2\,\lambda_2^3\,a_4(t)^{3/2} cg_{219}(t) + 2\,\lambda_2\,a_4(t)^{3/2}\,cg_{411}(x,t) \tag{4.24}$$

$$U(x,t) = -\int \sqrt{\frac{3}{2}}\,c_{315}\lambda_2\left(\frac{a_{3t}(t)}{a_3(t)}\sqrt{a_4(t)} + \frac{a_3(t)}{\sqrt{a_4(t)}}\left(-\frac{a_4(t)a_{3t}(t)}{a_3^2(t)} + \frac{a_{4t}(t)}{a_3(t)}\right)\right) dx \tag{4.25}$$

$$L(x,t) = \int \left(\frac{1}{2\sqrt{a_4(t)}}\lambda_2\,cf_{411}(x,t)\,a_{4t}(t) + \lambda_2\sqrt{a_4(t)}\,cg_{411}^{(1,0)}(x,t)\right) dx \tag{4.26}$$

$$h(x,t) = \left(\int \left(-\sqrt{6}\,c_{315}\lambda_2\sqrt{a_4(t)}\,cf_{411}(x,t) + \lambda_2\sqrt{a_4(t)}\,cf_{411}(x,t)\right) dx\right) a_{4,t}(t) \tag{4.27}$$

- **Simplified general solutions:**

$$\psi_2(x,t) = c_{1110}\ \exp[\int ((\frac{g(t) - \ 2a_4(t)(U(x,t)+L(x,t)) + h(x,t)}{2\ a_4(t)^{3/2}}\,dt) + s(x,t)\,dx)] \tag{4.28}$$

$$\phi_2(x,t) = c_{1120}\ \exp[\int \lambda_2\ cg_{411}(x,t)dx - i\lambda_2^2\int (6\ c_{315}^2\ a_1(t) + i\ cg_{21}(t) + i\ cg_{219}(t))dt] \tag{4.29}$$

with:

$$s(x,t) = \lambda^2 cg_{411}(x,t) - \sqrt{6} c_{315} \lambda^2 \tag{4.30}$$

Using the trivial seed solution $\psi_0(x,t)$ of the Hirota equation, and the substitutions $\phi_2 = -\psi_1^*$ and $\psi_2 = \phi_1^*$, the system yields:

$$\psi_1^*(x,t) = -c_{1120} \exp[\int \lambda_2 \; cg_{411}(x,t)dx - i\lambda_2^2 \int (6 \; c_{315}^2 \; a_1(t) + i \; cg_{21}(t) + i \; cg_{219}(t))dt] \tag{4.31}$$

$$\phi_1^*(x,t) = c_{1110} \; \exp[\int ((\frac{g(t) - \; 2a_4(t)(U(x,t) + L(x,t)) + h(x,t)}{2 \; a_4(t)^{3/2}} \; dt) + s(x,t) \; dx)] \tag{4.32}$$

$$\psi_2(x,t) = c_{1110} \; \exp[\int ((\frac{g(t) - \; 2a_4(t)(U(x,t) + L(x,t)) + h(x,t)}{2 \; a_4(t)^{3/2}} \; dt) + s(x,t) \; dx)] \tag{4.33}$$

$$\phi_2(x,t) = c_{1120} \; \exp[\int \lambda_2 \; cg_{411}(x,t)dx - i\lambda_2^2 \int (6 \; c_{315}^2 \; a_1(t) + i \; cg_{21}(t) + i \; cg_{219}(t))dt] \tag{4.34}$$

where c_{1110} and c_{1120} are real arbitrary constants of integration. We consider the Darboux transformation:

$$\psi[1] = \psi\Lambda - \sigma\psi, \tag{4.35}$$

where

$$\sigma = \psi_0 \, \Lambda \, \psi_0^{-1}. \tag{4.36}$$

The transformed operator is given by:

$$U_0[1] = \sigma U \sigma^{-1} + \sigma_x \sigma^{-1}. \tag{4.37}$$

Fixing the parameters:

$$\lambda_1 = -1, \quad \lambda_2 = 1, \quad c_{315} = 1, \quad cg_{411}(x,t) = x, \quad cf_{411}(x,t) = t,$$

$$c_{1110} = c_{1120} = 1, \quad cg_{21}(t) = 5, \quad cg_{219}(t) = 2,$$

2-4-2 Lax pair:

where

$$Y(x,t) = c_2(t)^2(-i\ (a_1(t) + c_4(t)\ a_3(t))\ \psi_0(x,t)\ \psi_0(x,t) + \ a_3(t)(\psi_0^*(x,t) \\ \psi_0^{(1,0)}(x,t) - \psi_0(x,t)\ \psi_0^{(1,0)}(x,t))) \tag{4.38}$$

$$L(x,t) = i\ c_2(t) \exp[G(x,t)]\ (-(c_4(t)\ a_1(t) + c_4(t)^2\ a_3(t))\ \psi_0(x,t)) - i\ (a_1(t) \\ + c_4(t)a_3(t))\ \psi_0^{(1,0)}(x,t) + a_3(t)\ \psi_0^{(2,0)}(x,t) + \frac{1}{3}a_4(t)\ \psi_0(x,t)^2\ \psi_0^*(x,t) \tag{4.39}$$

$$k(x,t) = -i\ c_2(t) \exp[-G(x,t)]\ (-(c_4(t)\ a_1(t) + c_4(t)^2\ a_3(t))\ \psi_0^*(x,t) + i\ (a_1(t) \\ + c_4(t)\ a_3(t))\ \psi_0^{(1,0)}(x,t)^* + a_3(t)\ \psi_0^{(2,0)}(x,t)^* + \frac{1}{3}\ a_4(t)\ \psi_0^*(x,t)^2\ \psi_0(x,t)) \tag{4.40}$$

$$P(x,t) = -c_2(t)^2\ (-i\ (a_1(t) + c_4(t)\ a_3(t))\ \psi_0(x,t)\ \psi_0^*(x,t) + a_3(t)\ (\psi_0^*(x,t) \\ \psi_0^{(1,0)}(x,t) - \psi_0(x,t)\ \psi_0^{(1,0)}(x,t)^*)) \tag{4.41}$$

$$Z(x,t) = \sqrt{\frac{a_4(t)}{a_3(t)}}\ c_{315}\ (-i\ a_1(t)\ \psi_0(x,t) + a_3(t)\ \psi_0^{(1,0)}(x,t)) \tag{4.42}$$

$$T(x,t) = \ \mathrm{c}g_{411}(x,t) - \frac{1}{\sqrt{6}}\ c_{315}\ a_4(t)\ \psi_0(x,t)\ \psi_0^*(x,t) \tag{4.43}$$

Where:

$c_2(t) = i\ \sqrt{\frac{a_4(t)}{6\ a_3(t)}}$, $cf_{411}(x,t)^{(0,1)} = cg_{411}^{(1,0)}(x,t)$, $G(x,t) = 0$, $c_3 = 0$, $c_4(t) = 0$,
$\psi(x,t)^{(1,0)} = \frac{\partial\psi(x,t)}{\partial x}$,
$\psi(x,t)^{(0,1)} = \frac{\partial\psi(x,t)}{\partial t}$.

2-4-4-2 Breather solution

First case: The breather solution of Higher Hirota Equation:

$$\psi(x,t) = -\ \frac{\exp(\ ix)\ Q(x,t)}{Q_1(x,t)} \tag{4.44}$$

where: where $c_1 = -c_2$, $\lambda_1 = -\lambda_2$, $cg_{411}(x,t) = 1, cf_{411}(x,t) = 1, cg_{21}(t) = 1, cg_{219}(t) = 1$.

$$Q(x,t) = A\cosh[\frac{1}{36}(6\ \sqrt{3}\ x - C\int a_3(t)dt)](-B\cosh[\frac{1}{36}B(6\sqrt{3} - D\int a_3(t)dt)] + W\sinh[\frac{1}{36}B(6\sqrt{3}x - D\int a_3(t)dt)]) + \sinh[\frac{1}{36}A(6\sqrt{3}x - C\int a_3(t)dt)] \quad (4.45)$$
$$(iMB\cosh[\frac{1}{36}\ B\ (6\ \sqrt{3}\ x - D\int a_3(t)\ dt)] + N\sinh\ [\frac{1}{36}B\ (6\sqrt{3}\ x - D\int a_3(t)\ dt)])$$

$$Q_1(x,t) = (A\cosh[\frac{1}{36}A(6\ \sqrt{3}\ x - C\int a_3(t)dt)](B\cosh[\frac{1}{36}B(6\ \sqrt{3}\ x - D\int a_3(t)dt)] M\sinh[\frac{1}{36}B(6\sqrt{3}x - D\int a_3(t)dt)]) + \sinh[\frac{1}{36}A(6\sqrt{3}x - C\int a_3(t)dt)] \quad (4.46)$$
$$(WB\cosh[\frac{1}{36}B(6\ \sqrt{3}\ x - D\int a_3(t)dt)] + Y\sinh[\frac{1}{36}B(6\sqrt{3}x - D\int a_3(t)dt)])$$

and:

$$A = \sqrt{-1 - 6\ i\ \sqrt{6}\ c315\ \lambda_2 + 18\ c315^2\ \lambda_2^2} \quad (4.47)$$

$$B = \sqrt{-1 + 6\ i\ \sqrt{6}\ c315\ \lambda_2 + 18\ c315^2\ \lambda_2^2} \quad (4.48)$$

$$C = \sqrt{3} - 9\ i\ \sqrt{2}\ c315\ \lambda_2 + 36\ \sqrt{3}\ c315^2\ \lambda_2^2 \quad (4.49)$$

$$D = \sqrt{3} + 9\ i\ \sqrt{2}\ c315\ \lambda_2 + 36\ \sqrt{3}\ c315^2\ \lambda_2^2 \quad (4.50)$$

$$M = \sqrt{3} + 3\ i\ \sqrt{2}\ c315\ \lambda_2 \quad (4.51)$$

$$N = -5 - 12\ i\ \sqrt{6}\ c315\ \lambda_2 + 54\ \sqrt{3}\ c315^2\ \lambda_2^2 \quad (4.52)$$

$$W = -\ i\ \sqrt{3} + 9\ \sqrt{2}\ c315\ \lambda_2 \quad (4.53)$$

$$Y = 5 + 18\ c315^2\ \lambda_2^2 \tag{4.54}$$

Second case: the solution of Standard Hirota Equation:

$$\psi(x,t) = \frac{-(\lambda_1 - \lambda_2)\, e^{\frac{1}{6}x(A+3M_2)}\, B(x,t)\, P(x,t) + e^{ix} Y_2(x,t)}{\sqrt{\frac{a_4(t)}{a_3(t)}}\, Y_2(x,t)} \tag{4.55}$$

where

$$\begin{aligned}
A &= -3\sqrt{6}\, c_{315}\lambda_1 + 3i, \\
A_2 &= -3\sqrt{6}\, c_{315}\lambda_1 - 3i, \\
B &= \sqrt{3}\sqrt{18c_{315}^2\lambda_1^2 + 6i\sqrt{6}c_{315}\lambda_1 - 5}, \\
B_2 &= \sqrt{3}\sqrt{18c_{315}^2\lambda_1^2 - 6i\sqrt{6}c_{315}\lambda_1 - 5}, \\
M &= -\sqrt{6}c_{315}\lambda_1 - i, \\
M_2 &= -\sqrt{6}c_{315}\lambda_1 + i,
\end{aligned}$$

$$
\begin{aligned}
S &= \sqrt{-\frac{2}{3} + (\sqrt{6}c_{315}\lambda_1 + i)^2},\\
S_2 &= \sqrt{-\frac{2}{3} + (\sqrt{6}c_{315}\lambda_1 - i)^2},\\
T &= 3\sqrt{6}\, c_{315}\lambda_1 + 3i,\\
Z(t) &= \frac{a_3(t)\Big(324\sqrt{3}\, c_{315}^4\lambda_1^4 + 162i\sqrt{2}\, c_{315}^3\lambda_1^3 - 18\sqrt{3}\, c_{315}^2\lambda_1^2 + 9i\sqrt{2}\, c_{315}\lambda_1 + 10\sqrt{3}\Big)}{18\sqrt{18c_{315}^2\lambda_1^2 + 6i\sqrt{6}c_{315}\lambda_1 - 5}},\\
Z_2(t) &= \frac{a_3(t)\Big(324\sqrt{3}\, c_{315}^4\lambda_1^4 - 162i\sqrt{2}\, c_{315}^3\lambda_1^3 - 18\sqrt{3}\, c_{315}^2\lambda_1^2 - 9i\sqrt{2}\, c_{315}\lambda_1 + 10\sqrt{3}\Big)}{18\sqrt{18c_{315}^2\lambda_1^2 - 6i\sqrt{6}c_{315}\lambda_1 - 5}},\\
Y(x,t) &= \cosh\Big(\frac{Sx}{2} - \int Z(t)\, dt\Big)\cosh\Big(\frac{S_2x}{2} - \int Z_2(t)\, dt\Big),\\
B_2(x,t) &= T\cosh\Big(\frac{B_2x}{6} - \int Z_2(t)\, dt\Big) - B\sinh\Big(\frac{B_2x}{6} - \int Z_2(t)\, dt\Big),\\
H_2(x,t) &= TB_2(x,t)\cosh\Big(\frac{Bx}{6} - \int Z(t)\, dt\Big) + B\big(-B_2(x,t)\big)\sinh\Big(\frac{Bx}{6} - \int Z(t)\, dt\Big),\\
Y_2(x,t) &= e^{\frac{1}{6}x(A+A_2)}H_2(x,t) + 6e^{\frac{1}{2}x(M+M_2)}Y(x,t),\\
P(x,t) &= 6\sqrt{6}\, c_{315}\cosh\Big(\frac{S_2x}{2} - \int Z_2(t)\, dt\Big),\\
B(x,t) &= T\cosh\Big(\frac{Bx}{6} - \int Z(t)\, dt\Big) - B\sinh\Big(\frac{Bx}{6} - \int Z(t)\, dt\Big)
\end{aligned}
$$

.

2-4-4-3 Breather solution

The breather solution of satsa satsuma equation:

$$\psi(x,t) = \frac{i\,(H(x,t) + G(x)M(x,t) - L(x,t))}{H(x,t)L(x,t)} \tag{4.56}$$

Here, the functions $H(x,t)$, $M(x,t)$, $L(x,t)$, and $G(x)$ are constructed from combinations of exponential and hyperbolic functions arising from the spectral problem. These terms encode the interaction between different modes associated with the eigenvalues $\lambda_1, \lambda_2, \lambda_3$.

The function $G(x)$ is given by:

$$G(x) = \frac{1}{4} u_{133} \exp\left(-\frac{x\left(\sqrt{3\lambda_1^2 u_{133}^2 - 4} + \sqrt{3\lambda_2^2 u_{133}^2 - 4} + \sqrt{3\lambda_3^2 u_{133}^2 - 4}\right)}{2\sqrt{3}} \right)$$

The remaining components $H(x,t)$, $M(x,t)$, and $L(x,t)$ are expressed through combinations of:

* exponential functions $e^{K_i x + S_i(t)}$, * hyperbolic functions $\sinh(\cdot)$ and $\cosh(\cdot)$, * and auxiliary phase functions.

$$\begin{aligned}
H(x,t) = &\left(2c_8 e^{\frac{K_3 x}{2} + S_3(t)} \sinh(A_3(x,t)) - \frac{1}{2} c_7 D_3(x,t)\right) \\
&\times \left[\frac{1}{6}\left(2c_2 e^{\frac{K_2 x}{2} + S_2(t)} \cosh(A_2(x,t)) + \frac{1}{2} c_1 D_2(x,t)\right)\right. \\
&\quad \times \left(e^{\frac{K_1 x}{2} + S_1(t)} (6c_5 K_1 \cosh(B_1(x,t)) + 2c_5 T_1 \sinh(B_1(x,t)))\right) \\
&\quad - \frac{1}{6}\left(2c_5 e^{S_1(t) + \frac{x K_1}{2}} \cosh(A_1(x,t)) + \frac{1}{2} c_4 D_1(x,t)\right) \\
&\quad \left. \times \left(e^{\frac{K_2 x}{2} + S_2(t)} (6c_2 K_2 \cosh(B_2(x,t)) + 2c_2 T_2 \sinh(B_2(x,t)))\right)\right]
\end{aligned}$$

$$
\begin{aligned}
M(x,t) =& \lambda_3 \left(c_7 e^{E_3(t)+K_3 x+\frac{1}{2}x\sqrt{\lambda_3^2 u_{133}^2-\frac{4}{3}}} - 2e^{\frac{K_3 x}{2}} \left((c_9-c_8)\sinh(Z_3(x,t)) + (c_8+c_9)\cosh(Z_3(\right. \right. \\
& \times \left(2c_4 \left((c_3-c_2)\sinh(R_2(t)) + (c_2+c_3)\cosh(R_2(t)) \right) e^{\frac{1}{6}x(6K_1+3K_2+T_1)+P_1(t)} \right. \\
& \left. \left. - 2c_1 e^{\frac{1}{6}x(3K_1+6K_2+T_2)+P_2(t)} \left((c_6-c_5)\sinh(Z_1(x,t)) + (c_5+c_6)\cosh(Z_1(x,t)) \right) \right) \right. \\
& - 2\lambda_1 \left(c_4 e^{E_1(t)+\frac{1}{2}\sqrt{K_1^2-\frac{4}{3}}x+K_1 x} - 4\cosh\left(F_1 + \frac{xT_1}{3} \right) e^{\frac{K_1 x}{2}+\frac{S_1(t)}{2}} \right) \\
& \times \left(c_2 c_7 e^{\left(\frac{1}{9}(3a_5 K_2^2 T_2^2+2a_5 T_2+9S_2(t))+\frac{1}{6}x(3K_2+6K_3+T_3)+P_3(t)\right)} \right. \\
& - 2c_1 \cosh\left(F_3 + \frac{xT_3}{3} \right) e^{\frac{1}{6}x(6K_2+3K_3+T_2)+P_2(t)+\frac{S_3(t)}{2}} \\
& \left. + c_3 c_7 e^{\frac{1}{6}x(3K_2+6K_3+2T_2+T_3)+P_3(t)+S_2(t)} \right) \\
& + 2\lambda_2 \left(c_1 e^{E_2(t)+K_2 x+\frac{1}{2}x\sqrt{\lambda_2^2 u_{133}^2-\frac{4}{3}}} - 4\cosh\left(F_2 + \frac{xT_2}{3} \right) e^{\frac{K_2 x}{2}+S_2(t)} \right) \\
& \times \left(c_7 \cosh\left(F_1 + \frac{xT_1}{3} \right) e^{K_1 x+\frac{P_3(t)}{9}+\frac{S_1(t)}{2}+xK_2} \right. \\
& \left. \left. - c_4 e^{\frac{1}{6}x(6K_1+3K_3+T_1)+P_1(t)} \left(c_8 e^{F_3+S_3(t)} + c_9 e^{-F_3+S_3(t)+\frac{T_3 x}{3}} \right) \right) \right)
\end{aligned}
$$

$$
\begin{aligned}
L(x,t) = &\left(2c_2 e^{\frac{K_2 x}{2}+S_2(t)}\cosh(A_2(x,t)) - \frac{1}{2}c_1 D_2(x,t)\right)\\
&\times\left[\frac{1}{6}\left(2c_8 e^{\frac{K_3 x}{2}+S_3(t)}\cosh(A_3(x,t)) + \frac{1}{2}c_7 D_3(x,t)\right)\right.\\
&\quad\times\left(e^{\frac{K_1 x}{2}+S_1(t)}(6c_5 K_1\cosh(B_1(x,t)) + 2c_5 T_1\sinh(B_1(x,t)))\right)\\
&\quad-\frac{1}{6}\left(2c_5 e^{\frac{K_1 x}{2}+S_1(t)}\cosh(A_1(x,t)) + \frac{1}{2}c_4 D_1(x,t)\right)\\
&\quad\left.\times\left(e^{\frac{K_3 x}{2}+S_3(t)}(6c_9 K_3\sinh(B_3(x,t)) + 2c_9 T_3\cosh(B_3(x,t)))\right)\right]\\
&+\left(2c_5 e^{\frac{K_1 x}{2}+S_1(t)}\cosh(A_1(x,t)) - \frac{1}{2}c_4 D_1(x,t)\right)\\
&\times\left[\frac{1}{6}\left(2c_8 e^{\frac{K_3 x}{2}+S_3(t)}\cosh(A_3(x,t)) + \frac{1}{2}c_7 D_3(x,t)\right)\right.\\
&\quad\times\left(e^{\frac{K_2 x}{2}+S_2(t)}(6c_2 K_2\cosh(B_2(x,t)) + 2c_2 T_2\sinh(B_2(x,t)))\right)\\
&\quad-\frac{1}{6}\left(2c_2 e^{\frac{K_2 x}{2}+S_2(t)}\cosh(A_2(x,t)) + \frac{1}{2}c_1 e^{E_2(t)+K_2 x}\right)\\
&\quad\left.\times\left(e^{\frac{K_3 x}{2}+S_3(t)}(6c_9 K_3\sinh(B_3(x,t)) + 2c_9 T_3\cosh(B_3(x,t)))\right)\right]
\end{aligned}
$$

The key quantities are defined as:

$$
\begin{aligned}
K_i &= \lambda_i u_{133},\\
T_i &= \sqrt{9\lambda_i^2 u_{133}^2 - 12},\\
F_i &= \frac{1}{18}\left(3a_5\lambda_i^2 u_{133}^2\sqrt{9\lambda_i^2 u_{133}^2 - 12} + 2a_5\sqrt{9\lambda_i^2 u_{133}^2 - 12}\right).
\end{aligned}
\tag{4.57}
$$

for $i = 1, 2, 3$.

The phase functions are given by:

$$
\begin{aligned}
A_i(x,t) &= \frac{1}{6}xT_i - \frac{1}{9}\int\left(3a_5\lambda_i^2 u_{133}^2 T_i + 2a_5 T_i\right)dt,\\
B_i(x,t) &= \frac{1}{6}xT_i + \frac{1}{9}\int\left(3a_5\lambda_i^2 u_{133}^2 T_i + 2a_5 T_i\right)dt.\\
D_i(x,t) &= \exp\left(\lambda_i^2\int(v_{233}(t) + \lambda_i v_{333}(t))dt + \lambda_i u_{133}x\right), for \text{ i=1,2,3}.
\end{aligned}
\tag{4.58}
$$

$$
\begin{aligned}
Z_1(x,t) =& \frac{1}{9}\int \Big(9a_5\lambda_1^3 u_{133}^3 - 3a_5\lambda_1^2 u_{133}^2\sqrt{9\lambda_1^2u_{133}^2-12} \\
&- 2a_5\sqrt{9\lambda_1^2u_{133}^2-12} + 9\lambda_1^2 v_{233}(t) + 9\lambda_1^3 v_{333}(t)\Big)\,dt \\
&+ \frac{x}{3}\sqrt{9\lambda_1^2u_{133}^2-12}, \\
Z_3(x,t) =& \frac{1}{9}\int \Big(9a_5\lambda_3^3 u_{133}^3 - 3a_5\lambda_3^2 u_{133}^2\sqrt{9\lambda_3^2u_{133}^2-12} \\
&- 2a_5\sqrt{9\lambda_3^2u_{133}^2-12} + 9\lambda_3^2 v_{233}(t) + 9\lambda_3^3 v_{333}(t)\Big)\,dt \\
&+ \frac{x}{3}\sqrt{9\lambda_3^2u_{133}^2-12}.
\end{aligned}
\tag{4.59}
$$

Additional auxiliary functions are defined as:

$$
\begin{aligned}
S_i(t) =& \int \left(a_5\lambda_i^3 u_{133}^3 + \lambda_i^2 v_{233}(t) + \lambda_i^3 v_{333}(t)\right)dt, \\
E_i(t) =& \lambda_i^2 \int \left(v_{233}(t) + \lambda_i v_{333}(t)\right)dt, \\
P_i(t) =& \lambda_i^2 \int \Big(v_{233}(t) + \lambda_i v_{333}(t)\Big)\,dt, for \text{ i=1,2,3}.
\end{aligned}
\tag{4.60}
$$

$$
\begin{aligned}
R_2(t) =& \frac{1}{9}\int \Big(9a_5\lambda_2^3 u_{133}^3 + 3a_5\lambda_2^2 u_{133}^2\sqrt{9\lambda_2^2u_{133}^2-12} \\
&+ 2a_5\sqrt{9\lambda_2^2u_{133}^2-12} + 9\lambda_2^2 v_{233}(t) + 9\lambda_2^3 v_{333}(t)\Big)\,dt,
\end{aligned}
\tag{4.61}
$$

2-4-5-2 Solitonic solution of sse

Our equations are simplified into :

$$eqt1x = \psi_1^{(1,0)}(x,t) - \lambda_1 u_{111}\psi_2(x,t). \tag{4.62}$$

$$eqt2x = \psi_2^{(1,0)}(x,t) - \lambda_2 u_{111}\psi_2(x,t) \tag{4.63}$$

$$eqt3x = \psi_3^{(1,0)}(x,t) - \lambda_3 u_{111}\psi_3(x,t) \tag{4.64}$$

$$eqt4x = \phi_1^{(1,0)}(x,t) - \lambda_1 u_{133}\phi_1(x,t) \tag{4.65}$$

$$eqt5x = \phi_2^{(1,0)}(x,t) - \lambda_2 u_{133}\phi_2(x,t) \tag{4.66}$$

$$eqt6x = \phi_3^{(1,0)}(x,t) - \lambda_3 u_{133}\phi_3(x,t) \tag{4.67}$$

$$eqt7x = \chi_1^{(1,0)}(x,t) - \lambda_1 u_{133}\chi_1(x,t) \tag{4.68}$$

$$eqt8x = \chi_2^{(1,0)}(x,t) - \lambda_2 u_{133}\chi_2(x,t) \tag{4.69}$$

$$eqt9x = \chi_3^{(1,0)}(x,t) - \lambda_3 u_{133}\chi_3(x,t) \tag{4.70}$$

$$eqt1t = \lambda_1^2\psi_1(x,t)\left(\lambda_1\left(\mathrm{a_3}(\mathrm{u_{111}} - \mathrm{u_{133}})^3 - \mathrm{v_{333}}(t)\right) - \mathrm{v_{233}}(t)\right) + \psi_1^{(0,1)}(x,t) \tag{4.71}$$

$$eqt2t = \lambda_2^2\psi_2(x,t)\left(\lambda_2\left(a_3A^3 - v_{333}(t)\right) - v_{233}(t)\right) + \psi_2^{(0,1)}(x,t) \tag{4.72}$$

$$eqt3t = \lambda_3^2\psi_3(x,t)\left(\lambda_3\left(a_3A^3 - v_{333}(t)\right) - v_{233}(t)\right) + \psi_3^{(0,1)}(x,t) \tag{4.73}$$

$$eqt4t = -\lambda_1^2 v_{233}(t)\phi_1(x,t) + \lambda_1^3(-v_{333}(t))\phi_1(x,t) + \phi_1^{(0,1)}(x,t) \tag{4.74}$$

$$eqt5t = -\lambda_1^2 v_{233}(t)\phi_1(x,t) + \lambda_1^3(-v_{333}(t))\phi_1(x,t) + \phi_1^{(0,1)}(x,t) \tag{4.75}$$

$$eqt6t = -\lambda_3^2 v_{233}(t)\phi_3(x,t) + \lambda_3^3(-v_{333}(t))\phi_3(x,t) + \phi_3^{(0,1)}(x,t) \tag{4.76}$$

$$eqt7t = -\lambda_1^2 v_{233}(t)\chi_1(x,t) + \lambda_1^3(-v_{333}(t))\chi_1(x,t) + \chi_1^{(0,1)}(x,t) \tag{4.77}$$

$$eqt8t = -\lambda_2^2 v_{233}(t)\chi_2(x,t) + \lambda_2^3(-v_{333}(t))\chi_2(x,t) + \chi_2^{(0,1)}(x,t) \tag{4.78}$$

$$eqt9t = -\lambda_3^2 v_{233}(t)\chi_3(x,t) + \lambda_3^3(-v_{333}(t))\chi_3(x,t) + \chi_3^{(0,1)}(x,t) \tag{4.79}$$

remember: $A = u_{111} - u_{133}$

Thus, the answer will be in the linear system. :

$$\psi_1(x,t) = c_{111}(t)e^{\lambda_1 u_{111}x} \tag{4.80}$$

$$\psi_2(x,t) = c_{112}(t)e^{\lambda_2 u_{111}x} \tag{4.81}$$

$$\psi_3(x,t) = c_{113}(t)e^{\lambda_3 u_{111}x} \tag{4.82}$$

$$\phi_1(x,t) = c_{114}(t)e^{\lambda_1 u_{133}x} \tag{4.83}$$

$$\phi_2(x,t) = c_{115}(t)e^{\lambda_2 u_{133}x} \tag{4.84}$$

$$\phi_3(x,t) = c_{116}(t)e^{\lambda_3 u_{133}x} \tag{4.85}$$

$$\chi_1(x,t) = c_{117}(t)e^{\lambda_1 u_{133}x} \tag{4.86}$$

$$\chi_2(x,t) := c_{118}(t)e^{\lambda_2 u_{133}x} \tag{4.87}$$

$$\chi_3(x,t) = c_{119}(t)e^{\lambda_3 u_{133}x} \tag{4.88}$$

With $c_{111}(t), c_{112}(t), c_{113}(t), c_{114}(t), c_{115}(t), c_{116}(t), c_{117}(t), c_{118}(t)$and $c_{119}(t)$ are given by:

$$c_{111}(t) = c_{1110} \exp\left(\int_1^t \Big(- a_3\lambda_1^3 u_{111}^3 + 3a_3\lambda_1^3 u_{111}^2 u_{133} - 3a_3\lambda_1^3 u_{111} u_{133}^2 + a_3\lambda_1^3 u_{133}^3 + \lambda_1^2 v_{233}(t) + \lambda_1^3 v_{333}(t) \Big) \, dt \right) \tag{4.89}$$

$$c_{112}(t) = c_{1120} \exp\left(\int_1^t \Big(- a_3\lambda_2^3 u_{111}^3 + 3a_3\lambda_2^3 u_{111}^2 u_{133} - 3a_3\lambda_2^3 u_{111} u_{133}^2 + a_3\lambda_2^3 u_{133}^3 + \lambda_2^2 v_{233}(t) + \lambda_2^3 v_{333}(t) \Big) \, dt \right) \tag{4.90}$$

$$c_{113}(t) = c_{1130} \exp\left(\int_1^t \Big(- a_3\lambda_3^3 u_{111}^3 + 3a_3\lambda_3^3 u_{111}^2 u_{133} - 3a_3\lambda_3^3 u_{111} u_{133}^2 + a_3\lambda_3^3 u_{133}^3 + \lambda_3^2 v_{233}(t) + \lambda_3^3 v_{333}(t) \Big) \, dt \right) \tag{4.91}$$

$$\mathrm{c}_{114}(t) = \mathrm{c}_{1140} \exp\left(\int_1^t \left(\lambda_1^2 v_{233}(t) + \lambda_1^3 v_{333}(t) \right) \, dt \right) \tag{4.92}$$

$$\mathrm{c}_{115}(t) = \mathrm{c}_{1150} \exp\left(\int_1^t \left(\lambda_2^2 v_{233}(t) + \lambda_2^3 v_{333}(t) \right) \, dt \right) \tag{4.93}$$

$$\mathrm{c}_{116}(t) = \mathrm{c}_{1160} \exp\left(\int_1^t \left(\lambda_3^2 v_{233}(t) + \lambda_3^3 v_{333}(t) \right) \, dt \right) \tag{4.94}$$

$$\mathrm{c}_{117}(t) = \mathrm{c}_{1170} \exp\left(\int_1^t \left(\lambda_1^2 v_{233}(t) + \lambda_1^3 v_{333}(t) \right) \, dt \right) \tag{4.95}$$

$$\mathrm{c}_{118}(t) = \mathrm{c}_{1180} \exp\left(\int_1^t \left(\lambda_2^2 v_{233}(t) + \lambda_2^3 v_{333}(t) \right) \, dt \right) \tag{4.96}$$

$$\mathrm{c}_{119}(t) = \mathrm{c}_{1190} \exp\left(\int_1^t \left(\lambda_3^2 v_{233}(t) + \lambda_3^3 v_{333}(t) \right) \, dt \right) \tag{4.97}$$

Therefore, we reduce the answer to :

$$\psi_1(x,t) = c_{1110} \exp\left(\int_1^t \lambda_1^2 \left(\lambda_1 \left(\mathrm{v}_{333}(t) - \mathrm{a}_3(\mathrm{u}_{111} - \mathrm{u}_{133})^3 \right) + \mathrm{v}_{233}(t) \right) \, dt + \lambda_1 \mathrm{u}_{111} x \right) \tag{4.98}$$

$$\psi_2(x,t) = c_{1120} \exp\left(\int_1^t \lambda_2^2 \left(\lambda_2 \left(\mathrm{v}_{333}(t) - \mathrm{a}_3 (\mathrm{u}_{111} - \mathrm{u}_{133})^3 \right) + \mathrm{v}_{233}(t) \right) \, dt + \lambda_2 \mathrm{u}_{111} x \right) \tag{4.99}$$

$$\psi_3(x,t) = c_{1130} \exp\left(\int_1^t \lambda_3^2 \left(\lambda_3 \left(\mathrm{v}_{333}(t) - \mathrm{a}_3 (\mathrm{u}_{111} - \mathrm{u}_{133})^3 \right) + \mathrm{v}_{233}(t) \right) \, dt + \lambda_3 \mathrm{u}_{111} x \right) \tag{4.100}$$

$$\phi_1(x,t) = c_{1140} \exp\left(\int_1^t \lambda_1^2 \left(\mathrm{v}_{233}(t) + \lambda_1 \mathrm{v}_{333}(t) \right) \, dt + \lambda_1 \mathrm{u}_{133} x \right) \tag{4.101}$$

$$\phi_2(x,t) = c_{1150} \exp\left(\int_1^t \lambda_2^2 \left(\mathrm{v}_{233}(t) + \lambda_2 \mathrm{v}_{333}(t) \right) \, dt + \lambda_2 \mathrm{u}_{133} x \right) \tag{4.102}$$

$$\phi_3(x,t) = c_{1160} \exp\left(\int_1^t \lambda_3^2 \left(\mathrm{v}_{233}(t) + \lambda_3 \mathrm{v}_{333}(t) \right) \, dt + \lambda_3 \mathrm{u}_{133} x \right) \tag{4.103}$$

$$\chi_1(x,t) = c_{1170} \exp\left(\int_1^t \lambda_1^2 \left(\mathrm{v}_{233}(t) + \lambda_1 \mathrm{v}_{333}(t) \right) \, dt + \lambda_1 \mathrm{u}_{133} x \right) \tag{4.104}$$

$$\chi_2(x,t) = c_{1180} \exp\left(\int_1^t \lambda_2^2 \left(\mathrm{v}_{233}(t) + \lambda_2 \mathrm{v}_{333}(t) \right) \, dt + \lambda_2 \mathrm{u}_{133} x \right) \tag{4.105}$$

$$\chi_3(x,t) = c_{1190} \exp\left(\int_1^t \lambda_3^2 \left(\mathrm{v}_{233}(t) + \lambda_3 \mathrm{v}_{333}(t) \right) \, dt + \lambda_3 \mathrm{u}_{133} x \right) \tag{4.106}$$

The solution of SSE is:

$$\psi(x,t) = \frac{144\, a_3^2\, c_{1110}^2\, c_{1140}^2\, \lambda_3^2 \;\exp\left[4\lambda_3 \left(4a_3\lambda_3^2(t-1) + x\right)\right]}{\left(2a_5 c_{1140}^2 \exp\left(16a_3\lambda_3^3(t-1)\right) + 3a_3 c_{1110}^2 \exp(4\lambda_3 x)\right)^2} \tag{4.107}$$

Appendix B

3-2 Lax pair

where:

$$G(x,t) = \tfrac{1}{2} i \sqrt{\frac{-3\; a_2(t)}{2\; a_1(t)}} e^{-i \frac{a_1(t)}{3\; a_3(t)} x} \left(-\frac{3\; a_2(t)\; a_3(t)\; \Psi^2 \Psi^*}{2\; a_1(t)} - \frac{2\; a_1(t)^2\, \Psi}{9\, a_3(t)} + \frac{2}{3} i\; a_1(t)\; \Psi_x - a_3(t) \Psi_{xx} \right).$$

$$Z(x,t) = \frac{a_2(t)(3\, a_3(t)\, (\Psi_x \Psi^* - \Psi \Psi_x^*) - 2\; i\; a_1(t)\, \Psi\; \Psi^*)}{8\, a_1(t)}.$$

$A(x,t) = \frac{3\ a_2(t)\ a_3(t)\,(u_{133}\ u_{111})\Psi\,\Psi^*}{4\ a_1(t)} - \frac{a_1(t)^2(u_{111}-u_{133})}{3\ a_3(t)} + cv_{133}(t).$
$B(x,t) = \frac{3\ a_2(t)\ a_3(t)\ (u_{111}-u_{133}).\Psi\,\Psi^*}{8\ a_1(t)} + cv_{133}(t).$
$C(x,t) = -\frac{(u_{111}-u_{133})\sqrt{-\frac{a_2(t)}{a_1(t)}}e^{-\frac{i\,x\,a_1(t)}{3\,a_3(t)}}\,(a_1(t)\ \Psi+3\,i\,a_3(t)\Psi_x)}{2\sqrt{6}},$
$D(x,t) = -\frac{3\,a_2(t)\ a_3(t)\ (u_{111}-u_{133})\ e^{-\frac{2\ i\ x\ a_1(t)}{3\ a_3(t)}}}{8\ a_1(t)}\Psi^2.$
$K(x,t) = -\frac{1}{2}i\,\sqrt{\frac{-\,3\ a_2(t)}{2\ a_1(t)}}\ a_3(t)\ (u_{111}-u_{133})^2 e^{-\,i\,\frac{a_1(t)}{3\ a_3(t)}\,x}\ \Psi,$
$h = (u_{111}-u_{133})^3.$
we applying the DT we find the solitonic solution of HNLS:

$$\psi(x,t) = -\frac{8i\sqrt{\frac{2}{3}}\,c_{1110}c_{1170}\lambda_3\,e^{z(x,t)}}{\sqrt{-\frac{a_2(t)}{a_1(t)}}\left(c_{1110}^2 e^{f(x,t)} - 2c_{1170}^2 e^{h(x,t)}\right)} \tag{4.108}$$

where:

$$f(x,t) = 2\lambda_3\int\left[\lambda_3^2(8a_3(t)+v_{311}(t)) + \mathbf{cv}_{133}(t)\right]\,dt$$
$$h(x,t) = \frac{2}{3}\lambda_3\left(\int\left[3\left(\mathbf{cv}_{133}(t)+\lambda_3^2 v_{311}(t)\right) - \frac{2a_1(t)^2}{a_3(t)}\right]\,dt + 6x\right)$$
$$z(x,t) = \frac{1}{3}\Bigg(\lambda_3\Big(\int\left[3\left(\mathbf{cv}_{133}(t)+\lambda_3^2 v_{311}(t)\right) - \frac{2a_1(t)^2}{a_3(t)}\right]dt + 3\int\left[\lambda_3^2(8a_3(t)+v_{311}(t)) + \mathbf{cv}_{133}(t)\right]dt + 6x\Big) + \frac{ixa_1(t)}{a_3(t)}\Bigg)$$

3-3 Solitonic solution of hnls

In this case, we consider the seed solution $\psi_0(x,t) = 0$. By deriving the compatibility conditions, we obtain a total of 18 equations: 8 related the temporal and 8 related the spatial :

$$\mathbf{eq_{1x}} = \psi_1^{(1,0)}(x,t) - \lambda_1\mathbf{u}_{111}\psi_1(x,t) \tag{4.109}$$

$$\mathbf{eq}_{2x} = \phi_1^{(1,0)}(x,t) - \lambda_1 u_{133}\phi_1(x,t) \tag{4.110}$$

$$\mathbf{eq}_{3x} = \chi_1^{(1,0)}(x,t) - \lambda_1 u_{133}\chi_1(x,t) \tag{4.111}$$

$$\mathbf{eq_{4x}} = \psi_2^{(1,0)}(x,t) - \lambda_2 u_{111}\psi_2(x,t) \tag{4.112}$$

$$\mathbf{eq_{5x}} = \phi_2^{(1,0)}(x,t) - \lambda_2 u_{133}\phi_2(x,t) \tag{4.113}$$

$$\mathbf{eq_{6x}} = \chi_2^{(1,0)}(x,t) - \lambda_2 u_{111}\chi_2(x,t) \tag{4.114}$$

$$\mathbf{eq_{7x}} = \psi_3^{(1,0)}(x,t) - \lambda_3 u_{111}\psi_3(x,t) \tag{4.115}$$

$$\mathbf{eq_{8x}} = \phi_3^{(1,0)}(x,t) - \lambda_3 u_{133}\phi_3(x,t) \tag{4.116}$$

$$\mathbf{eq_{9x}} = \chi_3^{(1,0)}(x,t) - \lambda_3 u_{133}\chi_3(x,t) \tag{4.117}$$

$$\mathbf{eq_{1t}} = -\lambda_1\psi_1(x,t)\left(\mathbf{cv}_{133}(t) - \frac{a_1(t)^2(u_{111}-u_{133})}{3a_3(t)}\right) + \lambda_1^3(-v_{311}(t))\psi_1(x,t) + \psi_1^{(0,1)}(x,t) \tag{4.118}$$

$$\mathbf{eq_{2t}} = \lambda_1^3\phi_1(x,t)\left(-\left(a_3(t)(u_{111}-u_{133})^3 + v_{311}(t)\right)\right) - \lambda_1\,\mathbf{cv}_{133}(t)\,\phi_1(x,t) + \phi_1^{(0,1)}(x,t) \tag{4.119}$$

$$\mathbf{eq_{3t}} = \lambda_1^3\chi_1(x,t)\left(-\left(a_3(t)(u_{111}-u_{133})^3 + v_{311}(t)\right)\right) - \lambda_1\,\mathbf{cv}_{133}(t)\,\chi_1(x,t) + \chi_1^{(0,1)}(x,t) \tag{4.120}$$

$$\mathbf{eq_{4t}} = -\lambda_2\psi_2(x,t)\left(\mathbf{cv}_{133}(t) - \frac{a_1(t)^2(u_{111}-u_{133})}{3a_3(t)}\right) + \lambda_2^3(-v_{311}(t))\psi_2(x,t) + \psi_2^{(0,1)}(x,t) \tag{4.121}$$

$$\mathbf{eq_{5t}} = \lambda_2^3\phi_2(x,t)\left(-\left(a_3(t)(u_{111}-u_{133})^3 + v_{311}(t)\right)\right) - \lambda_2\,\mathbf{cv}_{133}(t)\,\phi_2(x,t) + \phi_2^{(0,1)}(x,t) \tag{4.122}$$

$$\mathbf{eq_{6t}} = \lambda_2^3\chi_2(x,t)\left(-\left(a_3(t)(u_{111}-u_{133})^3 + v_{311}(t)\right)\right) - \lambda_2\,\mathbf{cv}_{133}(t)\,\chi_2(x,t) + \chi_2^{(0,1)}(x,t) \tag{4.123}$$

$$\mathbf{eq_{7t}} = -\lambda_3\psi_3(x,t)\left(\mathbf{cv}_{133}(t) - \frac{a_1(t)^2(u_{111}-u_{133})}{3a_3(t)}\right) + \lambda_3^3(-v_{311}(t))\psi_3(x,t) + \psi_3^{(0,1)}(x,t) \tag{4.124}$$

$$\mathbf{eq_{8t}} = \lambda_3^3 \phi_3(x,t) \left(- \left(a_3(t)(u_{111} - u_{133})^3 + v_{311}(t) \right) \right) - \lambda_3 \, \mathbf{cv}_{133}(t) \, \phi_3(x,t) + \phi_3^{(0,1)}(x,t) \tag{4.125}$$

$$\mathbf{eq_{9t}} = \lambda_3^3 \chi_3(x,t) \left(- \left(a_3(t)(u_{111} - u_{133})^3 + v_{311}(t) \right) \right) - \lambda_3 \, \mathbf{cv}_{133}(t) \, \chi_3(x,t) + \chi_3^{(0,1)}(x,t) \tag{4.126}$$

Applying the seed $\psi_0(x,t) = 0$, $\psi_0^*(x,t) = 0$, our equations are simplified into :

$$\mathbf{eq_{1x}} = \psi_1^{(1,0)}(x,t) - \lambda_1 \, u_{111} \, \psi_1(x,t) \tag{4.127}$$

$$\mathbf{eq_{2x}} = \phi_1^{(1,0)}(x,t) - \lambda_1 \, u_{111} \, \phi_1(x,t) \tag{4.128}$$

$$\mathbf{eq_{3x}} = \chi_1^{(1,0)}(x,t) - \lambda_1 \, u_{133} \, \chi_1(x,t) \tag{4.129}$$

$$\mathbf{eq_{4x}} = \psi_2^{(1,0)}(x,t) - \lambda_2 \, u_{111} \, \psi_2(x,t) \tag{4.130}$$

$$\mathbf{eq_{5x}} = \phi_2^{(1,0)}(x,t) - \lambda_2 \, u_{111} \, \phi_2(x,t) \tag{4.131}$$

$$\mathbf{eq_{6x}} = \chi_2^{(1,0)}(x,t) - \lambda_2 \, u_{133} \, \chi_2(x,t) \tag{4.132}$$

$$\mathbf{eq_{7x}} = \psi_3^{(1,0)}(x,t) - \lambda_3 \, u_{111} \, \phi_3(x,t) \tag{4.133}$$

$$\mathbf{eq_{8x}} = \phi_3^{(1,0)}(x,t) - \lambda_3 \, u_{111} \, \phi_3(x,t) \tag{4.134}$$

$$\mathbf{eq_{9x}} = \chi_3^{(1,0)}(x,t) - \lambda_3 \, u_{133} \, \chi_3(x,t) \tag{4.135}$$

$$\mathbf{eq_{1t}} = -\lambda_1 \, \psi_1(x,t) \left(\mathbf{cv}_{133}(t) - \frac{a_1(t)^2 (u_{111} - u_{133})}{3 \, a_3(t)} \right) + \lambda_1^3 \left(-v_{311}(t) \right) \psi_1(x,t) + \psi_1^{(0,1)}(x,t) \tag{4.136}$$

$$\mathbf{eq_{2t}} = \lambda_1^3 \, \phi_1(x,t) \left(- \left(a_3(t)(u_{111} - u_{133})^3 + v_{311}(t) \right) \right) - \lambda_1 \, \mathbf{cv}_{133}(t) \, \phi_1(x,t) + \phi_1^{(0,1)}(x,t) \tag{4.137}$$

$$\mathbf{eq_{3t}} = \lambda_1^3 \, \chi_1(x,t) \left(- \left(a_3(t)(u_{111} - u_{133})^3 + v_{311}(t) \right) \right) - \lambda_1 \, \mathbf{cv}_{133}(t) \, \chi_1(x,t) + \chi_1^{(0,1)}(x,t) \tag{4.138}$$

$$\mathbf{eq_{4t}} = -\lambda_2\,\psi_2(x,t)\left(\mathrm{cv}_{133}(t) - \frac{a_1(t)^2(u_{111}-u_{133})}{3\,a_3(t)}\right) + \lambda_2^3\,(-v_{311}(t))\,\psi_2(x,t) + \psi_2^{(0,1)}(x,t) \tag{4.139}$$

$$\mathbf{eq_{5t}} = \lambda_2^3\,\phi_2(x,t)\left(-\left(a_3(t)(u_{111}-u_{133})^3 + v_{311}(t)\right)\right) - \lambda_2\,\mathrm{cv}_{133}(t)\,\phi_2(x,t) + \phi_2^{(0,1)}(x,t) \tag{4.140}$$

$$\mathbf{eq_{6t}} = \lambda_2^3\,\chi_2(x,t)\left(-\left(a_3(t)(u_{111}-u_{133})^3 + v_{311}(t)\right)\right) - \lambda_2\,\mathrm{cv}_{133}(t)\,\chi_2(x,t) + \chi_2^{(0,1)}(x,t) \tag{4.141}$$

$$\mathbf{eq_{7t}} = -\lambda_3\,\psi_3(x,t)\left(\mathrm{cv}_{133}(t) - \frac{a_1(t)^2(u_{111}-u_{133})}{3\,a_3(t)}\right) + \lambda_3^3\,(-v_{311}(t))\,\psi_3(x,t) + \psi_3^{(0,1)}(x,t) \tag{4.142}$$

$$\mathbf{eq_{8t}} = \lambda_3^3\,\phi_3(x,t)\left(-\left(a_3(t)(u_{111}-u_{133})^3 + v_{311}(t)\right)\right) - \lambda_3\,\mathrm{cv}_{133}(t)\,\phi_3(x,t) + \phi_3^{(0,1)}(x,t) \tag{4.143}$$

$$\mathbf{eq_{9t}} = \lambda_3^3\,\chi_3(x,t)\left(-\left(a_3(t)(u_{111}-u_{133})^3 + v_{311}(t)\right)\right) - \lambda_3\,\mathrm{cv}_{133}(t)\,\chi_3(x,t) + \chi_3^{(0,1)}(x,t) \tag{4.144}$$

So, the linear system will have the solution :

$$\psi_1(x,t) = c_{111}(t)\,e^{\lambda_1 u_{111} x} \tag{4.145}$$

$$\psi_2(x,t) = c_{112}(t)\,e^{\lambda_2 u_{111} x} \tag{4.146}$$

$$\psi_3(x,t) = c_{113}(t)\,e^{\lambda_3 u_{111} x} \tag{4.147}$$

$$\phi_1(x,t) = c_{114}(t)\,e^{\lambda_1 u_{133} x} \tag{4.148}$$

$$\phi_2(x,t) = c_{115}(t)\,e^{\lambda_2 u_{133} x} \tag{4.149}$$

$$\phi_3(x,t) = c_{116}(t)\, e^{\lambda_3 u_{133} x} \tag{4.150}$$

$$\chi_1(x,t) = c_{117}(t)\, e^{\lambda_1 u_{133} x} \tag{4.151}$$

$$\chi_2(x,t) = c_{118}(t)\, e^{\lambda_2 u_{133} x} \tag{4.152}$$

$$\chi_3(x,t) = c_{119}(t)\, e^{\lambda_3 u_{133} x} \tag{4.153}$$

With $c_{111}(t)$,..., and $c_{119}(t)$ are given by:

$$c_{111}(t) = c_{1110} \exp \int_1^t \frac{1}{3a_3(t)} \Big(-\lambda_1 u_{111} a_1(t)^2 + \lambda_1 u_{133} a_1(t)^2 + 3\lambda_1 a_3(t) \mathrm{cv}_{133}(t) + 3\lambda_1^3 a_3(t) v_{311}(t) \Big)\, dt \tag{4.154}$$

$$c_{112}(t) = c_{1120} \exp \int_1^t \frac{1}{3a_3(t)} \Big(-\lambda_2 u_{111} a_1(t)^2 + \lambda_2 u_{133} a_1(t)^2 + 3\lambda_2 a_3(t) \mathrm{cv}_{133}(t) + 3\lambda_2^3 a_3(t) v_{311}(t) \Big)\, dt \tag{4.155}$$

$$c_{113}(t) = c_{1130} \exp \int_1^t \frac{1}{3a_3(t)} \Big(-\lambda_3 u_{111} a_1(t)^2 + \lambda_3 u_{133} a_1(t)^2 + 3\lambda_3 a_3(t) \mathrm{cv}_{133}(t) + 3\lambda_3^3 a_3(t) v_{311}(t) \Big)\, dt \tag{4.156}$$

$$c_{114}(t) = c_{1140} \exp \int_1^t \Big(\lambda_1^3 u_{111}^3 a_3(t) - 3\lambda_1^3 u_{111}^2 u_{133} a_3(t) + 3\lambda_1^3 u_{111} u_{133}^2 a_3(t) - \lambda_1^3 u_{133}^3 a_3(t) + \lambda_1\, \mathrm{cv}_{133}(t) + \lambda_1^3 v_{311}(t) \Big) dt \tag{4.157}$$

$$c_{115}(t) = c_{1150} \exp \int_1^t \Big(\lambda_2^3 u_{111}^3 a_3(t) - 3\lambda_2^3 u_{111}^2 u_{133} a_3(t) + 3\lambda_2^3 u_{111} u_{133}^2 a_3(t) - \lambda_2^3 u_{133}^3 a_3(t) + \lambda_2\, \mathrm{cv}_{133}(t) + \lambda_2^3 v_{311}(t) \Big) dt \tag{4.158}$$

$$c_{116}(t) = c_{1160} \exp \int_1^t \Big(\lambda_3^3 u_{111}^3 a_3(t) - 3\lambda_3^3 u_{111}^2 u_{133} a_3(t) + 3\lambda_3^3 u_{111} u_{133}^2 a_3(t) - \lambda_3^3 u_{133}^3 a_3(t) + \lambda_3 \, \mathbf{cv}_{133}(t) + \lambda_3^3 v_{311}(t) \Big) dt \tag{4.159}$$

$$c_{117}(t) = c_{1170} \exp \int_1^t \Big(\lambda_1^3 u_{111}^3 a_3(t) - 3\lambda_1^3 u_{111}^2 u_{133} a_3(t) + 3\lambda_1^3 u_{111} u_{133}^2 a_3(t) - \lambda_1^3 u_{133}^3 a_3(t) + \lambda_1 \, \mathbf{cv}_{133}(t) + \lambda_1^3 v_{311}(t) \Big) dt \tag{4.160}$$

$$c_{118}(t) = c_{1180} \exp \int_1^t \Big(\lambda_2^3 u_{111}^3 a_3(t) - 3\lambda_2^3 u_{111}^2 u_{133} a_3(t) + 3\lambda_2^3 u_{111} u_{133}^2 a_3(t) - \lambda_2^3 u_{133}^3 a_3(t) + \lambda_2 \, \mathbf{cv}_{133}(t) + \lambda_2^3 v_{311}(t) \Big) dt \tag{4.161}$$

$$c_{119}(t) = c_{1190} \exp \int_1^t \Big(\lambda_3^3 u_{111}^3 a_3(t) - 3\lambda_3^3 u_{111}^2 u_{133} a_3(t) + 3\lambda_3^3 u_{111} u_{133}^2 a_3(t) - \lambda_3^3 u_{133}^3 a_3(t) + \lambda_3 \, \mathbf{cv}_{133}(t) + \lambda_3^3 v_{311}(t) \Big) dt \tag{4.162}$$

So we simplify the solution into :

$$\phi_1(x,t) = c_{1140} \exp \left(\int \lambda_1 \left(\lambda_1^2 a_3(t)(u_{111} - u_{133})^3 + \mathbf{cv}_{133}(t) + \lambda_1^2 v_{311}(t) \right) dt + \lambda_1 u_{133} x \right) \tag{4.163}$$

$$\phi_2(x,t) = c_{1150} \exp \left(\int \lambda_2 \left(\lambda_2^2 a_3(t)(u_{111} - u_{133})^3 + \mathbf{cv}_{133}(t) + \lambda_2^2 v_{311}(t) \right) dt + \lambda_2 u_{133} x \right) \tag{4.164}$$

$$\phi_3(x,t) = c_{1160} \exp \left(\int \lambda_3 \left(\lambda_3^2 a_3(t)(u_{111} - u_{133})^3 + \mathbf{cv}_{133}(t) + \lambda_3^2 v_{311}(t) \right) dt + \lambda_3 u_{133} x \right) \tag{4.165}$$

$$\chi_1(x,t) = c_{1170}\exp\left(\int \lambda_1\left(\lambda_1^2 a_3(t)(u_{111}-u_{133})^3 + \mathbf{cv}_{133}(t) + \lambda_1^2 v_{311}(t)\right)dt + \lambda_1 u_{133}x\right) \tag{4.166}$$

$$\chi_2(x,t) = c_{1180}\exp\left(\int \lambda_2\left(\lambda_2^2 a_3(t)(u_{111}-u_{133})^3 + \mathbf{cv}_{133}(t) + \lambda_2^2 v_{311}(t)\right)dt + \lambda_2 u_{133}x\right) \tag{4.167}$$

$$\chi_3(x,t) = c_{1190}\exp\left(\int \lambda_3\left(\lambda_3^2 a_3(t)(u_{111}-u_{133})^3 + \mathbf{cv}_{133}(t) + \lambda_3^2 v_{311}(t)\right)dt + \lambda_3 u_{133}x\right) \tag{4.168}$$

$$\psi_1(x,t) = c_{1110}\exp\left(\int \frac{\lambda_1\left(a_1(t)^2(u_{133}-u_{111}) + 3a_3(t)(\mathbf{cv}_{133}(t) + \lambda_1^2 v_{311}(t))\right)}{3a_3(t)}dt + \lambda_1 u_{111}x\right) \tag{4.169}$$

$$\psi_2(x,t) = c_{1120}\exp\left(\int \frac{\lambda_2\left(a_1(t)^2(u_{133}-u_{111}) + 3a_3(t)(\mathbf{cv}_{133}(t) + \lambda_2^2 v_{311}(t))\right)}{3a_3(t)}dt + \lambda_2 u_{111}x\right) \tag{4.170}$$

$$\psi_3(x,t) = c_{1130}\exp\left(\int \frac{\lambda_3\left(a_1(t)^2(u_{133}-u_{111}) + 3a_3(t)(\mathbf{cv}_{133}(t) + \lambda_3^2 v_{311}(t))\right)}{3a_3(t)}dt + \lambda_3 u_{111}x\right) \tag{4.171}$$

where c_{1110} and c_{1190} are real arbitrary constants of integration consider the following version of the Darboux transformation:

$$\psi[1] = \psi\,\mathbf{\Lambda} - \sigma\,\psi \tag{4.172}$$

Where $\psi[1]$is the transformation field

$$\sigma = \psi_{\mathbf{0}}.\mathbf{\Lambda}.\psi^{-\mathbf{1}} \tag{4.173}$$

Here ψ_0 is a known (seed) solution of the linear system equations and for the transformed field $\psi[1]$ to be a solution of the linear system ,the matrix U for instance must be transformed

as:

$$\mathbf{U[1]} = \sigma \mathbf{U} \sigma^{\mathbf{-1}} + \sigma_{\mathbf{x}} \sigma^{\mathbf{-1}}, \tag{4.174}$$

Where:

$\mathrm{c}_{1140} = \mathrm{c}_{1170}$, $\lambda_1 = -\lambda_2 = -\lambda_3$,

$u_{111} = 1$, $u_{133} = -1$, $c_{1190} = \frac{c_{1110}(c_{1120}\, c_{1160} + c_{1130}\, (c_{1180} - c_{1150})) - 2 c_{1160}\, c_{1170}\, c_{1180}}{c_{1110}\, c_{1120} - 2\, c_{1150}\, c_{1170}}$. Following algebraic simplifications, the HNLS equation admits solitonic solutions; one such solution is expressed as:

$$\psi(x,t) = \; -\frac{8i\sqrt{\frac{2}{3}}\, c_{1110} c_{1170} \lambda_3\, e^{z(x,t)}}{\sqrt{-\frac{a_2(t)}{a_1(t)}} \left(c_{1110}^2 e^{f(x,t)} - 2 c_{1170}^2 e^{h(x,t)} \right)} \tag{4.175}$$

3-4 The Role of the Spectral Parameter (λ)

3-4-1 General Breather Regime

We derive the compatibility equations,we found 18 equations :9 equations for time and 9 equations for space ,we use seed $\sqrt{-\frac{a_1}{a_2}} e^{\frac{i\, x\, a_1}{3\, a_3}}$:

$$
\begin{aligned}
\text{eq1x} &= \frac{1}{4}\left(4\frac{\partial\psi_2}{\partial x} - i\sqrt{6}\,\phi_2 + i\sqrt{6}\,\chi_2 - 4u_{111}\lambda_2\psi_2\right) = 0 \\
\text{eq2x} &= \frac{\partial\phi_2}{\partial x} - u_{133}\lambda_2\phi_2 + \frac{i}{2}\sqrt{\frac{3}{2}}\,\psi_2 = 0 \\
\text{eq3x} &= \frac{\partial\chi_2}{\partial x} - u_{133}\lambda_2\chi_2 - \frac{i}{2}\sqrt{\frac{3}{2}}\,\psi_2 = 0 \\
\text{eq4x} &= \frac{1}{4}\left(4\frac{\partial\psi_1}{\partial x} - i\sqrt{6}\,\phi_1 + i\sqrt{6}\,\chi_1 - 4u_{111}\lambda_1\psi_1\right) = 0 \\
\text{eq5x} &= \frac{\partial\phi_1}{\partial x} - u_{133}\lambda_1\phi_1 + \frac{i}{2}\sqrt{\frac{3}{2}}\,\psi_1 = 0 \\
\text{eq6x} &= \frac{\partial\chi_1}{\partial x} - u_{133}\lambda_1\chi_1 - \frac{i}{2}\sqrt{\frac{3}{2}}\,\psi_1 = 0 \\
\text{eq7x} &= \frac{1}{4}\left(4\frac{\partial\psi_3}{\partial x} - i\sqrt{6}\,\phi_3 + i\sqrt{6}\,\chi_3 - 4u_{111}\lambda_3\psi_3\right) = 0 \\
\text{eq8x} &= \frac{\partial\phi_3}{\partial x} - u_{133}\lambda_3\phi_3 + \frac{i}{2}\sqrt{\frac{3}{2}}\,\psi_3 = 0 \\
\text{eq9x} &= \frac{\partial\chi_3}{\partial x} - u_{133}\lambda_3\chi_3 - \frac{i}{2}\sqrt{\frac{3}{2}}\,\psi_3 = 0
\end{aligned}
\tag{4.176}
$$

$$
\begin{aligned}
\text{eq1t} = \frac{1}{24a_3}\Bigg[& 24a_3\frac{\partial\psi_2}{\partial t} + i\left(2a_1^2 + 3a_3^2(2u_{111}^2\lambda_2^2 + 2u_{133}^2\lambda_2^2 - 4u_{111}u_{133}\lambda_2^2 - 3)\right)\sqrt{6}\,\phi_2 \\
& - i\sqrt{6}\left(2a_1^2 + 3a_3^2(2u_{111}^2\lambda_2^2 + 2u_{133}^2\lambda_2^2 - 4u_{111}u_{133}\lambda_2^2 - 3)\right)\chi_2 \\
& - 2\lambda_2\left(4(u_{133} - u_{111})a_1^2 + 9a_3^2(u_{111} - u_{133}) + 12a_3(\lambda_2^2 + 1)\right)\psi_2\Bigg] = 0
\end{aligned}
\tag{4.177}
$$

$$\text{eq2t} = \frac{1}{24a_3}\Bigg[24a_3\frac{\partial\phi_2}{\partial t} - 2i\sqrt{6}a_1^2\psi_2 \\ - 3a_3\lambda_2\left(8(\lambda_2^2+1) + a_3(u_{111}-u_{133})(8u_{111}^2\lambda_2^2 + 8u_{133}^2\lambda_2^2 - 16u_{111}u_{133}\lambda_2^2 - 3)\right)\phi_2 \\ + 9a_3^2(u_{133}-u_{111})\lambda_2\chi_2 \\ - 6i\sqrt{6}a_3^2u_{111}^2\lambda_2^2\psi_2 - 6i\sqrt{6}a_3^2u_{133}^2\lambda_2^2\psi_2 \\ + 12i\sqrt{6}a_3^2u_{111}u_{133}\lambda_2^2\psi_2 + 9i\sqrt{6}a_3^2\psi_2\Bigg] = 0 \tag{4.178}$$

$$\text{eq3t} = \frac{1}{24a_3}\Bigg[24a_3\frac{\partial\chi_2}{\partial t} + 2i\sqrt{6}a_1^2\psi_2 \\ + 9a_3^2(u_{133}-u_{111})\lambda_2\phi_2 \\ - 3a_3\lambda_2\left(8(\lambda_2^2+1) + a_3(u_{111}-u_{133})(8u_{111}^2\lambda_2^2 + 8u_{133}^2\lambda_2^2 - 16u_{111}u_{133}\lambda_2^2 - 3)\right)\chi_2\Bigg] = 0 \tag{4.179}$$

$$\text{eq4t} = \frac{1}{24a_3}\Bigg[24a_3\frac{\partial\psi_1}{\partial t} + i\left(2a_1^2 + 3a_3^2(2u_{111}^2\lambda_1^2 + 2u_{133}^2\lambda_1^2 - 4u_{111}u_{133}\lambda_1^2 - 3)\right)\sqrt{6}\,\phi_1 \\ - i\sqrt{6}\left(2a_1^2 + 3a_3^2(2u_{111}^2\lambda_1^2 + 2u_{133}^2\lambda_1^2 - 4u_{111}u_{133}\lambda_1^2 - 3)\right)\chi_1 \\ - 2\lambda_1\left(4(u_{133}-u_{111})a_1^2 + 9a_3^2(u_{111}-u_{133}) + 12a_3(\lambda_1^2+1)\right)\psi_1\Bigg] = 0 \tag{4.180}$$

$$\begin{aligned}\text{eq5t} = \frac{1}{24a_3}\Bigg[&24a_3\frac{\partial\phi_1}{\partial t} - 2i\sqrt{6}a_1^2\psi_1 \\ &- 3a_3\lambda_1\left(8(\lambda_1^2+1) + a_3(u_{111}-u_{133})(8u_{111}^2\lambda_1^2 + 8u_{133}^2\lambda_1^2 - 16u_{111}u_{133}\lambda_1^2 - 3)\right)\phi_1 \\ &+ 9a_3^2(u_{133}-u_{111})\lambda_1\chi_1 \\ &- 6i\sqrt{6}a_3^2u_{111}^2\lambda_1^2\psi_1 - 6i\sqrt{6}a_3^2u_{133}^2\lambda_1^2\psi_1 \\ &+ 12i\sqrt{6}a_3^2u_{111}u_{133}\lambda_1^2\psi_1 + 9i\sqrt{6}a_3^2\psi_1\Bigg] = 0\end{aligned} \tag{4.181}$$

$$\begin{aligned}\text{eq6t} = \frac{1}{24a_3}\Bigg[&24a_3\frac{\partial\chi_1}{\partial t} + 2i\sqrt{6}a_1^2\psi_1 \\ &+ 9a_3^2(u_{133}-u_{111})\lambda_1\phi_1 \\ &- 3a_3\lambda_1\left(8(\lambda_1^2+1) + a_3(u_{111}-u_{133})(8u_{111}^2\lambda_1^2 + 8u_{133}^2\lambda_1^2 - 16u_{111}u_{133}\lambda_1^2 - 3)\right)\chi_1\Bigg] = 0\end{aligned} \tag{4.182}$$

$$\begin{aligned}\text{eq7t} = \frac{1}{24a_3}\Bigg[&24a_3\frac{\partial\psi_3}{\partial t} + i\left(2a_1^2 + 3a_3^2(2u_{111}^2\lambda_3^2 + 2u_{133}^2\lambda_3^2 - 4u_{111}u_{133}\lambda_3^2 - 3)\right)\sqrt{6}\,\phi_3 \\ &- i\sqrt{6}\left(2a_1^2 + 3a_3^2(2u_{111}^2\lambda_3^2 + 2u_{133}^2\lambda_3^2 - 4u_{111}u_{133}\lambda_3^2 - 3)\right)\chi_3 \\ &- 2\lambda_3\left(4(u_{133}-u_{111})a_1^2 + 9a_3^2(u_{111}-u_{133}) + 12a_3(\lambda_3^2+1)\right)\psi_3\Bigg] = 0\end{aligned} \tag{4.183}$$

$$\text{eq8t} = \frac{1}{24a_3}\Bigg[24a_3\frac{\partial\phi_3}{\partial t} - 2i\sqrt{6}a_1^2\psi_3 - 3a_3\lambda_3\left(8(\lambda_3^2+1) + a_3(u_{111}-u_{133})(8u_{111}^2\lambda_3^2 + 8u_{133}^2\lambda_3^2 - 16u_{111}u_{133}\lambda_3^2 - 3)\right)\phi_3 + 9a_3^2(u_{133}-u_{111})\lambda_3\chi_3 - 6i\sqrt{6}a_3^2u_{111}^2\lambda_3^2\psi_3 - 6i\sqrt{6}a_3^2u_{133}^2\lambda_3^2\psi_3 + 12i\sqrt{6}a_3^2u_{111}u_{133}\lambda_3^2\psi_3 + 9i\sqrt{6}a_3^2\psi_3\Bigg] = 0 \tag{4.184}$$

$$\text{eq9t} = \frac{1}{24a_3}\Bigg[24a_3\frac{\partial\chi_3}{\partial t} + 2i\sqrt{6}a_1^2\psi_3 + 9a_3^2(u_{133}-u_{111})\lambda_3\phi_3 - 3a_3\lambda_3\left(8(\lambda_3^2+1) + a_3(u_{111}-u_{133})(8u_{111}^2\lambda_3^2 + 8u_{133}^2\lambda_3^2 - 16u_{111}u_{133}\lambda_3^2 - 3)\right)\chi_3\Bigg] = 0 \tag{4.185}$$

After integrating the spatial and temporal equations, we obtain:

$$\begin{aligned}
\phi_2(x,t) = \tfrac{1}{2}\Bigg[& e^{\lambda_2\left(t(a_3(u_{111}-u_{133})^3+1)\lambda_2^2+t+u_{133}x\right)}(c_1+c_2) \\
& + \frac{e^{\frac{1}{12}\left(\frac{ty}{a_3}+6xz\right)}}{hl^2n}\Bigg((2ka_1^2+3a_3^2m)\cosh\left(\tfrac{tw}{12a_3}\right) \\
& \times\Big[(c_1-c_2)g\Big(k\cosh\left(\tfrac{fx}{2}\right) + f(u_{133}-u_{111})\lambda_2\sinh\left(\tfrac{fx}{2}\right)\Big) \\
& - i\sqrt{6}c_3fhl\sinh\left(\tfrac{fx}{2}\right)\Big] \\
& + w\Big[gk\Big((c_1-c_2)(u_{111}-u_{133})\lambda_2 + c_3i\sqrt{6}\Big)\cosh\left(\tfrac{fx}{2}\right) \\
& + f\Big(-(c_1-c_2)g(u_{111}-u_{133})^2\lambda_2^2 - i\sqrt{6}c_3(g-hl)(u_{111}-u_{133})\lambda_2 \\
& + 3(c_2-c_1)hl\Big)\sinh\left(\tfrac{fx}{2}\right)\Big]
\end{aligned}$$

$$\times \sinh\left(\tfrac{tw}{12a_3}\right)\Bigg)\Bigg]$$

$$\chi_2(x,t) = \tfrac{1}{2}\Bigg[e^{\lambda_2\left(t(a_3(u_{111}-u_{133})^3+1)\lambda_2^2+t+u_{133}x\right)}(c_1+c_2)$$
$$+ \frac{e^{\frac{1}{12}\left(\frac{ty}{a_3}+6xz\right)}}{hl^2n}\Bigg((2ka_1^2+3a_3^2m)\cosh\left(\tfrac{tw}{12a_3}\right)$$
$$\times\Bigg[(c_2-c_1)gk\cosh\left(\tfrac{fx}{2}\right)+f\Big((c_1-c_2)g(u_{111}-u_{133})\lambda_2+c_3hil\sqrt{6}\Big)\sinh\left(\tfrac{fx}{2}\right)\Bigg]$$
$$+ w\Bigg[gk\Big(-(c_1-c_2)(u_{111}-u_{133})\lambda_2+c_3(-i)\sqrt{6}\Big)\cosh\left(\tfrac{fx}{2}\right)$$
$$+ f\Big((c_1-c_2)g(u_{111}-u_{133})^2\lambda_2^2+c_3i(g-hl)(u_{111}-u_{133})\sqrt{6}\lambda_2$$
$$+ 3(c_1-c_2)hl\Big)\sinh\left(\tfrac{fx}{2}\right)\Bigg]$$
$$\times \sinh\left(\tfrac{tw}{12a_3}\right)\Bigg)\Bigg]$$

$$\psi_2(x,t) = \frac{e^{\frac{1}{12}\left(\frac{ty}{a_3}+6xz\right)}}{2hl^2n}\Bigg[(2ka_1^2+3a_3^2m)\cosh\left(\tfrac{tw}{12a_3}\right)$$
$$\times\Big(2c_3hkl\cosh\left(\tfrac{fx}{2}\right)+f\Big(2c_3hl(u_{111}-u_{133})\lambda_2+(c_1-c_2)gi\sqrt{6}\Big)\sinh\left(\tfrac{fx}{2}\right)\Big)$$
$$+ w\Big(fg\Big(i\sqrt{6}(c_1-c_2)(u_{111}-u_{133})\lambda_2-6c_3\Big)\sinh\left(\tfrac{fx}{2}\right)$$
$$+ hl\Big(2c_3(u_{133}-u_{111})\lambda_2-i\sqrt{6}c_1+i\sqrt{6}c_2\Big)$$
$$\times\Big(k\cosh\left(\tfrac{fx}{2}\right)+f(u_{111}-u_{133})\lambda_2\sinh\left(\tfrac{fx}{2}\right)\Big)\Big)$$
$$\times \sinh\left(\tfrac{tw}{12a_3}\right)\Bigg]$$

$$\phi_1(x,t) = \tfrac{1}{2}\Bigg[e^{\lambda_1\left(t(a_3(u_{111}-u_{133})^3+1)\lambda_1^2+t+u_{133}x\right)}(c_4+c_5)$$
$$+ \frac{e^{\frac{1}{12}\left(\frac{ty_1}{a_3}+6xz_1\right)}}{h_1l_1^2n_1}\Bigg((2k_1a_1^2+3a_3^2m_1)\cosh\left(\tfrac{tw_1}{12a_3}\right)$$
$$\times\Big[(c_4-c_5)g_1\Big(k_1\cosh\left(\tfrac{f_1x}{2}\right)+f_1(u_{133}-u_{111})\lambda_1\sinh\left(\tfrac{f_1x}{2}\right)\Big)$$
$$- i\sqrt{6}c_6f_1h_1l_1\sinh\left(\tfrac{f_1x}{2}\right)\Big]$$
$$+ w_1\Big[g_1k_1\Big((c_4-c_5)(u_{111}-u_{133})\lambda_1+c_6i\sqrt{6}\Big)\cosh\left(\tfrac{f_1x}{2}\right)$$

$$+ f_1\Big(- (c_4 - c_5)g_1(u_{111} - u_{133})^2\lambda_1^2 - i\sqrt{6}c_6(g_1 - h_1l_1)(u_{111} - u_{133})\lambda_1$$
$$+ 3(c_5 - c_4)h_1l_1\Big)\sinh\left(\tfrac{f_1x}{2}\right)\Big]$$
$$\times \sinh\left(\tfrac{tw_1}{12a_3}\right)\Big)\Big]$$

$$\chi_1(x,t) = \tfrac{1}{2}\Bigg[e^{\lambda_1\left(t(a_3(u_{111}-u_{133})^3+1)\lambda_1^2+t+u_{133}x\right)}(c_4 + c_5)$$
$$+ \frac{e^{\frac{1}{12}\left(\frac{ty_1}{a_3}+6xz_1\right)}}{h_1l_1^2n_1}\Bigg((2k_1a_1^2 + 3a_3^2m_1)\cosh\left(\tfrac{tw_1}{12a_3}\right)$$
$$\times \Big[(c_5 - c_4)g_1k_1\cosh\left(\tfrac{f_1x}{2}\right) + f_1\Big((c_4 - c_5)g_1(u_{111} - u_{133})\lambda_1 + c_6h_1il_1\sqrt{6}\Big)\sinh\left(\tfrac{f_1x}{2}\right)\Big]$$
$$+ w_1\Big[g_1k_1\Big(- (c_4 - c_5)(u_{111} - u_{133})\lambda_1 + c_6(-i)\sqrt{6}\Big)\cosh\left(\tfrac{f_1x}{2}\right)$$
$$+ f_1\Big((c_4 - c_5)g_1(u_{111} - u_{133})^2\lambda_1^2 + c_6i(g_1 - h_1l_1)(u_{111} - u_{133})\sqrt{6}\lambda_1$$
$$+ 3(c_4 - c_5)h_1l_1\Big)\sinh\left(\tfrac{f_1x}{2}\right)\Big]$$
$$\times \sinh\left(\tfrac{tw_1}{12a_3}\right)\Big)\Bigg]$$

$$\psi_1(x,t) = \frac{e^{\frac{1}{12}\left(\frac{ty_1}{a_3}+6xz_1\right)}}{2h_1l_1^2n_1}\Bigg[(2k_1a_1^2 + 3a_3^2m_1)\cosh\left(\tfrac{tw_1}{12a_3}\right)$$
$$\times \Big(2c_6h_1k_1l_1\cosh\left(\tfrac{f_1x}{2}\right) + f_1\Big(2c_6h_1l_1(u_{111} - u_{133})\lambda_1 + (c_4 - c_5)g_1i\sqrt{6}\Big)\sinh\left(\tfrac{f_1x}{2}\right)\Big)$$
$$+ w_1\Big(f_1g_1\Big(i\sqrt{6}(c_4 - c_5)(u_{111} - u_{133})\lambda_1 - 6c_6\Big)\sinh\left(\tfrac{f_1x}{2}\right)$$
$$+ h_1l_1\Big(2c_6(u_{133} - u_{111})\lambda_1 - i\sqrt{6}c_4 + i\sqrt{6}c_5\Big)$$
$$\times \Big(k_1\cosh\left(\tfrac{f_1x}{2}\right) + f_1(u_{111} - u_{133})\lambda_1\sinh\left(\tfrac{f_1x}{2}\right)\Big)\Big)$$
$$\times \sinh\left(\tfrac{tw_1}{12a_3}\right)\Bigg]$$

$$\phi_3(x,t) = \tfrac{1}{2}\Bigg[e^{\lambda_3\left(t(a_3(u_{111}-u_{133})^3+1)\lambda_3^2+t+u_{133}x\right)}(c_7 + c_8)$$
$$+ \frac{e^{\frac{1}{12}\left(\frac{ty_3}{a_3}+6xz_3\right)}}{h_3l_3^2n_3}\Bigg((2k_3a_1^2 + 3a_3^2m_3)\cosh\left(\tfrac{tw_3}{12a_3}\right)$$
$$\times \Big[(c_7 - c_8)g_3\Big(k_3\cosh\left(\tfrac{f_3x}{2}\right) + f_3(u_{133} - u_{111})\lambda_3\sinh\left(\tfrac{f_3x}{2}\right)\Big)$$
$$- i\sqrt{6}c_9f_3h_3l_3\sinh\left(\tfrac{f_3x}{2}\right)\Big]$$

$$
\begin{aligned}
&+ w_3\Bigg[g_3k_3\Big((c_7-c_8)(u_{111}-u_{133})\lambda_3 + c_9 i\sqrt{6}\Big)\cosh\left(\tfrac{f_3x}{2}\right)\\
&+ f_3\Big(-(c_7-c_8)g_3(u_{111}-u_{133})^2\lambda_3^2 - i\sqrt{6}c_9(g_3-h_3l_3)(u_{111}-u_{133})\lambda_3\\
&+ 3(c_8-c_7)h_3l_3\Big)\sinh\left(\tfrac{f_3x}{2}\right)\Bigg]\\
&\times\sinh\left(\tfrac{tw_3}{12a_3}\right)\Bigg)\Bigg]
\end{aligned}
$$

$$
\begin{aligned}
\chi_3(x,t) = \tfrac{1}{2}\Bigg[&e^{\lambda_3\left(t(a_3(u_{111}-u_{133})^3+1)\lambda_3^2+t+u_{133}x\right)}(c_7+c_8)\\
&+ \frac{e^{\frac{1}{12}\left(\frac{ty_3}{a_3}+6xz_3\right)}}{h_3l_3^2n_3}\Bigg((2k_3a_1^2+3a_3^2m_3)\cosh\left(\tfrac{tw_3}{12a_3}\right)\\
&\times\Big[(c_8-c_7)g_3k_3\cosh\left(\tfrac{f_3x}{2}\right) + f_3\Big((c_7-c_8)g_3(u_{111}-u_{133})\lambda_3 + c_9h_3il_3\sqrt{6}\Big)\sinh\left(\tfrac{f_3x}{2}\right)\Big]\\
&+ w_3\Bigg[g_3k_3\Big(-(c_7-c_8)(u_{111}-u_{133})\lambda_3 + c_9(-i)\sqrt{6}\Big)\cosh\left(\tfrac{f_3x}{2}\right)\\
&+ f_3\Big((c_7-c_8)g_3(u_{111}-u_{133})^2\lambda_3^2 + c_9i(g_3-h_3l_3)(u_{111}-u_{133})\sqrt{6}\lambda_3\\
&+ 3(c_7-c_8)h_3l_3\Big)\sinh\left(\tfrac{f_3x}{2}\right)\Bigg]\\
&\times\sinh\left(\tfrac{tw_3}{12a_3}\right)\Bigg)\Bigg]
\end{aligned}
$$

$$
\begin{aligned}
\psi_3(x,t) = \frac{e^{\frac{1}{12}\left(\frac{ty_3}{a_3}+6xz_3\right)}}{2h_3l_3^2n_3}\Bigg[&(2k_3a_1^2+3a_3^2m_3)\cosh\left(\tfrac{tw_3}{12a_3}\right)\\
&\times\Big(2c_9h_3k_3l_3\cosh\left(\tfrac{f_3x}{2}\right) + f_3\Big(2c_9h_3l_3(u_{111}-u_{133})\lambda_3 + (c_7-c_8)g_3i\sqrt{6}\Big)\sinh\left(\tfrac{f_3x}{2}\right)\Big)\\
&+ w_3\Big(f_3g_3\Big(i\sqrt{6}(c_7-c_8)(u_{111}-u_{133})\lambda_3 - 6c_9\Big)\sinh\left(\tfrac{f_3x}{2}\right)\\
&+ h_3l_3\Big(2c_9(u_{133}-u_{111})\lambda_3 - i\sqrt{6}c_7 + i\sqrt{6}c_8\Big)\\
&\times\Big(k_3\cosh\left(\tfrac{f_3x}{2}\right) + f_3(u_{111}-u_{133})\lambda_3\sinh\left(\tfrac{f_3x}{2}\right)\Big)\Big)\\
&\times\sinh\left(\tfrac{tw_3}{12a_3}\right)\Bigg]
\end{aligned}
$$

where:

$$
\mathrm{w} = \sqrt{\left((u_{111}-u_{133})^2\lambda_2^2+3\right)\left(2a_1^2+3a_3^2(2u_{111}^2\lambda_2^2+2u_{133}^2\lambda_2^2-4u_{111}u_{133}\lambda_2^2-3)\right)^2}
$$

$$
\mathrm{w}_1 = \sqrt{\left((u_{111}-u_{133})^2\lambda_1^2+3\right)\left(2a_1^2+3a_3^2(2u_{111}^2\lambda_1^2+2u_{133}^2\lambda_1^2-4u_{111}u_{133}\lambda_1^2-3)\right)^2}
$$

$$w_3 = \sqrt{\left((u_{111}-u_{133})^2\lambda_3^2+3\right)\left(2a_1^2+3a_3^2(2u_{111}^2\lambda_3^2+2u_{133}^2\lambda_3^2-4u_{111}u_{133}\lambda_3^2-3)\right)^2}$$

$$y = 6\,a_3^2(u_{111}-u_{133})^3\lambda_2^3-2a_1^2u_{111}\lambda_2+2a_1^2u_{133}\lambda_2+12a_3(\lambda_2^3+\lambda_2)$$

$$y_1 = 6a_3^2(u_{111}-u_{133})^3\lambda_1^3-2a_1^2u_{111}\lambda_1+2a_1^2u_{133}\lambda_1+12a_3(\lambda_1^3+\lambda_1)$$

$$y_3 = 6a_3^2(u_{111}-u_{133})^3\lambda_3^3-2a_1^2u_{111}\lambda_3+2a_1^2u_{133}\lambda_3+12a_3(\lambda_3^3+\lambda_3)$$

$$f = \sqrt{(u_{111}-u_{133})^2\lambda_2^2+3},\quad f_1 = \sqrt{(u_{111}-u_{133})^2\lambda_1^2+3},\quad f_3 = \sqrt{(u_{111}-u_{133})^2\lambda_3^2+3}$$

$$z = (u_{111}+u_{133})\lambda_2,\quad z_1 = (u_{111}+u_{133})\lambda_1,\quad z_3 = (u_{111}+u_{133})\lambda_3$$

$$k = (u_{111}-u_{133})^2\lambda_2^2+3,\quad k_1 = (u_{111}-u_{133})^2\lambda_1^2+3,\quad k_3 = (u_{111}-u_{133})^2\lambda_3^2+3$$

$$n = k^2,\quad n_1 = k_1^2,\quad n_3 = k_3^2$$

$$l = 2\,a_1^2+3a_3^2(2u_{111}^2\lambda_2^2+2u_{133}^2\lambda_2^2-4u_{111}u_{133}\lambda_2^2-3)$$

$$l_1 = 2a_1^2+3a_3^2(2u_{111}^2\lambda_1^2+2u_{133}^2\lambda_1^2-4u_{111}u_{133}\lambda_1^2-3)$$

$$l_3 = 2a_1^2+3a_3^2(2u_{111}^2\lambda_3^2+2u_{133}^2\lambda_3^2-4u_{111}u_{133}\lambda_3^2-3)$$

$$m = 2\,u_{111}^4\lambda_2^4+2u_{133}^4\lambda_2^4-8u_{111}^3u_{133}\lambda_2^4+3u_{133}^2\lambda_2^2$$
$$-2u_{111}u_{133}(4u_{133}^2\lambda_2^2+3)\lambda_2^2+3u_{111}^2(4u_{133}^2\lambda_2^4+\lambda_2^2)-9$$

$$m_1 = 2u_{111}^4\lambda_1^4+2u_{133}^4\lambda_1^4-8u_{111}^3u_{133}\lambda_1^4+3u_{133}^2\lambda_1^2$$
$$-2u_{111}u_{133}(4u_{133}^2\lambda_1^2+3)\lambda_1^2+3u_{111}^2(4u_{133}^2\lambda_1^4+\lambda_1^2)-9$$

$$m_3 = 2u_{111}^4\lambda_3^4+2u_{133}^4\lambda_3^4-8u_{111}^3u_{133}\lambda_3^4+3u_{133}^2\lambda_3^2$$
$$-2u_{111}u_{133}(4u_{133}^2\lambda_3^2+3)\lambda_3^2+3u_{111}^2(4u_{133}^2\lambda_3^4+\lambda_3^2)-9$$

$$h = 4a_1^4+12a_3^2(u_{111}^2\lambda_2^2+u_{133}^2\lambda_2^2-2u_{111}u_{133}\lambda_2^2-3)a_1^2$$
$$-81a_3^4(u_{111}^2\lambda_2^2+u_{133}^2\lambda_2^2-2u_{111}u_{133}\lambda_2^2-1)$$

$$h_1 = 4a_1^4+12a_3^2(u_{111}^2\lambda_1^2+u_{133}^2\lambda_1^2-2u_{111}u_{133}\lambda_1^2-3)a_1^2$$
$$-81a_3^4(u_{111}^2\lambda_1^2+u_{133}^2\lambda_1^2-2u_{111}u_{133}\lambda_1^2-1)$$

$$h_3 = 4a_1^4+12a_3^2(u_{111}^2\lambda_3^2+u_{133}^2\lambda_3^2-2u_{111}u_{133}\lambda_3^2-3)a_1^2$$
$$-81a_3^4(u_{111}^2\lambda_3^2+u_{133}^2\lambda_3^2-2u_{111}u_{133}\lambda_3^2-1)$$

By applying the Darboux transformation (DT), we derive the breather solution of the HNLS equation as follows:

$$\Psi(x,t) = \Psi_0(x,t)\,\frac{f\lambda_3 z(u-v)\left(\sinh(fx)\,m_1(x,t) - \cosh(fx)\,m_2(x,t)\right) + f_1}{-f\lambda_3 z(u-v)\left(\sinh(fx)\,m_1(x,t) - \cosh(fx)\,m_2(x,t)\right) + f_2}, \quad (4.186)$$

where,

$$f = \sqrt{(u-v)^2\lambda_3^2 + 3}, z = f\left(2a_1^2 + 3a_3^2\left(2(u-v)^2\lambda_3^2 - 3\right)\right)$$

$$m_1(x,t) = \sinh\left(\frac{tz}{6a_3}\right)\left(\sqrt{6}c_3 - 2ic_2\lambda_3(u-v)\right)$$

$$m_2(x,t) = \cosh\left(\frac{tz}{6a_3}\right)\left(\sqrt{6}c_3 - 2ic_2\lambda_3(u-v)\right) + 2ic_2 f\sinh\left(\frac{tz}{6a_3}\right)$$

$f_1 = -24\,i\,a_3^2\,c_2\,u_{133}^6\,\lambda_3^6 + 144\,a_3^2\,c_2\,i\,u_{111}\,u_{133}^5\,\lambda_3^6 - 360\,i\,a_3^2\,c_2\,u_{111}^2\,u_{133}^4\,\lambda_3^6 + 480\,a_3^2\,c_2\,i\,u_{111}^3\,u_{133}^3\,\lambda_3^6 - 8i\,a_1^2\,c_2\,u_{111}^4\,\lambda_3^4 - 72\,i\,a3^2\,c_2\,u_{111}^4\,\lambda_3^4 - 48\,i\,a_1^2\,c_2\,u_{111}^2\,u_{133}^2\,\lambda_3^4 + 32\,a_1^2\,c_2\,i\,u_{111}^3\,u_{133}\,\lambda_3^4 + 288\,a_3^2\,c_2\,i\,u_{111}^3\,u_{133}\,\lambda_3^4 - 2\sqrt{6}\,a_1^2\,c_3\,u_{133}^3\,\lambda_3^3 - 9\sqrt{6}\,a_3^2\,c_3\,u_{133}^3\,\lambda_3^3 + 27\,a_3^2\,c_3\,u_{111}\,u_{133}^2\sqrt{6}\,\lambda_3^3 - 24\,i\,a_3^2\,c_2\,u_{111}^6\,\lambda_3^6 - 360\,i\,a_3^2\,c_2\,u_{111}^4\,u_{133}^2\,\lambda_3^6 + 144\,a_3^2\,c_2\,i\,u_{111}^5\,u_{133}\,\lambda_3^6 - 6\sqrt{6}\,a_3^2\,c_3\,u_{133}^5\,\lambda_3^5 + 30\,a_3^2\,c_3\,u_{111}\,u_{133}^4\sqrt{6}\,\lambda_3^5 - 60\,a_3^2\,c_3\,u_{111}^2\,u_{133}^3\sqrt{6}\,\lambda_3^5 - 30\sqrt{6}\,a_3^2\,c_3\,u_{111}^4\,u_{133}\,\lambda_3^5 + 6\,a_3^2\,c_3\,u_{111}^5\sqrt{6}\,\lambda_3^5 + 60\,a_3^2\,c_3\,u_{111}^3\,u_{133}^2\sqrt{6}\,\lambda_3^5 - 8\,i\,a_1^2\,c_2\,u_{133}^4\,\lambda_3^4 - 72\,i\,a_3^2\,c_2\,u_{133}^4\,\lambda_3^4 + 32\,a_1^2\,c_2\,i\,u_{111}\,u_{133}^3\,\lambda_3^4 + 288\,a_3^2\,c_2\,i\,u_{111}\,u_{133}^3\,\lambda_3^4 - 432\,a_3^2\,c_2\,i\,u_{111}^2\,u_{133}^2\,\lambda_3^4 - 6\sqrt{6}\,a_1^2\,c_3\,u_{111}^2\,u_{133}\,\lambda_3^3 - 27\sqrt{6}\,a_3^2\,c_3\,u_{111}^2\,u_{133}\,\lambda_3^3 + 2\,a_1^2\,c_3\,u_{111}^3\sqrt{6}\,\lambda_3^3 + 9\,a_3^2\,c_3\,u_{111}^3\sqrt{6}\,\lambda_3^3 + 6\,a_1^2\,c_3\,u_{111}\,u_{133}^2\sqrt{6}\,\lambda_3^3 - 36\,i\,a_1^2\,c_2\,u_{133}^2\,\lambda_3^2 + 54\,a_3^2\,c_2\,i\,u_{133}^2\,\lambda_3^2 - 108\,a_3^2\,c_2\,i\,u_{111}\,u_{133}\,\lambda_3^2 - 36\,i\,c_2\,u_{111}^2\,\lambda_3^2\,a_1^2 + 72\,c_2\,i\,u_{111}\,u_{133}\,\lambda_3^2\,a_1^2 - 36\,c_2\,i\,a_1^2 - 6\sqrt{6}\,c_3\,u_{133}\,\lambda_3\,a_1^2 + 6\,c_3\,u_{111}\,\lambda_3\sqrt{6}\,a_1^2 + 54\,a_3^2\,c_2\,i\,u_{111}^2\,\lambda_3^2 + 162\,a_3^2\,c_2\,i - 27\sqrt{6}\,a_3^2\,c_3\,u_{111}\,\lambda_3 + 27\,a_3^2\,c_3\,u_{133}\,\lambda_3\sqrt{6}.$

$f_2 = -30\sqrt{6}\,a_3^2\,c_3\,u_{111}\,u_{133}^4\,\lambda_3^5 + 6\,a_3^2\,c_3\,u_{133}^5\sqrt{6}\,\lambda_3^5 + 60\,c_3^2\,c_3\,u_{111}^2\,u_{133}^3\sqrt{6}\,\lambda_3^5 - 6\sqrt{6}\,a_3^2\,c_3\,u_{111}^5\,\lambda_3^5 - 60\sqrt{6}\,a_3^2\,c_3\,u_{111}^3\,u_{133}^2\,\lambda_3^5 + 30\,a_3^2\,c_3\,u_{111}^4\,u_{133}\sqrt{6}\,\lambda_3^5 - 36\,i\,a_3^2\,c_2\,u_{133}^4\,\lambda_3^4 + 144\,a_3^2\,c_2\,i\,u_{111}\,u_{133}^3\,\lambda_3^4 - 216\,a_3^2\,c_2\,i\,u_{111}^2\,u_{133}^2\,\lambda_3^4 - 36\,i\,a_3^2\,c_2\,u_{111}^4\,\lambda_3^4 + 144\,a_3^2\,c_2\,i\,u_{111}^3\,u_{133}\,\lambda_3^4 - 6\sqrt{6}\,a_1^2\,c_3\,u_{111}\,u_{133}^2\,\lambda_3^3 - 27\sqrt{6}\,a_3^2\,c_3\,u_{111}\,u_{133}^2\,\lambda_3^3 + 2\,a_1^2\,c_3\,u_{133}^3\sqrt{6}\,\lambda_3^3 + 9\,a_3^2\,c_3\,u_{133}^3\sqrt{6}\,\lambda_3^3 + 27\,a_3^2\,c_3\,u_{111}^2\,u_{133}\sqrt{6}\,\lambda_3^3 - 2\sqrt{6}\,a_1^2\,c_3\,u_{111}^3\,\lambda_3^3 - 9\sqrt{6}\,a_3^2\,c_3\,u_{111}^3\,\lambda_3^3 + 6\,a_1^2\,c_3\,u_{111}^2\,u_{133}\sqrt{6}\,\lambda_3^3 - 12\,i\,a_1^2\,c_2\,u_{133}^2\,\lambda_3^2 - 54\,i\,a_3^2\,c_2\,u_{133}^2\,\lambda_3^2 + 24\,a_1^2\,c_2\,i\,u_{111}\,u_{133}\,\lambda_3^2 + 108\,a_3^2\,c_2\,i\,u_{111}\,u_{133}\,\lambda_3^2 - 12\,i\,c_2\,u_{111}^2\,\lambda_3^2 a_1^2 - 36\,c_2\,i\,a_1^2 - 6\sqrt{6}\,c_3\,u_{111}\,\lambda_3\,a_1^2 + 6\,c_3\,u_{133}\,\lambda_3\sqrt{6}\,a_1^2 - 54\,i\,a_3^2\,c_2\,u_{111}^2\,\lambda_3^2 + 162\,a_3^2\,c_2\,i - 27\sqrt{6}\,a_3^2\,c_3\,u_{133}\,\lambda_3 + 27\,a_3^2\,c_3\,u_{111}\,\lambda_3\sqrt{6}.$

4-2 Derivation of General Solutions for the Non-autonomous HNLS Equation

4-2-1 Breather Solutions via the Darboux Transformation

We derive the compatibility equations,we found 18 equations :9 equations for time and 9 equations for space ,we use seed $\sqrt{-\frac{a_1(t)}{a_2(t)}}e^{\frac{i\,x\,a_1(t)}{3\,a_3(t)}}$:

$$\text{eq1x} = \frac{1}{4}\left(4(\lambda_1 u133\,\psi_1(x,t) + \psi_1^{(1,0)}(x,t)) + i\sqrt{6}\chi_1(x,t) - i\sqrt{6}\phi_1(x,t)\right) = 0$$

$$\text{eq2x} = -\lambda_1 u_{133}\phi_1(x,t) + \frac{i}{2}\sqrt{\frac{3}{2}}\,\psi_1(x,t) + \phi_1^{(1,0)}(x,t) = 0$$

$$\text{eq3x} = -\lambda_1 u_{133}\chi_1(x,t) + \chi_1^{(1,0)}(x,t) - \frac{i}{2}\sqrt{\frac{3}{2}}\,\psi_1(x,t) = 0$$

$$\text{eq4x} = \frac{1}{4}\left(4(\lambda_2 u_{133}\psi_2(x,t) + \psi_2^{(1,0)}(x,t)) + i\sqrt{6}\,\chi_2(x,t) - i\sqrt{6}\,\phi_2(x,t)\right)$$
$$= 0$$

$$\text{eq5x} = -\lambda_2 u_{133}\phi_2(x,t) + \frac{i}{2}\sqrt{\frac{3}{2}}\,\psi_2(x,t) + \phi_2^{(1,0)}(x,t) = 0$$

$$\text{eq6x} = -\lambda_2 u_{133}\chi_2(x,t) + \chi_2^{(1,0)}(x,t) - \frac{i}{2}\sqrt{\frac{3}{2}}\,\psi_2(x,t) = 0$$

$$\text{eq7x} = \frac{1}{4}\left(4(\lambda_3 u_{133}\psi_3(x,t) + \psi_3^{(1,0)}(x,t)) + i\sqrt{6}\,\chi_3(x,t) - i\sqrt{6}\,\phi_3(x,t)\right) = 0$$

$$\text{eq8x} = -\lambda_3 u_{133}\phi_3(x,t) + \frac{i}{2}\sqrt{\frac{3}{2}}\,\psi_3(x,t) + \phi_3^{(1,0)}(x,t) = 0$$

$$\text{eq9x} = -\lambda_3 u_{133}\chi_3(x,t) + \chi_3^{(1,0)}(x,t) - \frac{i}{2}\sqrt{\frac{3}{2}}\,\psi_3(x,t) = 0$$

$$
\begin{cases}
\text{eq1t: } \frac{ia_1(t)^2}{12a_3(t)}\left(\sqrt{6}\phi_1-\sqrt{6}\chi_1+8iu_{133}\lambda_1\psi_1\right)-(\lambda_1^3+\lambda_1)\psi_1 \\
\quad +\frac{a_3(t)}{8}\left[i(8u_{133}^2\lambda_1^2-3)\sqrt{6}(\phi_1-\chi_1)+12u_{133}\lambda_1\psi_1\right]+\psi_1^{(0,1)} \\
\text{eq2t: } -\frac{ia_1(t)^2}{2\sqrt{6}a_3(t)}\psi_1-(\lambda_1^3+\lambda_1)\phi_1 \\
\quad +\frac{a_3(t)}{8}\left[(64u_{133}^3\lambda_1^3-6u_{133}\lambda_1)\phi_1+6u_{133}\lambda_1\chi_1+i(3-8u_{133}^2\lambda_1^2)\sqrt{6}\psi_1\right]+\phi_1^{(0,1)} \\
\text{eq3t: } \frac{ia_1(t)^2}{2\sqrt{6}a_3(t)}\psi_1-(\lambda_1^3+\lambda_1)\chi_1 \\
\quad +\frac{a_3(t)}{8}\left[6u_{133}\lambda_1\phi_1+(64u_{133}^3\lambda_1^3-6u_{133}\lambda_1)\chi_1+i(8u_{133}^2\lambda_1^2-3)\sqrt{6}\psi_1\right]+\chi_1^{(0,1)} \\
\text{eq4t–eq6t: same structure with } (\lambda_2,\phi_2,\chi_2,\psi_2) \\
\text{eq7t–eq9t: same structure with } (\lambda_3,\phi_3,\chi_3,\psi_3)
\end{cases}
\tag{4.187}
$$

After integrating the spatial and temporal equations, we obtain:

$$
\begin{aligned}
\chi_1(x,t) = \frac{1}{2}e^{u_{133}x\lambda_1+\int\left(-8u_{133}^3a_3(t)\lambda_1^3+\lambda_1^3+\lambda_1\right)dt}c_1 \\
+ c_3\exp\left\{\frac{1}{12}\left[\int\left(\frac{2(2u_{133}\lambda_1+\sqrt{4u_{133}^2\lambda_1^2+3})a_1(t)^2}{a_3(t)}+12(\lambda_1^3+\lambda_1)\right.\right.\right. \\
\left.\left.\left.+3a_3(t)\left(-16u_{133}^3\lambda_1^3+8u_{133}^2\sqrt{4u_{133}^2\lambda_1^2+3}\lambda_1^2-3\sqrt{4u_{133}^2\lambda_1^2+3}\right)\right)dt\right.\right. \\
\left.\left.-6x\sqrt{4u_{133}^2\lambda_1^2+3}\right]\right\} \\
+ c_2\exp\left\{\frac{1}{12}\left[\int\left(-\frac{2(\sqrt{4u_{133}^2\lambda_1^2+3}-2u_{133}\lambda_1)a_1(t)^2}{a_3(t)}+12(\lambda_1^3+\lambda_1)\right.\right.\right. \\
\left.\left.\left.-3\left(16u_{133}^3\lambda_1^3+8u_{133}^2\sqrt{4u_{133}^2\lambda_1^2+3}\lambda_1^2-3\sqrt{4u_{133}^2\lambda_1^2+3}\right)a_3(t)\right)dt\right.\right. \\
\left.\left.+6x\sqrt{4u_{133}^2\lambda_1^2+3}\right]\right\}
\end{aligned}
\tag{4.188}
$$

$$
\begin{aligned}
\chi_2(x,t) = \frac{1}{2} e^{u_{133}x\lambda_2 + \int \left(-8u_{133}^3 a_3(t)\lambda_2^3 + \lambda_2^3 + \lambda_2\right)dt} c_4 \\
+ c_6 \exp\Bigg\{ \frac{1}{12}\Bigg[\int \Bigg(\frac{2(2u_{133}\lambda_2 + \sqrt{4u_{133}^2\lambda_2^2+3})a_1(t)^2}{a_3(t)} + 12(\lambda_2^3+\lambda_2) \\
+ 3a_3(t)\Big(-16u_{133}^3\lambda_2^3 + 8u_{133}^2\sqrt{4u_{133}^2\lambda_2^2+3}\lambda_2^2 - 3\sqrt{4u_{133}^2\lambda_2^2+3}\Big)\Bigg) dt \\
- 6x\sqrt{4u_{133}^2\lambda_2^2+3}\Bigg]\Bigg\} \\
+ c_5 \exp\Bigg\{ \frac{1}{12}\Bigg[\int \Bigg(-\frac{2(\sqrt{4u_{133}^2\lambda_2^2+3} - 2u_{133}\lambda_2)a_1(t)^2}{a_3(t)} + 12(\lambda_2^3+\lambda_2) \\
- 3\Big(16u_{133}^3\lambda_2^3 + 8u_{133}^2\sqrt{4u_{133}^2\lambda_2^2+3}\lambda_2^2 - 3\sqrt{4u_{133}^2\lambda_2^2+3}\Big)a_3(t)\Bigg) dt \\
+ 6x\sqrt{4u_{133}^2\lambda_2^2+3}\Bigg]\Bigg\}
\end{aligned}
\tag{4.189}
$$

$$
\begin{aligned}
\chi_3(x,t) = \frac{1}{2} e^{u_{133}x\lambda_3 + \int \left(-8u_{133}^3 a_3(t)\lambda_3^3 + \lambda_3^3 + \lambda_3\right)dt} c_7 \\
+ c_9 \exp\Bigg\{ \frac{1}{12}\Bigg[\int \Bigg(\frac{2(2u_{133}\lambda_3 + \sqrt{4u_{133}^2\lambda_3^2+3})a_1(t)^2}{a_3(t)} + 12(\lambda_3^3+\lambda_3) \\
+ 3a_3(t)\Big(-16u_{133}^3\lambda_3^3 + 8u_{133}^2\sqrt{4u_{133}^2\lambda_3^2+3}\lambda_3^2 - 3\sqrt{4u_{133}^2\lambda_3^2+3}\Big)\Bigg) dt \\
- 6x\sqrt{4u_{133}^2\lambda_3^2+3}\Bigg]\Bigg\} \\
+ c_8 \exp\Bigg\{ \frac{1}{12}\Bigg[\int \Bigg(-\frac{2(\sqrt{4u_{133}^2\lambda_3^2+3} - 2u_{133}\lambda_3)a_1(t)^2}{a_3(t)} + 12(\lambda_3^3+\lambda_3) \\
- 3\Big(16u_{133}^3\lambda_3^3 + 8u_{133}^2\sqrt{4u_{133}^2\lambda_3^2+3}\lambda_3^2 - 3\sqrt{4u_{133}^2\lambda_3^2+3}\Big)a_3(t)\Bigg) dt \\
+ 6x\sqrt{4u_{133}^2\lambda_3^2+3}\Bigg]\Bigg\}
\end{aligned}
\tag{4.190}
$$

$$\psi_1(x,t) = i\sqrt{\frac{2}{3}}\, e^{-\frac{1}{2}x\sqrt{4u_{133}^2\lambda_1^2+3}}\Bigg[c_3\, e^{\frac{1}{12}\int\Big(\frac{2(2u_{133}\lambda_1+\sqrt{4u_{133}^2\lambda_1^2+3})a_1(t)^2}{a_3(t)}+12(\lambda_1^3+\lambda_1)}$$
$$+ 3a_3(t)\big(-16u_{133}^3\lambda_1^3+8u_{133}^2\sqrt{4u_{133}^2\lambda_1^2+3}\lambda_1^2-3\sqrt{4u_{133}^2\lambda_1^2+3}\big)\Big)\,dt$$
$$\times(2u_{133}\lambda_1+\sqrt{4u_{133}^2\lambda_1^2+3}) - c_2\, e^{\frac{1}{12}\int\Big(-\frac{2(\sqrt{4u_{133}^2\lambda_1^2+3}-2u_{133}\lambda_1)a_1(t)^2}{a_3(t)}+12(\lambda_1^3+\lambda_1)}$$
$$-3(16u_{133}^3\lambda_1^3+8u_{133}^2\sqrt{4u_{133}^2\lambda_1^2+3}\lambda_1^2-3\sqrt{4u_{133}^2\lambda_1^2+3})a_3(t)\Big)\,dt\Bigg],$$

$$\psi_2(x,t) = i\sqrt{\frac{2}{3}}\, e^{-\frac{1}{2}x\sqrt{4u_{133}^2\lambda_2^2+3}}\Bigg[c_6\, e^{\frac{1}{12}\int\Big(\frac{2(2u_{133}\lambda_2+\sqrt{4u_{133}^2\lambda_2^2+3})a_1(t)^2}{a_3(t)}+12(\lambda_2^3+\lambda_2)}$$
$$+ 3a_3(t)\big(-16u_{133}^3\lambda_2^3+8u_{133}^2\sqrt{4u_{133}^2\lambda_2^2+3}\lambda_2^2-3\sqrt{4u_{133}^2\lambda_2^2+3}\big)\Big)\,dt$$
$$\times(2u_{133}\lambda_2+\sqrt{4u_{133}^2\lambda_2^2+3}) - c_5\, e^{\frac{1}{12}\int\Big(-\frac{2(\sqrt{4u_{133}^2\lambda_2^2+3}-2u_{133}\lambda_2)a_1(t)^2}{a_3(t)}+12(\lambda_2^3+\lambda_2)}$$
$$-3(16u_{133}^3\lambda_2^3+8u_{133}^2\sqrt{4u_{133}^2\lambda_2^2+3}\lambda_2^2-3\sqrt{4u_{133}^2\lambda_2^2+3})a_3(t)\Big)\,dt\Bigg],$$

$$\psi_3(x,t) = i\sqrt{\frac{2}{3}}\, e^{-\frac{1}{2}x\sqrt{4u_{133}^2\lambda_3^2+3}}\Bigg[c_9\, e^{\frac{1}{12}\int\Big(\frac{2(2u_{133}\lambda_3+\sqrt{4u_{133}^2\lambda_3^2+3})a_1(t)^2}{a_3(t)}+12(\lambda_3^3+\lambda_3)}$$
$$+ 3a_3(t)\big(-16u_{133}^3\lambda_3^3+8u_{133}^2\sqrt{4u_{133}^2\lambda_3^2+3}\lambda_3^2-3\sqrt{4u_{133}^2\lambda_3^2+3}\big)\Big)\,dt$$
$$\times(2u_{133}\lambda_3+\sqrt{4u_{133}^2\lambda_3^2+3}) - c_8\, e^{\frac{1}{12}\int\Big(-\frac{2(\sqrt{4u_{133}^2\lambda_3^2+3}-2u_{133}\lambda_3)a_1(t)^2}{a_3(t)}+12(\lambda_3^3+\lambda_3)}$$
$$-3(16u_{133}^3\lambda_3^3+8u_{133}^2\sqrt{4u_{133}^2\lambda_3^2+3}\lambda_3^2-3\sqrt{4u_{133}^2\lambda_3^2+3})a_3(t)\Big)\,dt\Bigg]. \tag{4.191}$$

$$\phi_1(x,t) = \frac{1}{2}e^{u_{133}x\lambda_1+\int\left(-8u_{133}^3a_3(t)\lambda_1^3+\lambda_1^3+\lambda_1\right)dt}c_1$$
$$- c_3\exp\left\{\frac{1}{12}\left[\int\left(\frac{2(2u_{133}\lambda_1+\sqrt{4u_{133}^2\lambda_1^2+3})a_1(t)^2}{a_3(t)}+12(\lambda_1^3+\lambda_1)\right.\right.\right.$$
$$\left.\left.\left.+3a_3(t)\Big(-16u_{133}^3\lambda_1^3+8u_{133}^2\sqrt{4u_{133}^2\lambda_1^2+3}\lambda_1^2-3\sqrt{4u_{133}^2\lambda_1^2+3}\Big)\right)dt-\right.\right.$$
$$\left.\left.6x\sqrt{4u_{133}^2\lambda_1^2+3}\right]\right\}$$
$$- c_2\exp\left\{\frac{1}{12}\left[\int\left(-\frac{2(\sqrt{4u_{133}^2\lambda_1^2+3}-2u_{133}\lambda_1)a_1(t)^2}{a_3(t)}+12(\lambda_1^3+\lambda_1)\right.\right.\right.$$
$$\left.\left.\left.-3\Big(16u_{133}^3\lambda_1^3+8u_{133}^2\sqrt{4u_{133}^2\lambda_1^2+3}\lambda_1^2-3\sqrt{4u_{133}^2\lambda_1^2+3}\Big)a_3(t)\right)dt\right.\right.$$
$$\left.\left.+6x\sqrt{4u_{133}^2\lambda_1^2+3}\right]\right\} \tag{4.192}$$

$$\phi_2(x,t) = \frac{1}{2}e^{u_{133}x\lambda_2+\int\left(-8u_{133}^3a_3(t)\lambda_2^3+\lambda_2^3+\lambda_2\right)dt}c_4$$
$$- c_6\exp\left\{\frac{1}{12}\left[\int\left(\frac{2(2u_{133}\lambda_2+\sqrt{4u_{133}^2\lambda_2^2+3})a_1(t)^2}{a_3(t)}+12(\lambda_2^3+\lambda_2)\right.\right.\right.$$
$$\left.\left.\left.+3a_3(t)\Big(-16u_{133}^3\lambda_2^3+8u_{133}^2\sqrt{4u_{133}^2\lambda_2^2+3}\lambda_2^2-3\sqrt{4u_{133}^2\lambda_2^2+3}\Big)\right)dt-\right.\right.$$
$$\left.\left.6x\sqrt{4u_{133}^2\lambda_2^2+3}\right]\right\}$$
$$- c_5\exp\left\{\frac{1}{12}\left[\int\left(-\frac{2(\sqrt{4u_{133}^2\lambda_2^2+3}-2u_{133}\lambda_2)a_1(t)^2}{a_3(t)}+12(\lambda_2^3+\lambda_2)\right.\right.\right.$$
$$\left.\left.\left.-3\Big(16u_{133}^3\lambda_2^3+8u_{133}^2\sqrt{4u_{133}^2\lambda_2^2+3}\lambda_2^2-3\sqrt{4u_{133}^2\lambda_2^2+3}\Big)a_3(t)\right)dt\right.\right.$$
$$\left.\left.+6x\sqrt{4u_{133}^2\lambda_2^2+3}\right]\right\} \tag{4.193}$$

$$
\begin{aligned}
\phi_3(x,t) = \frac{1}{2} e^{u_{133}x\lambda_3 + \int \left(-8u_{133}^3 a_3(t)\lambda_3^3 + \lambda_3^3 + \lambda_3\right) dt} c_7 \\
- c_9 \exp\Bigg\{ \frac{1}{12}\Bigg[\int \Bigg(\frac{2(2u_{133}\lambda_3 + \sqrt{4u_{133}^2\lambda_3^2 + 3})a_1(t)^2}{a_3(t)} + 12(\lambda_3^3 + \lambda_3) \\
+ 3a_3(t)\Big(-16u_{133}^3\lambda_3^3 + 8u_{133}^2\sqrt{4u_{133}^2\lambda_3^2 + 3}\lambda_3^2 - 3\sqrt{4u_{133}^2\lambda_3^2 + 3}\Big)\Bigg) dt - \\
6x\sqrt{4u_{133}^2\lambda_3^2 + 3}\Bigg]\Bigg\} \\
- c_8 \exp\Bigg\{ \frac{1}{12}\Bigg[\int \Bigg(- \frac{2(\sqrt{4u_{133}^2\lambda_3^2 + 3} - 2u_{133}\lambda_3)a_1(t)^2}{a_3(t)} + 12(\lambda_3^3 + \lambda_3) \\
- 3\Big(16u_{133}^3\lambda_3^3 + 8u_{133}^2\sqrt{4u_{133}^2\lambda_3^2 + 3}\lambda_3^2 - 3\sqrt{4u_{133}^2\lambda_3^2 + 3}\Big)a_3(t)\Bigg) dt \\
+ 6x\sqrt{4u_{133}^2\lambda_3^2 + 3}\Bigg]\Bigg\}
\end{aligned}
\tag{4.194}
$$

By applying the Darboux transformation (DT), we derive the breather solution of the HNLS equation as follows:

$$
\Psi(x,t) = \Psi_0 \frac{2Be^{F(x,t)}\cosh[H(x,t)] + 4\lambda_3 u_{111} e^{Z(x,t)}\sinh[M(x,t)] - T(x)}{2Be^{F(x,t)}\cosh[H(x,t)] + 4\lambda_3 u_{133} e^{Z(x,t)}\sinh[M(x,t)]}. \tag{4.195}
$$

The functions $M(x,t)$, $H(x,t)$, $Z(x,t)$ and $F(x,t)$, which encode the complex spatiotemporal dynamics, are defined as follows:

$$
H(x,t) = A(t) - \frac{1}{12}\int \left(\frac{4\lambda_3 u_{133} a_1(t)^2}{a_3(t)} - 3\,P\,a_3(t) + W \right) dt + \lambda_3 u_{133} x, \tag{4.196}
$$

$$
F(x,t) = \frac{1}{12}\int \left(-\frac{4\lambda_3 u_{133} a_1(t)^2}{a_3(t)} + 3\,S\,a_3(t) + Y(t) \right) dt + Bx + \lambda_3 u_{133} x, \tag{4.197}
$$

$$
M(x,t) = \frac{1}{12}\int \left(-\frac{4\lambda_3 u_{133} a_1(t)^2}{a_3(t)} + 3\,S\,a_3(t) + Y(t) \right) dt + \frac{Bx}{2}, \tag{4.198}
$$

$$
Z(x,t) = A(t) + \frac{1}{12}\int \left(-\frac{4\lambda_3 u_{133} a_1(t)^2}{a_3(t)} + 3\,P\,a_3(t) - W \right) dt + \frac{Bx}{2} + 2\lambda_3 u_{133} x. \tag{4.199}
$$

The auxiliary complex functions and constants required for the construction of the DT

matrix are as follows:

$$
\begin{aligned}
T(x) &= \lambda_3(u_{133} - u_{111})e^{\frac{Bx}{2}+\lambda_3 u_{133}x}, \\
A(t) &= \int \left(-8\lambda_3^3 u_{133}^3 a_3(t) + \lambda_3^3 + \lambda_3\right) dt, \\
Y(t) &= \frac{2a_1(t)^2(2\lambda_3 u_{133} - B)}{a_3(t)}, \\
W &= 12(\lambda_3^3 + \lambda_3), \\
B &= \sqrt{4\lambda_3^2 u_{133}^2 + 3}, \\
P &= 16\lambda_3^3 u_{133}^3, \\
S &= 3B - 8B\lambda_3^2 u_{133}^2.
\end{aligned}
$$

Bibliography

[1] N. Akhmediev and A. Ankiewicz (eds.), *Solitons: Nonlinear Pulses and Beams*, Chapman & Hall, 1997.

[2] M. Onorato, S. Residori, U. Bortolozzo, A. Montina, and F. T. Arecchi, "Rogue waves and their generating mechanisms in different physical contexts," *Physics Reports*, vol. 528, pp. 47–89, 2013.

[3] G. B. Whitham, *Linear and Nonlinear Waves*, Wiley-Interscience, 1974.

[4] Y. S. Kivshar and G. P. Agrawal, *Optical Solitons: From Fibers to Photonic Crystals*, Academic Press, 2003.

[5] N. J. Zabusky and M. D. Kruskal, "Interaction of solitons in a collisionless plasma and the recurrence of initial states," *Physical Review Letters*, vol. 15, pp. 240–243, 1965.

[6] V. E. Zakharov and A. B. Shabat, "Exact theory of self-focusing and self-modulation of waves in nonlinear media," *Soviet Physics JETP*, vol. 34, pp. 62–69, 1972.

[7] M. J. Ablowitz and H. Segur, *Solitons and the Inverse Scattering Transform*, SIAM, 1981.

[8] M. J. Ablowitz and P. A. Clarkson, *Solitons, Nonlinear Evolution Equations and Inverse Scattering*, Cambridge University Press, 1991.

[9] J. M. Dudley, G. Genty, A. Mussot, A. Chabchoub, and F. Dias, "Rogue waves and analogies in optics and oceanography," *Nature Reviews Physics*, vol. 1, no. 11, pp. 675–689, 2019.

[10] N. Akhmediev *et al.*, "Rogue waves of the Hirota equation and the role of the spectral parameter," *Physical Review E*, vol. 98, p. 062210, 2018.

[11] V. E. Zakharov, "Stability of periodic waves of finite amplitude on the surface of a deep fluid," *Journal of Applied Mechanics and Technical Physics*, vol. 9, pp. 190–194, 1968.

[12] F. Mitschke, "Soliton content of fiber-optic light pulses," *Applied Sciences*, vol. 7, no. 6, p. 635, 2017.

[13] A. Ankiewicz and N. Akhmediev, "Higher-order nonlinear SchrÃ¶dinger equations and their solitary wave solutions," *Physics Letters A*, vol. 384, no. 15, p. 126322, 2020.

[14] R. Guo and H. J. Li, "Darboux transformations and localized wave solutions for higher-order integrable systems," *Nonlinear Dynamics*, vol. 112, pp. 450–468, 2024.

[15] V. B. Matveev, "Darboux transformation and explicit solutions of the Kadomtsev–Petviashvili equation," *Letters in Mathematical Physics*, vol. 3, pp. 213–216, 1979.

[16] F. Baronio, "Mixed rogue wave patterns of the coupled nonlinear SchrÃ¶dinger equations," *Physical Review E*, vol. 100, p. 032214, 2019.

[17] T. Xu and M. S. Maniandara, "Non-autonomous nonlinear waves: dispersion and nonlinearity management," *Chaos, Solitons & Fractals*, vol. 168, p. 113152, 2023.

[18] T. R. Taha and M. J. Ablowitz, "Analytical and numerical methods for periodic solutions of the nonlinear SchrÃ¶dinger equation," *Journal of Computational Physics*, vol. 55, pp. 203–230, 1984.

[19] P. G. Drazin and R. S. Johnson, *Solitons: An Introduction*, Cambridge University Press, 1989.

[20] Y. S. Zhang *et al.*, "Rational solution of the nonlocal nonlinear SchrÃ¶dinger equation and its application in optics," *Romanian Journal of Physics*, 2017.

[21] Z. X. Zhou, "Darboux transformation and global solutions for a nonlocal derivative nonlinear SchrÃ¶dinger equation," *Communications in Nonlinear Science and Numerical Simulation*, 2018.

[22] M. J. Ablowitz *et al.*, "Integrable nonlocal nonlinear SchrÃ¶dinger equation," *Physical Review Letters*, 2013.

[23] M. J. Ablowitz *et al.*, "Inverse scattering transform for the integrable nonlocal nonlinear SchrÃ¶dinger equation," *Nonlinearity*, 2016.

[24] M. J. Ablowitz *et al.*, "Integrable nonlocal nonlinear SchrÃ¶dinger equation," *Studies in Applied Mathematics*, 2017.

[25] M. J. Ablowitz *et al.*, "Inverse scattering transform for the integrable nonlocal nonlinear SchrÃ¶dinger equation with nonzero boundary conditions," *Journal of Mathematical Physics*, 2018.

[26] N. Akhmediev *et al.*, "Modulation instability and periodic solutions of the nonlinear SchrÃ¶dinger equation," *Theoretical and Mathematical Physics*, 1986.

[27] L. An *et al.*, "Darboux transformation and solutions of nonlocal Hirota and Maxwell–Bloch equations," *Studies in Applied Mathematics*, 2021.

[28] R. Hirota, "Exact envelope-soliton solutions of a nonlinear wave equation," *Journal of Mathematical Physics*, vol. 14, pp. 805–809, 1973.

[29] S. W. Xu and J. S. He, "The Darboux transformation of the derivative nonlinear SchrÃ¶dinger equation," *Journal of Physics A*, 2011.

[30] B. L. Guo, L. M. Ling, and Q. P. Liu, "High-order solutions and generalized Darboux transformations of the derivative nonlinear SchrÃ¶dinger equation," *Studies in Applied Mathematics*, vol. 130, pp. 317–344, 2013.

[31] L. L. Wu, Z. Wu, L. Wang, and J. He, "Higher-order rogue waves for the Hirota equation," *Annals of Physics*, vol. 334, pp. 198–211, 2013.

[32] V. E. Zakharov, "Stability of periodic waves of finite amplitude on the surface of a deep fluid," *Journal of Applied Mechanics and Technical Physics*, vol. 22, pp. 190–194, 1968.

[33] V. E. Zakharov and A. B. Shabat, "Exact theory of two-dimensional self-focusing and one-dimensional self-modulation of waves in nonlinear media," *Soviet Physics JETP*, vol. 34, pp. 62–69, 1972.

[34] G. Darboux, "Sur une proposition relative aux Ã©quations linÃ©aires," *Comptes Rendus de l'AcadÃ©mie des Sciences*, vol. 94, pp. 1456–1459, 1882.

[35] V. B. Matveev, "Darboux transformation and explicit solutions of the Kadomtsev–Petviashvili equation," *Letters in Mathematical Physics*, vol. 3, pp. 213–216, 1979.

[36] F. Baronio, A. Degli Esposti Onorato, S. Chen, S. Trillo, and S. Wabnitz, "Solutions of the mixed coupled nonlinear SchrÃ¶dinger equations," *Physical Review Letters*, vol. 109, p. 044102, 2012.

[37] V. E. Zakharov and A. B. Shabat, "Interaction between waves in a dispersive medium," *Soviet Physics JETP*, vol. 37, pp. 823–828, 1973.

[38] V. E. Zakharov (ed.), *What Is Integrability?*, Springer, 1991.

[39] M. Dunajski, *Integrable Systems*, Cambridge University Press, 2012.

[40] P. D. Lax, "Integrals of nonlinear equations of evolution and solitary waves," *Communications on Pure and Applied Mathematics*, vol. 21, pp. 467–490, 1968.

[41] "arXiv:2111.03266v1 [nlin.SI]," 2021.

[42] D. Grahelj, *Solitons in Optics*, University of Ljubljana, 2010.

[43] H. Belkroukra, *Binary mixtures with a time-dependent variational approach: new families of breathers in two-component condensates*, Ph.D. dissertation, University of Chlef, Algeria, 2022.

[44] K. E. Strecker, G. B. Partridge, A. G. Truscott, and R. G. Hulet, "Formation and propagation of matter-wave soliton trains," *Nature*, vol. 417, pp. 150–153, 2002.

[45] L. Khaykovich *et al.*, "Formation of a matter-wave bright soliton," *Science*, vol. 296, pp. 1290–1293, 2002.

[46] G. P. Agrawal, *Nonlinear Fiber Optics*, 6th ed., Academic Press, 2019.

[47] S. Burger *et al.*, "Dark solitons in Bose–Einstein condensates," *Physical Review Letters*, vol. 83, pp. 5198–5201, 1999.

[48] J. Denschlag *et al.*, "Generating solitons by phase engineering of a Bose–Einstein condensate," *Science*, vol. 287, pp. 97–101, 2000.

[49] A. C. Scott, *Nonlinear Science: Emergence and Dynamics of Coherent Structures*, 2nd ed., Oxford University Press, 2003.

[50] M. S. Petrovic, A. I. Strinic, and M. R. Belic, "Nonlinear wave dynamics," *Physica Scripta*, vol. 85, p. 015403, 2012.

[51] A. Hasegawa and F. Tappert, "Transmission of stationary nonlinear optical pulses in dispersive dielectric fibers," *Applied Physics Letters*, vol. 23, pp. 142–144, 1973.

[52] D. Mandelik *et al.*, "Band-gap structure of waveguide arrays and excitation of Floquet–Bloch solitons," *Physical Review Letters*, vol. 90, p. 253902, 2003.

[53] B. A. Malomed, *Soliton Management in Periodic Systems*, Springer, 2006.

[54] J. N. Kutz and S. G. Evangelides, "Stabilized pulse propagation in nonlinear optical fibers," *Optics Letters*, vol. 23, pp. 685–687, 1998.

[55] W. C. Chen and W. C. Xu, "Nonlinear pulse propagation in semiconductor photonics," *Semiconductor Photonics and Technology*, 2002.

[56] A. Trombettoni and A. Smerzi, "Discrete solitons and breathers with dilute Bose–Einstein condensates," *Physical Review Letters*, vol. 86, pp. 2353–2356, 2001.

[57] S. F. Mingaleev, Y. S. Kivshar, and R. A. Sammut, "Long-range interaction and nonlinear localized modes in photonic crystals," *Physical Review E*, vol. 62, pp. 5777–5782, 2000.

[58] F. M. Russell *et al.*, "Nonlinear excitations in lattices," *Physical Review B*, vol. 55, pp. 6304–6312, 1997.

[59] B. I. Swanson *et al.*, "Observation of intrinsic localized modes," *Physical Review Letters*, vol. 82, pp. 3288–3291, 1999.

[60] K. W. Chow, R. H. J. Grimshaw, and E. Ding, "Nonlinear wave propagation," *Wave Motion*, vol. 43, pp. 158–166, 2005.

[61] A. V. Slyunyaev, "Nonlinear wave evolution," *Journal of Experimental and Theoretical Physics*, vol. 92, pp. 529–536, 2001.

[62] K. G. Lamb *et al.*, "Rogue waves in shallow water," *Physical Review E*, vol. 75, p. 046306, 2007.

[63] Z. T. Fu, S. D. Liu, and S. K. Liu, "Exact solutions of nonlinear wave equations," *Physics Letters A*, vol. 368, pp. 238–244, 2007.

[64] E. A. Kuznetsov, "Solitons in a parametrically unstable plasma," *Soviet Physics Doklady*, vol. 22, pp. 507–508, 1977.

[65] Kawata, T. and Inoue, H., "Inverse scattering method for nonlinear evolution equations under non-vanishing conditions," *J. Phys. Soc. Jpn.*, vol. 44, no. 5, pp. 1722–1729, 1978.

[66] Zakharov, V.E. and Shabat, A.B., "Interaction between solutions in a stable medium," *Zh. Eksp. Teor. Fiz.*, vol. 64, no. 5, pp. 1627–1639, 1973.

[67] Akhmediev, N.N. and Korneev, V.I., "Modulation instability and periodic solutions of the nonlinear Schrödinger equation," *Theor. Math. Phys.*, 1986.

[68] Akhmediev, N.N., Eleonskii, V.M. and Kulagin, N.E., "Exact first-order solutions of the nonlinear Schrödinger equation," *Theor. Math. Phys.*, vol. 72, no. 2, pp. 809–818, 1987.

[69] Kharif, C. and Pelinovsky, E., *Eur. J. Mech. B*, vol. 22, p. 603, 2003.

[70] Dysthe, K., Krogstad, H.E. and Muller, P., *Annu. Rev. Fluid Mech.*, vol. 40, p. 287, 2008.

[71] Pelinovsky, E. and Kharif, C., *Extreme Ocean Waves*, Springer, New York, 2008.

[72] Osborne, A.R., *Nonlinear Ocean Waves*, Academic Press, New York, 2009.

[73] Kharif, C., Pelinovsky, E. and Slunyaev, A., *Rogue Waves in the Ocean*, Springer, New York, 2009.

[74] Didenkulova, I. and Pelinovsky, E., *Nonlinearity*, vol. 24, p. R1, 2011.

[75] Draper, L., *Oceanus*, vol. 10, p. 13, 1964.

[76] Yan, Z.Y., *Phys. Lett. A*, vol. 374, p. 672, 2010.

[77] Akhmediev, N. and Pelinovsky, E. (eds.), "Rogue waves: towards a unifying concept," *Eur. Phys. J. Spec. Top.*, vol. 185, 2010.

[78] Solli, D.R., Ropers, C., Koonath, P. and Jalali, B., "Optical rogue waves," *Nature*, vol. 450, p. 1054, 2007.

[79] Garrett, C. and Gemmrich, J., "Rogue waves," *Phys. Today*, vol. 62, p. 62, 2009.

[80] Wabnitz, S., Finot, C., Fatome, J. and Millot, G., "Shallow water rogue wavetrains in nonlinear optical fibers," *Phys. Lett. A*, vol. 377, p. 9329, 2013.

[81] Peregrine, D.H., "Water waves, nonlinear Schrödinger equations and their solutions," *J. Aust. Math. Soc. Ser. B*, vol. 25, pp. 16–43, 1983.

[82] Akhmediev, N. and Pelinovsky, E., *Eur. Phys. J. Spec. Top.*, vol. 185, p. 1, 2010.

[83] Dysthe, K., Krogstad, H.E. and Muller, P., *Annu. Rev. Fluid Mech.*, vol. 40, p. 287, 2008.

[84] Akhmediev, N.N., Korneev, V.I. and Kuz'menko, Y.V., "Generation of periodic trains of picosecond pulses in an optical fiber: exact solutions," *Sov. Phys. JETP*, vol. 61, pp. 62–67, 1985.

[85] Kibler, B. et al., "The Akhmediev breather as a theory of rogue waves: an experimental perspective," *Nat. Phys.*, vol. 6, pp. 790–795, 2010.

[86] Benjamin, T.B. and Feir, J.E., "The disintegration of wave trains on deep water Part 1: Theory," *J. Fluid Mech.*, vol. 27, pp. 417–430, 1967.

[87] Dysthe, K.B. and Trulsen, K., "Evolution of a narrow-band spectrum of random surface gravity waves," *Phys. Scr.*, vol. T82, pp. 48–52, 1999.

[88] Kivshar, Y.S. and Luther-Davies, B., "Dark solitons in nonlinear optics," *Phys. Rep.*, vol. 298, pp. 81–197, 1998.

[89] Das, A., *Integrable Models*, World Scientific, Singapore, 1989.

[90] Matveev, V.B. and Salle, M.A., *Darboux Transformations and Solitons*, Springer, Berlin, 1991.

[91] Gu, C.H., Hu, H. and Zhou, Z., *Darboux Transformations in Integrable Systems*, Springer, 2005.

[92] Hirota, R., "Exact envelope-soliton solutions of a nonlinear wave equation," *J. Math. Phys.*, vol. 14, pp. 805–809, 1973.

[93] Kodama, Y., "Optical solitons in a monomode fiber," *J. Stat. Phys.*, vol. 39, pp. 597–614, 1985.

[94] Matveev, V.B. and Salle, M.A., *Darboux Transformations and Solitons*, Springer, 1991.

[95] Rogers, C. and Schief, W.K., *Bäcklund and Darboux Transformations*, Cambridge University Press, 2002.

[96] Guo, B., Ling, L. and Liu, Q.P., "Generalized Darboux transformation and rogue wave solutions," *Phys. Rev. E*, vol. 85, 026607, 2012.

[97] Yousefi, Y. and Muminov, K.K., "A Simple Classification of Solitons," arXiv:1206.1294, 2012.

[98] Akhmediev, N., Eleonskii, V.M. and Kulagin, N.E., *Theor. Math. Phys.*, vol. 72, pp. 809–818, 1987.

[99] Kuznetsov, E.A., *Sov. Phys. JETP*, vol. 41, pp. 164–169, 1976.

[100] Solli, D.R. et al., *Nature*, vol. 450, pp. 1054–1057, 2007.

[101] Kibler, B. et al., *Nat. Phys.*, vol. 6, pp. 790–795, 2010.

[102] Agrawal, G.P., *Nonlinear Fiber Optics*, 5th ed., Academic Press, 2013.

[103] Tchofo-Dinda, P. and Govindarajan, A., *Mech. Res. Commun.*, vol. 124, 104022, 2022.

[104] Samet, H.C. et al., *Adv. Math. Phys.*, 2014, 323591.

[105] Durmus, S.A. et al., *Opt. Quantum Electron.*, vol. 56, p. 794, 2024.

[106] Miri, F. and Sheikhi, M., *Optik*, vol. 297, 171019, 2024.

[107] Vinayagam, P.S. et al., *Rom. Rep. Phys.*, vol. 77, 101, 2025.

[108] Jordan, D.W. and Smith, P., *Nonlinear Ordinary Differential Equations*, 2007.

[109] Su, C.Q. et al., *Commun. Nonlinear Sci. Numer. Simul.*, vol. 36, pp. 457–467, 2016.

[110] Wang, L.H. et al., *Phys. Rev. E*, vol. 87, 053202, 2013.

[111] Akhmediev, N.N. and Korneev, V.I., *Theor. Math. Phys.*, vol. 69, pp. 1089–1093, 1986.

[112] Dudley, J.M. et al., *Opt. Express*, vol. 16, pp. 3644–3651, 2008.

[113] Ma, Y.C., *Stud. Appl. Math.*, vol. 60, pp. 43–58, 1979.

[114] Emplit, P.; Hamaide, J.P.; Reynaud, F.; Froehly, G.; Barthelemy, A., *Opt. Commun.*, vol. 62, p. 374, 1987.

[115] Weller, A.; Ronzheimer, J.P.; Gross, C.; Esteve, J.; Oberthaler, M.K.; Frantzeskakis, D.J.; Theocharis, G.; Kevrekidis, P.G., "Experimental observation of oscillating and interacting matter-wave dark solitons," *Phys. Rev. Lett.*, vol. 101, 130401.

[116] Hasegawa, A.; Kodama, Y., *Solitons in Optical Communications*, Oxford University Press, Oxford, UK, 1995.

[117] YongHui, K.; Bolin, M.; Xin, W., "Higher-order soliton solutions for the SasaâSatsuma equation revisited via difference method," *J. Nonlinear Math. Phys.*, vol. 30, pp. 1821–1833, 2023.

[118] Yang, J., *Nonlinear Waves in Integrable and Nonintegrable Systems*, SIAM, Philadelphia, 2021.

[119] Peregrine, D.H., "Water waves, nonlinear Schrödinger equations and their solutions," *J. Aust. Math. Soc. Ser. B*, vol. 25, pp. 16–43, 1983.

[120] Ankiewicz, A.; Soto-Crespo, J.M.; Akhmediev, N., "Rogue waves and rational solutions of the Hirota equation," *Phys. Rev. E*, vol. 81, 046602, 2010.

[121] Yan, Z., "Nonautonomous rogons in the inhomogeneous nonlinear Schrödinger equation," *Phys. Lett. A*, vol. 374, pp. 672–679, 2010.

[122] Al Khawaja, U., *J. Phys. A: Math. Gen.*, vol. 39, 2006.

[123] Ablowitz, M.J.; Segur, H., "The inverse scattering transform: Semi-infinite interval," *J. Math. Phys.*, vol. 15, no. 9, pp. 1292–1303, 1974.

[124] Kodama, Y., "Optical soliton in a monomode fiber," *J. Stat. Phys.*, vol. 39, pp. 597–614.

[125] Samet, H.C.; Sakthivinayagam, P.; Al Khawaja, U.; Benarous, M.; Belkroukra, H., "Peregrine soliton management of breathers in coupled GrossâPitaevskii equations," *Phys. Wave Phenom.*, vol. 28, pp. 305–312, 2020.

[126] Mourachkine, A., arXiv:cond-mat/0411452, 2004.

[127] Bobenko, A.I., "Surfaces in terms of 2Ã2 matrices: old and new integrable cases," 1994.

[128] Korteweg, D.J.; de Vries, H., "On the change of form of long waves advancing in a canal," *Philos. Mag.*, vol. 39, pp. 422–443, 1895.

[129] Chachou, H., *Dynamics of a trapped Bose gas at finite temperature*, PhD thesis, Chlef University, 2014.

[130] Engels, P.; Atherton, C., "Stationary and nonstationary fluid flow of a BoseâEinstein condensate," *Phys. Rev. Lett.*, vol. 99, 160405, 2007.

[131] Pattinson, R.W., PhD thesis, 2014.

[132] Strecker, K.; Partridge, G.; Truscott, A.; Hulet, R., *Nature*, vol. 417, p. 150, 2002.

[133] Khaykovich, L. et al., *Science*, vol. 296, p. 1290, 2002.

[134] Cornish, S.; Thompson, S.; Wieman, C., *Phys. Rev. Lett.*, vol. 96, 170401, 2006.

[135] Yesmakhanova, K. et al., *J. Phys. Conf. Ser.*, vol. 804, 012004, 2017.

[136] Serikbayev, N.; Saparbekova, A., *Int. J. Geom. Methods Mod. Phys.*, vol. 20, 2350172, 2023.

[137] Shaikhova, G. et al., *Geom. Integr. Quantization*, vol. 21, pp. 265–271, 2020.

[138] Sasa, N.; Satsuma, J., *J. Phys. Soc. Jpn.*, vol. 60, pp. 409–417, 1991.

[139] Dutton, Z. et al., "Observation of quantum shock waves," *Science*, vol. 293, pp. 663–668, 2001.

[140] Emplit, P. et al., "Picosecond steps and dark pulses," *Opt. Commun.*, vol. 62, pp. 374–379, 1987.

[141] Hasegawa, A.; Tappert, F., *Appl. Phys. Lett.*, vol. 23, pp. 142–144, 1973.

[142] Kaup, D.J.; Newell, A.C., *J. Math. Phys.*, vol. 19, pp. 798–801, 1978.